2014-01-08

Molecular mechanisms of DNA translocation through a biological nanopore alpha-hemolysin

Markosyan, Suren

UNIVERSITY OF CALGARY

Molecular mechanisms of DNA translocation through a biological nanopore alpha-hemolysin

by

Suren Markosyan

A THESIS

SUBMITTED TO THE FACULTY OF GRADUATE STUDIES

IN PARTIAL FULFILMENT OF THE REQUIREMENTS FOR THE

DEGREE OF MASTER OF SCIENCE

DEPARTMENT OF BIOLOGICAL SCIENCES

CALGARY, ALBERTA

JANUARY 2014

Abstract

The transport of genetic material across biomembranes through pore-forming proteins is a process of great biological and medicinal interest (Szabo et al 1998). Alpha-Hemolysin, a pore-forming protein, was identified as a macromolecular device for DNA and RNA transport and detection. This protein may have a potential use in nanopore sequencing. The nanopore sequencing technique measures the effect of the captured single-stranded (ss) DNA blockade on the ion current across the nanopore. However, designing a nanopore that gives an ideal resolution at the single-base level is challenging due to the absence of detailed information on the behaviour of a DNA within the nanopore. This research project was able to confirm that several factors govern DNA behaviour inside the nanopore. In addition, novel software has been developed and validated for DNA-nanopore studies and for fast screening of multiple mutant nanopores.

Acknowledgments

This research work and thesis is accomplished thanks to the support of my supervisor Dr. Sergei Noskov. He has been an excellent mentor during the three and a half years that I have spent in the Masters of Science program. Thank you for giving me an opportunity to work on this fascinating project and helping to improve my abilities of scientific thinking, researching, reporting and presenting, drastically.

I am thankful to my committee members Dr. Elmar Prenner, Dr. Dennis Salahub, and Dr. Raymond Turner for their valuable suggestions and constructive feedback on my research throughout the degree program and during the committee meetings and personal communications.

My entire academic path from college to graduate studies would not be possible without my parents (Mr. Mekhak Markosyan and Mrs. Varduhi Soghomonyan) and my wife (Anahit Petoyan). I acknowledge them for their patience, support, and for always being on my side whatever I went through.

Table of Contents

List of Tables

List of Figures

List of Symbols and Abbreviations

(A/C) contrast ..... Adenine/Cytosine contrast

aa……amino acid

BD ..... Brownian Dynamics

CG ..... Coarse Grained

CHARMM ..... Chemistry at Harvard Macromolecular Mechanics

CMAP ..... Corrective Map

DIST ..... Distance

DPPC 1,2-dipalmitoyl-sn-glycero-3-phosphocholine

ds……..double-stranded

EBS ..... Electronic BioSciences

GC ..... Grand Canonical

GCMC ..... Grand Canonical Monte Carlo

GCMC/BD ..... Grand Canonical Monte Carlo/Brownian Dynamics

GCP ..... Geometric Centre of Phosphates

LJ ..... Lennard-Jones

MD ..... Molecular Dynamics

MspA ..... Mycobacterial porin A

PB ..... Poisson Boltzmann

PBC ..... Periodic Boundary Conditions

PDB ..... Protein Data Bank

PEG ..... Polyethylene glycol

PME ..... Particle Mesh Ewald

PMF.....Potential of Mean Force

POPC..... 1-palmitoyl,2-oleoyl-sn-glycero-3-phosphocholine

RDF..... Radial Distribution Function

REMD.....Replica Exchange Molecular Dynamics

RMSD ..... Root Mean Square Displacement

SR..... Short Range

ss ……...single-stranded

vdW..... van der Waals

WT ..... Wild Type

αHL .....alpa-Hemolysin

CHAPTER 1 – BACKGROUND AND SIGNIFICANCE

1.1 Literature review

1.1.1 Biopolymer translocation across alpha-hemolysin toxin

The passage of mRNA through nuclear pore complexes, the translocation of proteins across biological membranes, or the transport of DNA/RNA in and out of mitochondria are a few of many examples of biopolymer translocation (Somasundaran et al 1994). Bacterial ion channels and porins are involved in the transport of biological polymers across biological membranes often underlying bacterial pathogenicity. One particular bacterial protein capable of translocating small ions, organic molecules, and even poly-nucleic acids is alpha-hemolysin (αHL). αHL is secreted by the human pathogen *Staphylococcus aureus*. αHL appears as a monomer or heptamer, and as a monomer is capable of binding on human endothelial cells, lymphocytes, monocytes, erythrocytes and platelets (Bhakdi et al 1991). However to achieve its cytotoxic activity the monomers must insert into the membrane of a target cell and oligomerize to form heptamerical channels with a molecular weight of about 234 kDa and large conductance (more than 1nS) with a definite anion selectivity. Song and coworkers identified the structure of αHL in 1996. This mushroom-shaped protein is a bacterial toxin and is mostly composed of β strands. The protein is ~100 Å (10 nm) in length with the radius of the water-filled nanopore varying from 14 Å (1.4 nm) to 26 Å (2.6 nm) (figure 1.1). Structurally it consists of cap and stem regions. The cap is composed of α helices and β sheets and it represents the bulky and wider part of the channel. The stem region is mainly composed of β sheets and represents the narrow, β barrel part of the channel. The narrowest part of the channel (1.4 nm), called the constriction zone, is located here. The primary mechanism by which αHL damages the cell is a

leakage of ions, water, and low molecular weight molecules in to and out of the cell (Bhakdi et al 1991).

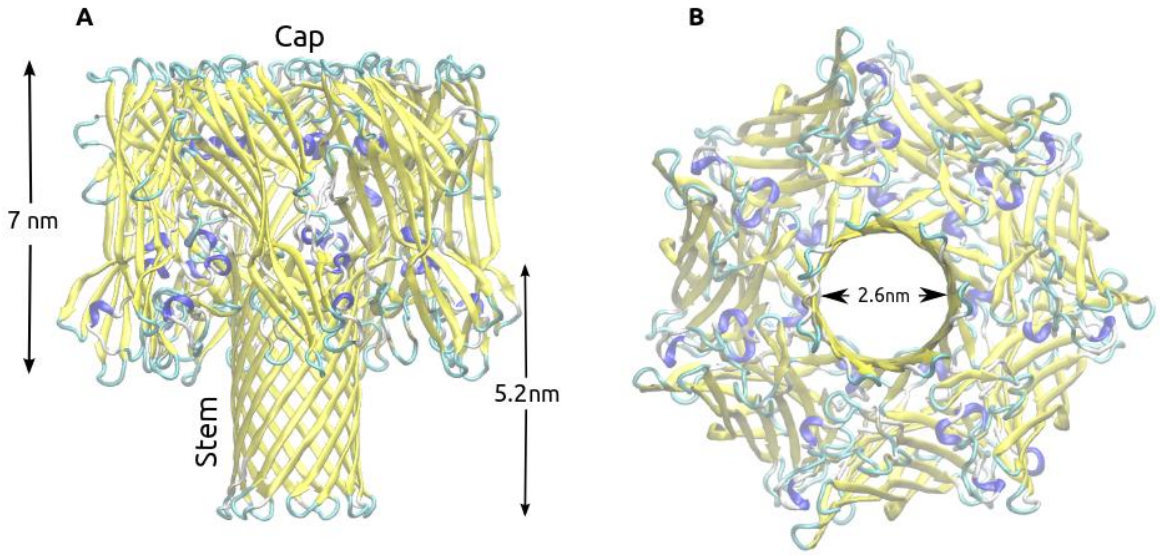

Figure 1.1 Structure of the alpha-hemolysin ion channel secreted by human pathogen *Staphylococcus aureus*.

Side view of the channel (panel A): the protein is a mixture of α - helices (in dark blue) and β - sheets (in yellow), loops are represented in light blue. Top view of the channel (panel B): the diameter of water-filled nanopore can reach up to 2.6 nm.

The structure was taken from protein data bank (PDB entry: 7AHL) and visualized using VMD.

1.1.2 Nanopore sequencing

Intense exploration of αHL's biophysical properties began in the early 90s; and was prompted by the potential applications of this protein in biotechnology. Since then, it has been firmly established that αHL can be used for controlled delivery of biopolymers to target cells. First, Bezrukov and coworkers (1996) showed that polyethylene glycol (PEG) was capable of diffusing through the aqueous pore of αHL and that the nanopore can be used as a single-molecule clock, counting every translocation event. Next, Kasianowicz et al (1996) illustrated that single-stranded (ss) DNA can also move through the αHL channel when an electric field was applied across the channel. They also detected ion currents through the αHL pores due to the presence of 1M salt (KCl) concentration on both sides of the lipid membrane. While the ss-DNA molecule was moving through the αHL nanopore, the ion current measurements fluctuated in a nucleotide-dependent manner. Eventually they were able to show that these current levels are directly related to the translocation events of ss-DNA and depended on its sequence. In particular, temporary decreases of the current level indicated that the ss-DNA molecule has blocked the channel (figure 1.2).

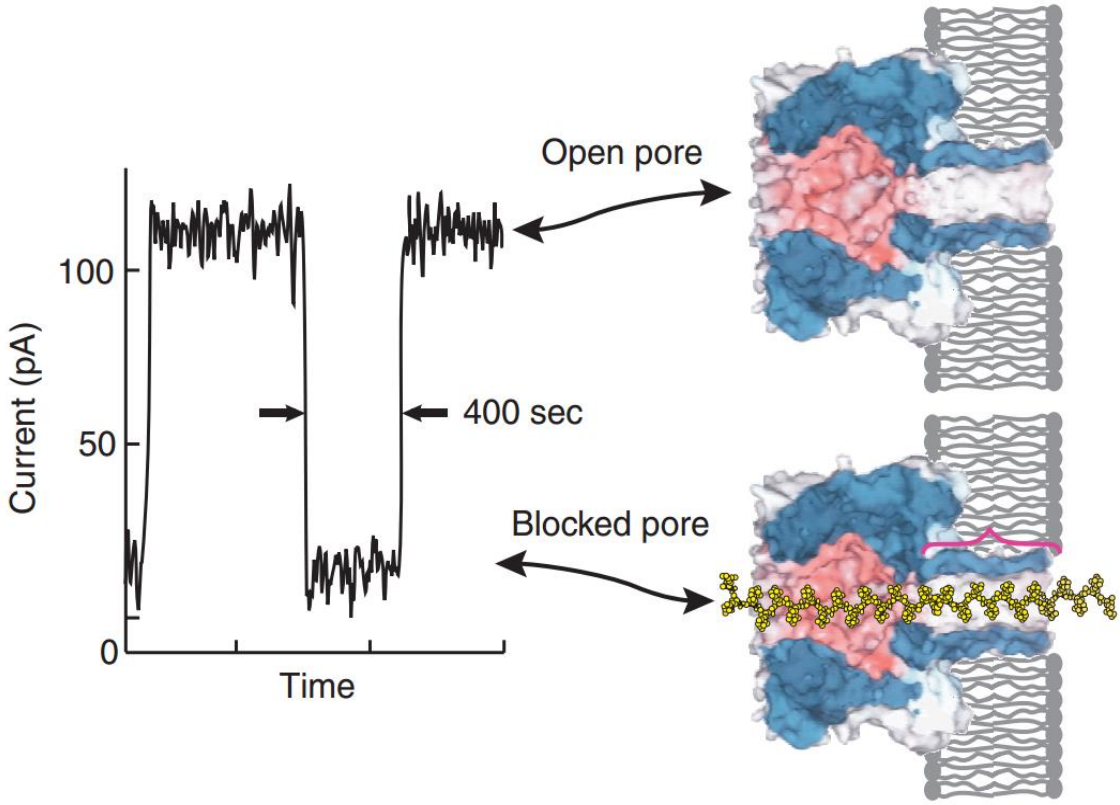

Figure 1.2 Strand-sequencing using ionic current blockages.

A typical trace of the ionic current amplitude through a αHL nanopore clearly differentiates between an open-pore (top right) and one blocked by a strand of DNA (bottom right) but cannot distinguish between the 12 nucleotides that simultaneously block the narrow transmembrane channel domain (red bracket). Taken from Branton et al (2008).

The time interval during which the current level remains decreased is proportional to the length of the molecule that blocks the nanopore (Kasianowicz et al 1996).This can be used to assess the translocation dynamics.

The next milestone in the development of nanopore sequencing happened in 1999, when Akeson et al found that αHL could act as a highly sensitive detector of single molecule RNA translocation events. Akeson et al 1999 performed sets of experiments where they separated homo-polymers (containing only one type of nucleotide: either adenine or cytosine) or hetero-polymers (a mixture of the two nucleotides) translocated through the αHL nanopore. As a result, the ion currents were blocked and the current levels were recorded. Subsequently, they illustrated that αHL is capable of "differentiating" between purine and pyrimidine bases based on analysis of the blocked current levels. Moreover, they found that poly-cytosine blocks more than poly-adenine, even though cytosine is smaller than adenine. However, this research group could not establish a clear discrimination between nucleotides of a DNA molecule.

One of the first attempts to observe nucleotide discrimination for a DNA molecule by the αHL nanopore was reported in 2000. Meller et al (2000) performed intensive research to study the translocation of individual single strands (ss) of DNA through the nanopore and to test whether αHL can "distinguish" between nucleotides. Their approach to the problem was successful to some extent. They were able to show that the nanopore could actually detect whether the single-stranded molecule represented homo-purine ($poly(dA)_{100}$) or homo-pyrimidine ($poly(dC)_{100}$) when it moved through and blocked the pore. Unfortunately, it was not sensitive enough to detect individual nucleotides within the hetero-polymer strand. However Meller et al (2000) revealed information about some other factors that influence these translocation events inside the nanopore. In particular, the translocation rate of the single

stranded polymers changes based upon changes in temperature, which in turn may influence the secondary structure and conformational behaviour of the polymers. For instance, poly(dA) exhibits completely different conformations at low (largely stacked) and high (coiled) temperatures (Luzzati et al 1964). Meller et al (2000) also illustrated that the direction of single stranded polymers is important: i.e. whether the polymers enter the nanopore with 3'- 5' or 5'- 3' directions affects the translocation speed and the blocked current levels.

Now we have learned that single stranded (ss) DNA molecules can move through the αHL nanopore under an applied electric field. However, this still begs the question what is the speed at which the channels transport the DNA and is it sufficient for sequencing purposes. Meller et al (2001) have addressed this question. It has been found that the translocation rate of ss-DNA depends on both the applied electric field and the length of the molecule itself. The experimental estimates (Meller et al 2001) showed that the average translocation velocity of a deoxyadenylic acid monomer (the equivalent of a single adenine nucleotide) was 1.4 Å /μs (at 2^{o} C and 120mV). Moreover, there is a threshold length for the ss-DNA molecule. The threshold length is described to be an oligomer composed of 12 nucleotides (~ 48 Å). This length almost matches the contour length of the β barrel region of the αHL nanopore (~ 52 Å). The polymers shorter than the threshold value move faster than those that are longer than the threshold. The translocation velocity increases non-linearly with the increase in the applied electric field (Meller et al 2001).

This marked the beginning of a new era in biotechnology with great promises of using nanopores for rapid DNA sequencing. Since αHL is capable of differentiating nucleotide bases, scientists have come to the idea that they can use that ability to sequence the human genome. Subsequently a new approach is being developed towards DNA sequencing. Nanopore

sequencing is a so-called "3rd generation" sequencing technology. The main goal of the nanopore sequencing is not just to achieve genome sequencing, but perform it for under $1000 and much faster than already existing sequencing technologies including 1st generation or Sanger-based and 2nd or the next-generation sequencing (Branton et al 2008).

1.1.3 Other sequencing techniques

For the past three decades, Sanger sequencing was the only DNA sequencing technology on the market. It was developed by Sanger and colleagues (Sanger et al 1977) and works via in-vitro DNA replication during which DNA polymerase integrates chain-terminating dideoxynucleotides. The length of polymer that this method can sequence per run varies from 400 to 900 base pairs or a total of 115 kbp (115,000 base pairs) per day. For example, the human genome contains 3.2 billion base pairs, therefore, sequencing it by the Sanger technique is slow and expensive. Consequently, there was a need to speed up and to minimize the cost of the sequencing process. That is when (2001) the next-generation sequencing techniques started to be developed. The main advantage of these techniques is the inexpensive production of a large volume of sequencing data (Metzker 2010). In addition, since the sequencing devices are massively parallel, sequencing is faster compared to the first generation devices (Mardis 2011). Roche/454, Life technologies SOLiD, Illumina, Pacific Biosciences RS are all examples of the 2nd or next-generation sequencing devices (Mardis 2011, Metzker 2010).

1.1.4 Limiting factors and challenges in nanopore sequencing

There are a number of factors that pose real limits for using nanopores for sequencing purposes.

Translocation speed: One of those factors is the rate at which DNA moves through the pore. For instance, the rate of translocation of a monomer of deoxyadenylic acid (at 2 ^{o}C and 120 mV)

is ~1.4 Å/μs (Meller et al 2001). Recent experiments show that to enable the identification of single nucleotides using nanopore devices one will need slow down the moving chain of DNA must move slowly enough so that each nucleotide can stay inside the "sensing region" for more than one millisecond (Deamer and Branton. 2002). Otherwise, the nucleotide identification will be impossible due to the sampling frequency that is accessible to low-noise electrophysiology. Unfortunately, the DNA molecule moves through the nanopore much faster than needed, which makes it very difficult for the nanopore to resolve the individual nucleotides. The production of a chip-based nanopore platform was not sufficient to produce the necessary statistical coverage to rebuild sequences long enough to piece together a complex genome.

Nanopore confinement: It has been previously stated that the αHL nanopore can accommodate 10-12 nucleotides. This implies that all of those nucleotides may contribute to the overall blockade of ionic current. Consequently, it becomes very difficult to achieve single nucleotide resolution based on the ion current traces alone. Moreover, no natural or human made channels possess such a geometry, which would allow for detecting only one nucleotide at a time (Branton et al 2008).

Excess noise: Another limiting factor in high-sensitivity sequencing with nanopores is related to excess noise in measurements. The noise has a well-defined 1/f dependence, where f is the frequency on an interval bounded away from zero and infinity. This noise is a canonical signature of slow conformational dynamics affecting fast degrees of freedom such as an ion permeating rapidly through the channel in the slowly evolving electrical field due to ss-DNA conformational dynamics. To reduce this noise one has to understand the potential surface of the system that defines DNA switching from one to another conformational state. Although everybody agrees that specific DNA-channel interactions are responsible for the differential

blockade by DNA, how exactly the nucleotides interact with the amino acid side-chains (e.g. which part of the protein, spatial and per-residue contributions) remains unknown.

1.1.5 Statement of the problem

In the past two decades intense studies have been focused on the transport of DNA across αHL and its many mutants. Several important factors were proposed to aid base recognition. The presence of some key amino acids inside the channel (constriction zone), which might make a vital contribution to the base-specific interactions with DNA (figure 1.3) is one of the most important factors.

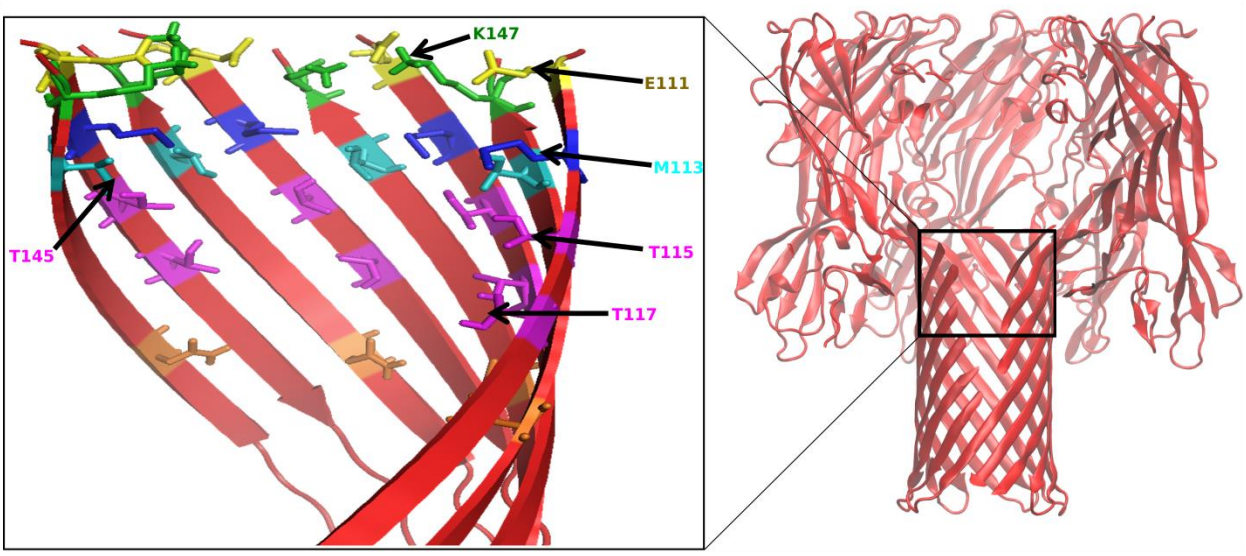

Figure 1.3 Constriction schematic.

The key amino acid residues residing in the constriction (the narrowest part) of alpha-hemolysin nanopore are represented with different colors.

However much remains unknown about the interactions of DNA and αHL. For example, most of the studies investigated the primary constriction zone formed by K147, but experimental evidence shows that αHL possesses at least three well-separated sensing zones responsible for contrast between different nucleotides (Stoddart et al 2009). The molecular mechanism by which DNA is transported through the channel has yet to be established. The orientation and conformational dynamics of ss-DNA inside the channel also remain largely unknown. Theoretical studies aimed at resolving the molecular interactions between DNA/RNA and ion channels can potentially help us to understand the transport machinery by which biopolymers move across the channels.

1.2 Objectives of the research

(a). to establish a clear understanding of the behaviour of a DNA molecule within the nanopore.

We want to understand where the direct contacts are between DNA and the protein, how strong these interactions (in terms of energy) are and how the DNA molecule behaves inside the pore. This sort of information may help in finding solutions for polymer (DNA/RNA) transport problems in affected cells.

(b). to confirm the targeted mutagenesis and to provide molecular details for the improvement of the (A/C) contrast

We will perform (via computational simulations) targeted modification of "key amino acids" to confirm the results obtained by our experimental collaborators and to collect molecular level details that will allow us to improve the contrast between different bases. First, we want to run simulations to measure the ionic current through open-pores of mutated and wild-type αHL protein. Then we want to measure the ion current through the blocked (by adenine or cytosine homo-polymers) pores of mutated and wild type αHL protein.

$$\left(\frac{A}{C}\right) contrast = \frac{I_C - I_A}{I_o} * 100\% \quad (1)$$

I_C and I_A are the ion current measurements from the pores blocked by cytosine and adenine homo-polymers, respectively and I_O is the open-pore ion current. (A/C) contrast is one of the most important factors that determine the efficiency of a nanopore as a sequencing tool. The larger the (A/C) contrast, the easier it is to detect and differentiate between nucleotides moving through a nanopore. In other words, the bigger the (A/C) contrast, the better the nanopore.

(c). to aid in the computer program development for long-time DNA-αHL studies

We aim to design a program that will be used to perform long-term computer simulations on ss-DNA translocation through αHL nanopore. This tool will allow simulations that can reach up to the millisecond regime at very low computational power and cost. This program will enable us to establish a time bridge (opportunity for closing the time gap) between classic all-atom Molecular Dynamics (MD) simulations and real-time experiments.

CHAPTER 2 – METHODS AND MATERIALS

2.1 All – atom Molecular Dynamics

2.1.1 All-atom Molecular Dynamics simulation

According to Daan Frenkel and Berend Smit (2002) "Molecular Dynamics simulation is a technique for computing the equilibrium and transport properties of a classical many-body system." One idea that is common in both Molecular Dynamics (MD) simulations and in real experiments is the sequential order of events that happen similarly. In particular, to set up a real experiment, one starts to prepare a sample of a material of interest. Then the sample is introduced to a measuring/experimental tool (be it a thermometer or spectrophotometer) and the properties of interest are measured during a definite time interval for consistent time statistics. To account for experimental noise, one has to average over longer time regimes to obtain results that are more accurate. On the other hand, in MD simulations, we start the simulations by preparing a "sample system" and propagating a sampling by solving Newton's equation of motion until the properties of a system are near an equilibrium state for a given temperature/volume/pressure. To re-phrase it in MD language we have to sample our conformational space completely.

Moreover, errors in both real experiments and simulations are similar, too. For instance, poorly prepared sample of interest; insufficiently averaged measurements (very few replicates or too short simulation).

Sufficient sampling is always an issue with MD techniques. Therefore, to improve the sampling of the system, in some of the studies, we have used a technique called Temperature Replica-Exchange Molecular Dynamics (REMD) (Jiang and Roux 2010). This technique allows the system to sample the conformational space at different temperatures. When doing so, the energy barriers can be overcome leading to exploration of new conformational space.

2.1.2 A program and its key parameters for performing MD simulations

There are several programs for MD simulations available in the field. However, few are capable of performing simulations of large bio-molecular systems (~200000 and more atoms). In this research project, the NAMD (Phillips et al 2005) code has been used to carry out all – atom MD simulations.

Throughout this chapter, I will go through all the important approaches and parameters we have used in our simulations.

2.1.2.1 MD concept

As it was mentioned previously, the basic starting point for MD simulations is to solve Newton's equation of motion for all atoms in the system.

$$m_\alpha r_\alpha = -\frac{\partial}{\partial r_\alpha} U_{total}(r_1, r_{2,} \ldots, r_N) \quad (2)$$

where $\alpha = 1, 2 \ldots N$, m_α is the mass and r_α is the position of atom α. U_{total} is the total potential energy arising from all atomic positions in a system. In other words, U_{total} or the so-called "force field" represents a summary of the interactions between all atoms in a system. Therefore, it is considered one of the most vital attributes of MD simulation. The Noskov research group is participating in the force-field development for CHARMM/NAMD simulations, which, in turn, determined the choice of the program code.

2.1.2.2 The "force field" in NAMD

The potential energy function in NAMD is as follows:

$$U_{total} = U_{bond} + U_{angle} + U_{dihedral} + U_{vdW} + U_{Coulomb} \quad (3)$$

This expression can be divided into two parts: bonded and non-bonded interactions. The bonded interactions are U_{bond}, U_{angle} and $U_{dihedral}$ (see figure 2.1).

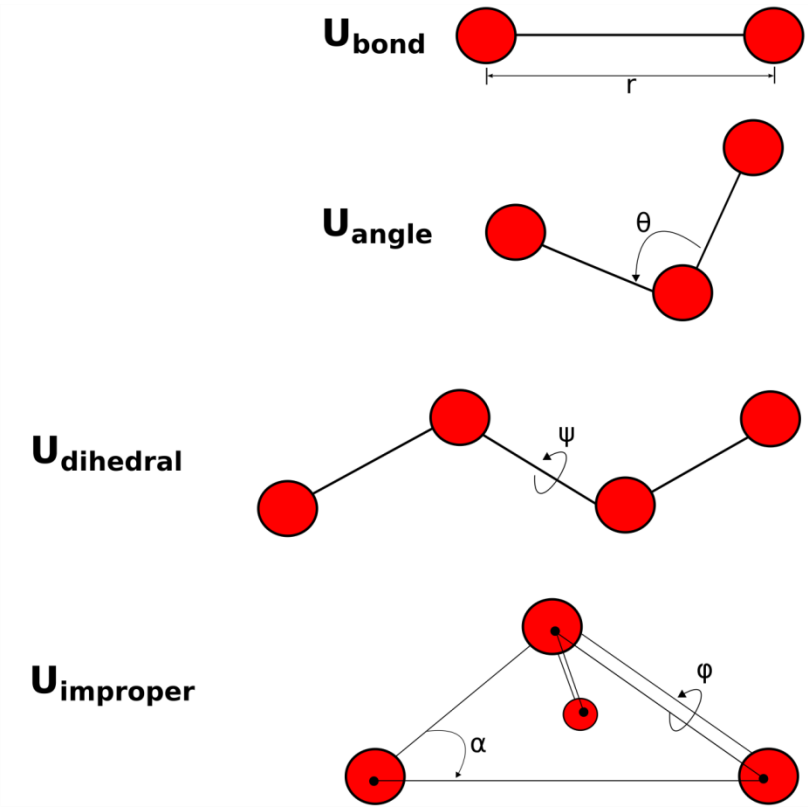

Figure 2.1 Internal coordinates for bonded interactions

r governs bond stretching; θ represents the bond angle term; ψ gives the dihedral angle; the small out-of-plane angle α is governed by the so-called "improper" dihedral angle φ

(Adopted from Phillips et al, JCC DOI 10.1002/jcc.20289)

The potential energy from bonds (U_{bond}) counts the sum of every covalent bond in the system and is introduced as a simple harmonic potential:

$$U_{bond} = k_{bond}(r_{ij} - r_0)^2 \quad (4)$$

Where i and j are the covalently bonded atoms, r_{ij} is the distance between these atoms, r_0 is the equilibrium distance and k_{bond} is the spring constant.

U_{angle} gives the potential energy sum of all angles between each pair of covalent bonds sharing a single atom at the vertex:

$$U_{angle} = k_\theta(\theta - \theta_0)^2 \quad (5)$$

Where θ_0 is the equilibrium value of bond angle, k_θ is the angle force constant.

The portion of potential energy that is responsible for intra-molecular – torsional dynamics ($U_{dihedral}$) is the sum of all atom pairs separated by exactly three covalent bonds with the central bond subject to the torsion angle φ. $U_{dihedral}$ also includes a term called "improper" dihedral that represents geometry of four planar, covalently bonded atoms.

$$U_{dihedral} = \begin{cases} k(1 + \cos(n\psi + \delta)), & n > 0 \\ k(\psi - \delta), & n = 0 \end{cases} \quad (6)$$

Where ψ is the dihedral angle, δ is the phase shift angle and k is the force constant.

Non-bonded interactions or long-range interactions (from equation 2) in turn can be divided into two parts: electrostatic ($U_{Coulomb}$) and van der Waals interactions (U_{vdW})

The potential energy portion coming from non-bonded electrostatic interactions is described as the sum of interactions of all charged atoms (q_i; q_j) that are at a distance r_{ij} from each other

$$U_{Coulomb} = \sum_i \sum_{j>i} \frac{q_i q_j}{4\pi\varepsilon_0 r_{ij}} \quad (7)$$

U_{vdW} represents the approximated Lennard-Jones 6-12 potential

$$U_{vdW} = \sum_i \sum_{j>i} 4\varepsilon_{ij} \left[\left(\frac{\sigma_{ij}}{r_{ij}}\right)^{12} - \left(\frac{\sigma_{ij}}{r_{ij}}\right)^{6} \right] \quad (8)$$

Where ε_{ij} is the depth of the potential well, σ_{ij} is the finite distance at which the inter-particle potential energy is zero and r_{ij} is the distance between the particles (i; j).

Based on the last two expressions, it becomes clear that long-range interactions ($U_{Coulomb}$+U_{vdW}) occur between every non-bonded pair of atoms in the system. Therefore, to compute the precise long-range interaction becomes non-trivial. To overcome this challenge NAMD has introduced user-specified cut-off for van der Waals interactions and a particle-mesh Ewald method for computing the long-range electrostatic interactions. van der Waals interactions display $1/R^6$ dependence on the distance and therefore are rapidly damped. In most simulations, no long-range correction is applied to the vdW part of the interaction potentials.

2.1.2.3 Periodic boundary condition (PBC)

In all MD simulations, among the other challenges one can encounter, are surface effects at the boundary of the simulated system. In other words, what are we to do when the molecule or its particles pass the borders of a simulation box? So-called periodic boundary conditions (PBC) were implemented to overcome the issue. This technique ensures that when a particle exits the central box on one side, its identical copy enters the box on the opposite side (figure 2.2). However, every particle in the central simulation box needs to be represented only once in the MD program, since all the others are the identical copies (images) of an original particle.

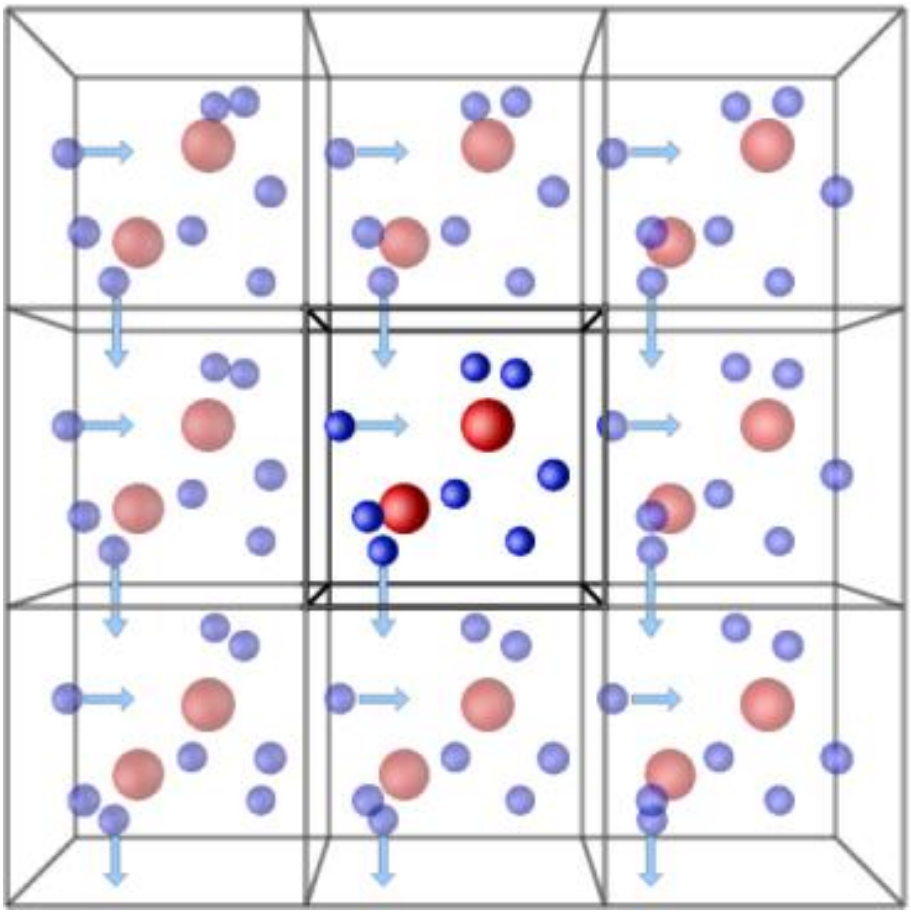

Figure 2.2 Schematic representation of the idea of periodic boundary conditions.

(Taken from http://isaacs.sourceforge.net/phys/pbc.html)

2.1.2.4 MD simulations for different ensembles

For different experiments (simulations) we need to have different set ups since the form of a partition function depends on the ensemble of interest.

In one case, we need to keep one variable constant (let us say temperature) and measure other properties of the system as a function of time, while in another case we want to keep the pressure constant. How to accomplish all these in MD simulations? Several ensembles are being used in MD simulations to satisfy specific needs.

To keep the temperature constant in MD simulations a method was implemented which couples the system of interest to a heating bath to maintain the desired temperature. The NPT or isothermal-isobaric ensemble is used for simulations with a constant number of atoms (N) constant pressure (P) and constant temperature (T). Usually, NPT ensemble is used to equilibrate the system. It is also more realistic, since in the real world most situations will occur at an almost constant pressure. NVT or canonical ensemble is used to perform MD simulations with a constant number of atoms (N), a constant volume (V) and a constant temperature (T). In this case, the simulation box size is fixed, so the volume does not vary.

2.2 Setting up molecular simulations

2.2.1 Protein of interest

The atomic structure of αHL was taken from the protein data bank (PDB entry: 7AHL). The coordinates of the following atoms were missing from the structure (residues dLys-30; gLys-70; aLys-70; dLys-240; fLys-282 and aArg-66). However, all of these atoms are accommodated on the peripheral region of αHL cap; therefore, we expect that their effect on this particular study is negligible. Since the crystal structure corresponds to the wild type αHL, we used the program scrwl4 to build the desired mutant proteins. It has been shown that scrwl4's algorithm effectively predicts and builds protein side-chains (Canutescu et al 2003). After we built the structure for the mutant protein, we repositioned it so that the center of the beta barrel region was aligned with the center of the lipid membrane at the origin in the z direction (z = 0). To reduce the computational cost and time we also truncated the intact αHL protein in a way that only the trans-membrane region has been kept for further studies. 1,2-dipalmitoyl-sn-glycero-3-phosphocholine (DPPC) phospholipid molecules were used to construct the lipid bilayer. This is one of the best-parameterized lipid molecules computationally. To solvate the system, TIP3P water molecules were placed in and around the bilayer and the protein. All the overlapping lipid and water molecules were carefully removed. K^+ and Cl^- ions were placed at random positions in the system in order to create a surrounding 1.0M salt concentration and to bring the system into neutral conditions (see figure 2.3).

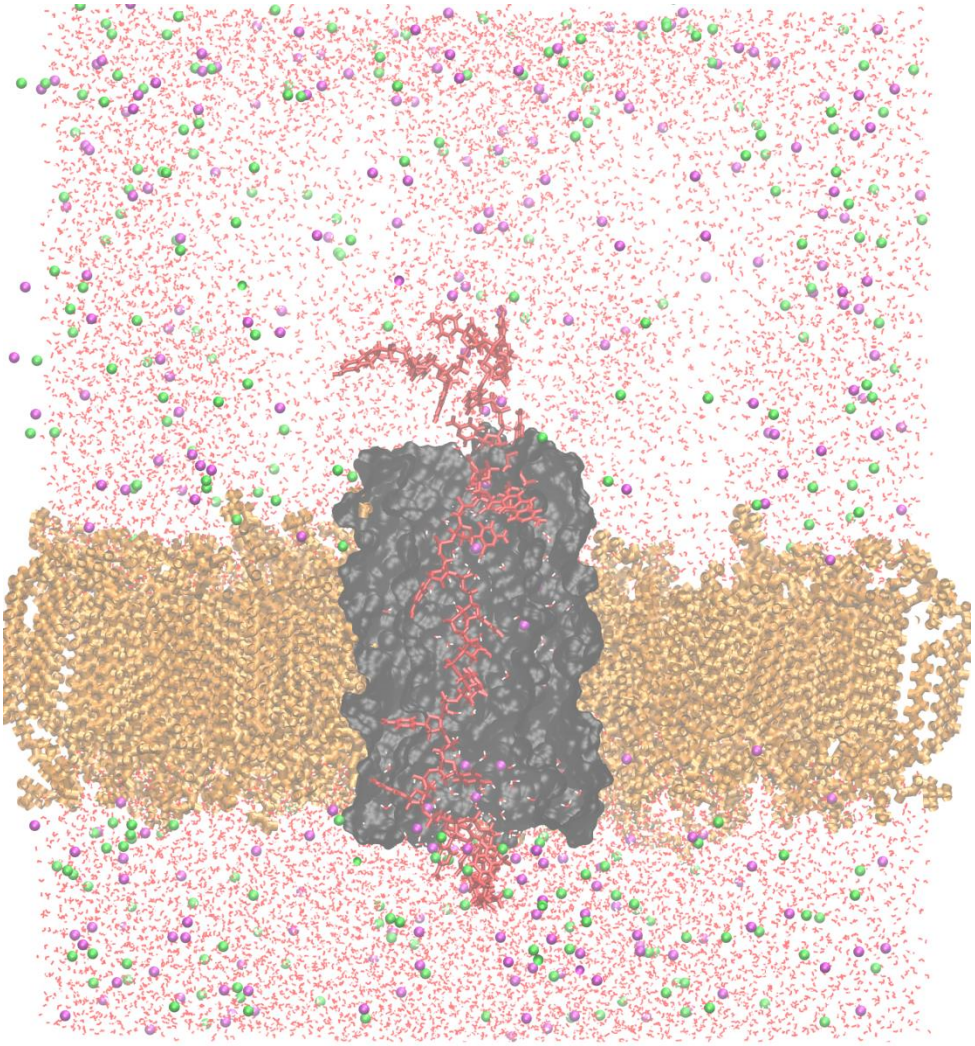

Figure 2.3 Schematic for all-atom Molecular Dynamics set up. The truncated αHL protein (black surf) is embedded in a DPPC lipid bilayer (orange sticks). TIP3P water (pink background) molecules have been used to solvate the protein, K^+ and Cl^- ions (green and magenta spheres) were added to have salt concentration of 1.0M. Single stranded DNA molecule (red chain) is threaded through the αHL pore.

2.2.2 Single stranded DNA molecule preparation and set up

Coordinates of single stranded (ss) DNA polymers were generated using 3D-DART (Lu and Olson 2003). In our study, we used two different homo-polymers: poly-adenine (as an example of a homo-purine) and poly-cytosine (as an example of a homo-pyrimidine) with a strand length equal to n bases (n can be anywhere from 25 to 40), each. Four different samples were prepared: poly(dA)n with 3' – 5' (a3p) and 5' – 3' (a5p); Poly(dC)n 3' – 5' (c3p) and 5' – 3' (c5p). The a3p and c3p samples (3' – 5') represent the orientation when the 3' end of ss-DNA is in the '-' region of the z-axis. a5p and c5p samples (5' – 3') represent exactly the reverse orientation where the 3' end appears in the '+' region of the z-axis (figure 2.4).When ss-DNA is oriented 3' – 5' (like in a3p and c3p) then nucleotides will be counted (1; 2; …; n-1; n) starting from the "–" z region. However, if ss-DNA is oriented 5' – 3' (like in a5p and c5p) then it is flipped and will be counted (n; n-1; …; 1) starting from the "+" z region (figure 2.4).

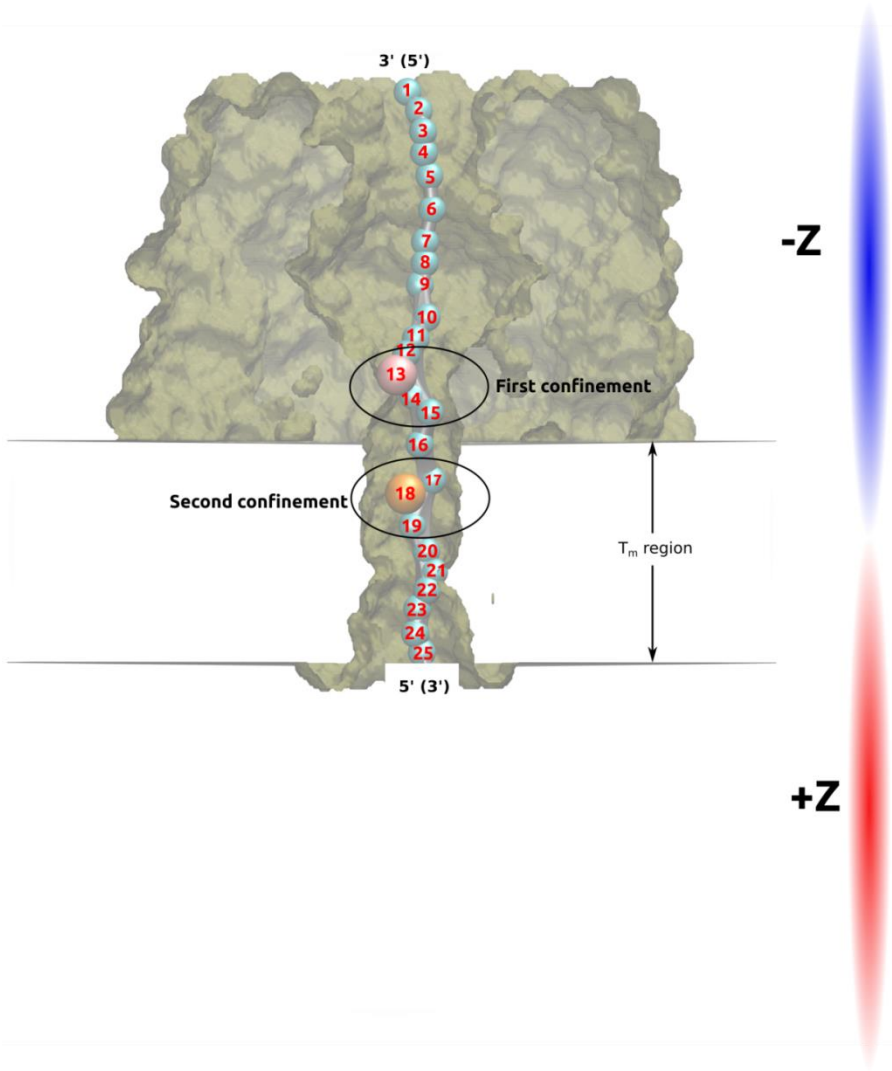

Figure 2.4 Schematic of a single stranded DNA molecule positioned inside the αHL pore. The ss-DNA molecule (a chain of numbered spheres) is either homo-poly-adenine (Poly(dA)n) or homo-poly-cytosine (Poly(dC)n) oriented in either 3' – 5' (3p) or 5' – 3' (5p) directions. In this case n = 25; however n can be a different value for different types of simulations throughout this project. The lipids are not shown in the transmembrane region (T_m region) for the sake of simplicity.

2.3 Data Analysis and Visualization

The post-processing and analysis of entire data sets obtained from all-atom MD simulations were carried out using tools from Charmm27 and in-house implemented python algorithms and scripts. To visualize the analyzed raw data, we used the OriginLab8 and Inkscape packages.

2.3.1 Interaction maps

The "INTE" module in Charmm27 was used to analyse the energy values of interactions between protein and DNA. Two kinds of non-bonded terms were considered: distance-dependent (screened) electrostatics and van der Waals: the smoothing function that begins to reduce a pair's energetic contribution was set to 12 (Å). A 16 (Å) distance cut-off was applied to generate the list of pairs. The distance cut-off at which energy contributions from a pair are eliminated was set to 14 (Å). The warning cut-off for the minimum distance between two atoms was set to 1.5 (Å) and the dielectric constant was set to 1.

The program gave the complete list of all interacting pairs based on the above criteria.

The file includes electrostatic, van der Waals and total energy values. The Python scripts and OriginLab8 were then used to visualize the raw data obtained.

2.3.2 End-to-end distance analysis

2.3.2.1 From MD simulations

The "DIST" module in Charmm27 was used to calculate the distance between the 5' end of nucleotide 1 and the 3' end of nucleotide n. The obtained data was plugged into OriginLab8 datasheets, the plots were constructed, then the plots were normalized and the probability distributions were obtained using analysis and statistics tools from OriginLab8

2.3.2.2 From BROMOC simulations

The distance between the first and last beads of nucleotide bases was measured using the VMD graphics plug-in. The obtained plots were then inputted into OriginLab8 to calculate the probability distributions and normalize the plots.

2.3 BROMOC

Our research group has developed a new computational tool to perform long-term Brownian Dynamics simulations on ss-DNA and protein interactions. I have contributed to it. In particular, I have tested the protocol on the system of interest, collected the results, and compared it with available experimental data to obtain realistic validation for our program. The next chapter of my thesis is a research article published in the *Journal of Chemical Theory and Computation* and it introduces our new computer program called BROMOC.

CHAPTER 3- BROMOC: Brownian dynamics/Monte-Carlo program suite to study ion and DNA permeation in nanopores

3.1 Author Contributions

Chapter 3 – "BROMOC: Brownian Dynamics/Monte-Carlo Program Suite to Study Ion and DNA Permeation in Nanopores" that was published in the Journal of Chemical Theory and Computation, **2012**, 8 (7), pp 2540–2551, **DOI**: 10.1021/ct3004244

Authors: Pablo M. De Biase[†]; Carlos J. F. Solano[†]; **Suren Markosyan**[†]; Luke Czapla and Sergei Yu. Noskov

[†] – Denotes equal contribution

Pablo M. De Biase: Worked on overall program development, contributed primarily to sections 1, 2, 4 and 5 in the paper.

Carlos J. F. Solano: Initiated the idea of developing a computational tool for long-term polymer-protein interaction studies, and contributed primarily to sections 1, 2, 4 and 5.

Suren Markosyan: Performed all test simulations, collected the entire set of data, analysed and compared them with existing experimental data and contributed primarily to sections 1, 3, 4 and 5

Luke Czapla: Ran initial MD simulations and developed analysis tools.

Sergei Yu. Noskov: Supervised the entire process of developing and reporting the research work.

3.2 Abstract

In this section a theoretical framework is presented to model ion and DNA translocation across a nanopore confinement under an applied electric field. A combined Grand Canonical Monte Carlo Brownian Dynamics (GCMC/BD) algorithm offers a general approach to study ion permeation through wide molecular pores with a direct account of ion−ion and ion−DNA correlations. This work extends previously developed theory by incorporating the recently developed coarse-grain polymer model of DNA by de Pablo and colleagues (Knotts et al 2007) with explicit ions for simulations of polymer dynamics. Atomistic MD simulations were used to guide the model development. The power of the developed scheme is illustrated using studies of single-stranded DNA (ss-DNA) oligomer translocation in two model cases: a cylindrical nanopore with a varying radius and a well-studied experimental system, the staphylococcal αHL (αHL) channel. The model shows good agreement with experimental data for model studies of two homo-polymers: ss-poly(dA)n and ss-poly(dC)n. The developed protocol allows for direct evaluation of different factors (charge distribution and nanopore shape and size) controlling DNA translocation in a variety of nanopores.

3.3 Introduction

Voltage-driven transport of biopolymers across cell membranes via wide pores is of central importance to normal cell function (Rostovtseva et al 2002) and bacterial pathogenicity (Finkelstein et al 2009; Basilio et al 2009). The ubiquity of these transport systems is most strikingly illustrated by their applications to a wide variety of problems spanning from analyte detection (Braha et al 2000; Bayley et al 2000; Gu et al 1999) to preparation of high-purity samples (Wanunu et al 2010) to the use of these proteins for rapid DNA sequencing (Branton et al 2008). The idea to use bacterial toxins for polymer counting and later as DNA sequencing devices was first formulated in the mid-1990s and then implemented with the α-hemolysin (αHL) channel by Kasianowic and colleagues (Kasianowicz et al 1996). In the following years a constantly growing number of papers addressing various aspects of DNA and ion dynamics in biological nanopores were published (Branton et al 2008; Deamer and Akeson 2000; Maglia et al 2010; Stoddart et al 2009). In the typical experimental setup, a nanopore forming protein is reconstituted into a lipid bilayer membrane that separates two chambers with symmetric or asymmetric ionic solutions. When a voltage is applied, the electric field drives ions through the nanopore and the ion current can be measured. Subsequently, DNA molecules are added to the solution bathing one side of the membrane. Since DNA molecules are charged, they will be driven by the electric potential through the nanopore where their blocking effect on the open-channel current is evaluated. While threading, the DNA molecule blocks the current of ions, and blockade events can be detected as a transient decrease in the ionic current that can be mapped to the sequence of nucleotides threaded through the pore. Thus, by monitoring the ion current, one can indirectly measure properties of the translocation process.

Although these advances in experimental studies suggest that such a system could be developed into an ultrafast method for DNA sequencing, it is necessary first to elucidate the physical mechanism underlying polymer translocation through these biological pores. An obvious problem is that single-stranded DNA (ss-DNA) is a large and floppy polymer that seems to be still fully or partially hydrated, and maintains a sufficient ionic atmosphere while in the nanopore and thus sensing has to rely on relatively weak forces between the wall of a nanopore and transported polymer, modification of DNA conformational dynamics by the nanopore confinement, and differences in nucleotide−ion interactions (Timp et al 2010; Aksimentiev 2010). Furthermore, DNA escape dynamics may not necessarily fit into exponential kinetics; it shows a nontrivial dependence on the voltage and temperature (Wiggin et al 2008). Because of the complexity of the translocation kinetics, very noisy recordings pose a natural challenge to obtaining a sufficient contrast in the signal between different nucleotides to the level required for accurate sequencing (Tabard-Cossa et al 2007; Wiggin et al 2007). There is a growing consensus that specific DNA−protein interactions could and should be exploited for amplification of the signal. However, targeted modification of a biological nanopore requires detailed information about the dynamics of a floppy ss-DNA molecule in confinement and its effect on ion currents (Stoddart et al 2010; Stoddart, Heron et al 2010).

Arguably, the best approach to this problem is to use modern atomistic simulations which explicitly account for ions, DNA, and protein dynamics (Aksimentiev 2010). While it is feasible to simulate a full assembly for hundreds of nanoseconds, direct evaluation of ion currents may represent a significant challenge that requires simulations using grand canonical ensembles with absorbing boundaries or dual-volume systems to manage accumulation of ions on one side of the membrane. The size of the system makes it prohibitive for brute-force microsecond simulations

that may be necessary to study the relevant conformational dynamics of flexible DNA chains, making every potential application of atomistic simulations to nanopores a tour-de-force exercise in computational power.

To reduce the dimensionality of the problem, several theoretical approaches have been used to study charged polymer translocation across membranes (Lubensky and Nelson 1999; Rabin and Tanaka 2005; Muthukumar 2007). Some of them focus on the DNA translocation dynamics alone and use implicit treatment for ion−ion and ion−DNA interactions, often representing the nanopore by cylindrical or conical confinement with uniform charge distribution. While this is an attractive route for studies of solid-state nanopores, it is limited in a realistic description of protein nanopores. One recent attempt to create an alternative approach was based on the application of Langevin dynamics to DNA translocation in the nanopore represented by a non-uniform 1D potential (Li and Talaga 2010). Another option may be to use a reduced representation of the modeled protein and solvent by solving the Poisson−Boltzmann equation for the electric field created by the nanopore and surrounding media, while still modeling DNA and ion translocation dynamics explicitly. For wide pores, such as nanopores, approaches based on Grand-Canonical Monte Carlo combined with Brownian Dynamics (GCMC/BD) have offered an excellent platform for studies of open-pore currents in αHL (Noskov et al 2004; Egwolf et al 2010; Luo et al 2010). Even with DNA blocking ionic currents, αHL retains relatively high levels of conductance, indicating a continuous water-filled pathway that has also been confirmed computationally using extensive MD simulations (Mathe et al 2005). Accordingly, in this paper, we present a theoretical strategy based on GCMC/BD that includes development of the parameters for ion−DNA interactions compatible with the established coarse-grained model for DNA published by de Pablo and colleagues (Knotts et al

2007) and its application to polymer dynamics and ion current simulations in cylindrical and arbitrarily shaped pores with non-uniform charge distribution (αHL).

3.4 Methods and computational models

In this section, we introduce basic approximations, simulation algorithms, and details of the force-field implementation and analysis for studies of DNA translocation with the previously developed GCMC/BD method (Im et al 2000). The Fortran-90 code for GCMC/BD simulations of DNA in nanopores is based on an earlier version of the GCMC/BD program (Noskov et al 2004; Im et al 2000; Im and Roux 2002). All of the developed programs (BROMOC and analysis suite) and documentation are freely available to the academic community upon request.

3.4.1 GCMC/BD algorithm

Brownian Dynamics (BD) represents an attractive computational approach for simulating the permeation process through wide channels over long time scales at the cost of treating solvent and membrane degrees of freedom implicitly, while describing ion dynamics explicitly. The approach consists of generating the trajectory of the ions as a function of time by numerically integrating the stochastic equation of motions using effective potential functions to calculate the microscopic forces acting on mobile particles in the system. From a microscopic point of view, this effective potential is a many-body potential of mean force (PMF or $W(r_1,r_2,...)$), which rigorously introduces a reversible thermodynamic work function (free energy) to assemble a particular configuration of the particles in the system while averaging over the remaining degrees of freedom as an effective mean field. In the case of wide aqueous pores, a continuum electrostatic description in which the solvent is represented as a featureless dielectric medium is often a useful and adequate approximation. Thus, the equation of motion governing

the dynamics of the system is a specific form of the general Langevin equation (Ermak and McCammon 1978):

$$r = -\frac{D_i(r_i)}{k_B T}\nabla_i W(r_1, r_2, \cdots) + \nabla_i D_i + \xi_i(\tau) \quad (9)$$

where $W(r_1,r_2,...)$ is a many-body PMF that describes interactions between ions, DNA sites and ion−DNA, the effect of applied membrane voltage, and the reaction field and static field emerging from a protein charges. D_i is a position-dependent diffusion coefficient which was kept to corresponding bulk diffusion values for both ions and nucleotides in the current study, and $\xi_i(\tau)$ is a term introducing a Gaussian random noise to the system dynamics. In the GCMC/BD scheme BD moves are coupled with the Grand Canonical Monte Carlo (GCMC) run, allowing the simulation of a fluctuating number of particles. In brief it consists of constructing a random walk (discrete time Markov chain) of the configuration of the system during which particle creation and destruction can occur, allowing for a constant chemical potential of the simulated system (Im et al 2000). The GCMC algorithm can be used to simulate equilibrium as well as non-equilibrium conditions of ion diffusion and permeation under an applied electric field. The GCMC/BD algorithm has been incorporated into the new code where the BD trajectory of ions is generated.

3.4.2 Mesoscale DNA model

A mesoscale model development for DNA has been described in the literature (Knotts et al 2007; Sambriski et al 2009). This DNA coarse-grain model reduces the complexity of a nucleotide to only three interaction sites, one each for the phosphate, sugar, and base. There are four different base sites, one for each type of base in DNA. The backbone phosphate and sugar sites are placed at the center of mass of the respective moiety. For purine bases (adenine and

guanine), the site is placed at the N1 position. For pyrimidine bases (cytosine and thymine), the site is placed at the N3 position. The coordinates for each of the sites just described were determined from the standard coordinates for the "B" isoform. The parameters for this DNA force field can be divided into bonded and non-bonded interactions, including an optional implicit representation of ions through Debye−Hückel Coulombic screening of the interactions between phosphates. The bonded interactions can be divided further into: (i) c*ovalent bonding interactions* (two-body contribution; U_{bond}), (ii) *bond angle interactions* (three-body contribution; U_{angle}), and (iii) *dihedral angle interactions* (four-body contribution; $U_{dihedral}$). The equilibrium distances and angles in these terms are set equal to the values obtained from the atomic coordinates of the standard model of the B form of double-stranded DNA (ds-DNA). The (pairwise) non-bonded interactions can be divided into (a) *intra-strand base-stacking interactions* (U_{stack}), (b) *hydrogen bonding interactions* (U_{bp}), (c) *excluded volume interactions* (U_{ex}), (d) C*oulomb interactions* (U_{ij}), and (e) *solvent-induced contributions* ($U_{solvent}$). The potential energy of the polymer (U_{DNA}) in this case is expressed as

$$U_{DNA} = U_{bond} + U_{angle} + U_{dihedral} + U_{stack} + U_{bp} + U_{ex} + U_{ij} + U_{solvent} \quad (10)$$

The base-stacking contribution (U_{stack}) accounts for the strong hydrophobic attraction between adjacent nucleotides and provides additional bending rigidity to the DNA molecule. Hydrogen bonding (U_{bp}), along with base-stacking interactions, provides structural stability in DNA duplexes while it may not be overly important for simulations of the fully stretched ss-DNA molecules. Nevertheless, the model allows for multiple inter- and intra-strand interactions, thus extending the range of applicability to both ds-DNA and ss-DNA (Buyukdagli et al 2006; Drukker and Schatz 2000; Drukker et al 2001; Mergell et al 2003; Sales-Pardo et al 2005). The next term (U_{ex}) accounting for excluded volume interactions are purely repulsive. Finally, the

solvent-induced contribution ($U_{solvent}$) is a novel ad hoc contribution introduced in the force field intended to represent (implicitly) many-body effects associated with the arrangement of water during the reversible denaturation of DNA. The interested reader is advised to refer to the original work of de Pablo and colleagues (Knotts et al 2007; Sambriski et al 2009). The DNA mesoscale model has been combined with the GCMC/BD algorithm described. The set of parameters for the coarse-grain model of the DNA force field is exactly the same as in Sambriski et al (2009). Bond constants, the bending constant, and the torsional constant were originally parameterized as a function of a ε parameter which we called the force field parameter. The "force field" parameter is used to control the depth of the well for potential in intra-strand base-stacking interactions, excluded volume interactions, and strength energy for the hydrogen bonding potential and can be modified. Forces for bonded interactions are derived by chain rule differentiation of the potential for bonds and angles and by using first principles of mechanics for dihedral forces. These dihedral force expressions require significantly fewer numerical operations and are equivalent to those more commonly used and obtained by mathematical differentiation (Bekker et al 1995).

3.4.3 Modeling of ss-DNA dynamics in the αHL channel

The structure for αHL was taken from Protein Data Bank (Protein Data Bank entry: 7ahl). In all GCMC/BD simulations, the protein was treated as a rigid structure with a dielectric constant of 2 surrounded by a high dielectric solvent (ε_m = 80) and embedded in a 32-Å-thick membrane (ε_m = 2). The choice of dielectric constant for the aqueous region was motivated by the large size of the pore, which can be safely assumed to be well-represented by a bulk continuum value and has been shown to provide an accurate approximation in the case of wide protein pores. The channel was positioned along the z-axis with the center of the membrane at z

= 34.1 Å. The salt concentrations of interest were maintained by two 3.5 Å buffers positioned from −90.75 to −87.75 Å and from 87.75 to 90.75 Å along the z-axis. A snapshot of the simulation system is shown in Figure 3.1. We have considered two different homo-polymeric strands (ss-poly(dA)x and ss-poly(dC)x, where x is the number of nucleotides) simulated at different voltages and electrolyte concentrations. A uniform diffusion coefficient of 0.001 $Å^2$/ps was assigned to all nucleotides. The explicit inclusion of the position-dependent diffusion may be important for obtaining 1:1 correspondence to the experimental data (Lee et al 2012; Simakov and Kurnikova 2010). It should be noted, however, that passive diffusion of the strand is a secondary factor in translocation under an applied force (see below) and in Meller et al (2001) and (Luan and Aksimentiev (2008)).

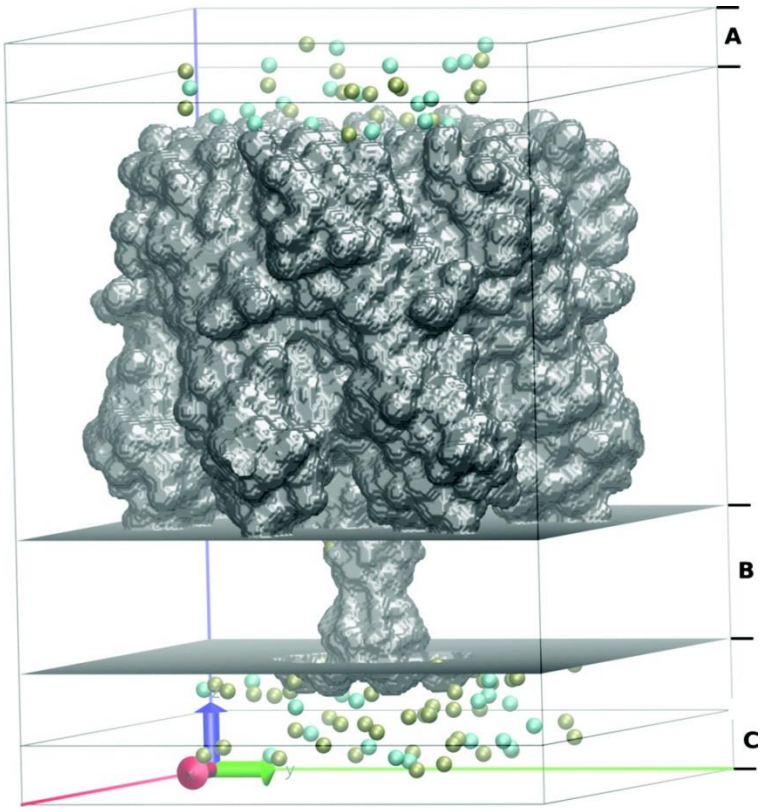

Figure 3.1 Molecular graphics view of the orthorhombic simulation box in GCMC/BD. The αHL nanopore (grey surf) is bathed in a 0.3 M KCl solution. K^+ (tan) and Cl^- (cyan) ions are located in the nanopore and in the buffer regions (A and C regions). Transmembrane zone is shown as region B.

A model for coarse-grained DNA has been previously developed for an implicit solvent model based on a canonical Debye−Hückel approximation (Knotts et al 2007). However, the main goal of recent development is to enable studies of DNA and ion dynamics. Therefore, we introduce potential terms that describe interactions of DNA sites and mobile ions modeled explicitly. The many-body Potential of Mean Force (PMF) that has been used to control the system dynamics is expressed as

$$W(r_1, r_2, \cdots) = U_{DNA} + \sum_{ij} U_{ij}(r_{ij}) + \sum_i U_{core}(r_i) + W_{sf}(r_1, r_2, \cdots) + W_{rf}(r_1, r_2, \cdots) \qquad (11)$$

where $W(r_1,r_2,...)$ is a many-body PMF that describes interactions between mobile particles and depends on all particle coordinates. U_{DNA} is the internal DNA potential described in eq. 10. U_{ij} is a pairwise particle interaction potential for DNA site−ion and ion−ion separated by distance r_{ij}. U_{core} is a repulsive core potential that prevents overlap between mobile particles and a protein or bilayer continuum, and it is a function of r_i, the Cartesian coordinate of particle i (ion or DNA site). W_{sf} is a static field potential for all charged particles that combines the effect of the protein static charges and the applied external electric potential. W_{rf} is a reaction field arising from the electrostatic polarization of the various dielectric boundaries and the implicit salt in the outer region.

More specifically, the direct pairwise particle interaction potential (U_{ij}) is described below:

$$U_{ij}(r_{ij}) = 4\varepsilon_{ij}\left[\left(\frac{\sigma_{ij}}{r_{ij}}\right)^{12} - \left(\frac{\sigma_{ij}}{r_{ij}}\right)^{6}\right] + \frac{q_i q_j}{4\pi\epsilon\, \varepsilon_{bulk}\, r_{ij}} + W_{sr}(r_{ij}) \qquad (12)$$

where ε_{ij} and σ_{ij} are the parameters of the Lennard-Jones 6−12 potential, q is the charge of the mobile particle i and j, ε is the vacuum permittivity, ε_{bulk} is the dielectric constant of the media (80 for water), and W_{sr} is the short-range potential.

Equation 4 is composed of (a) a primitive model potential term that has been extensively used in statistical mechanical studies of ionic solutions and (b) water-mediated short-range ion−ion and ion−DNA interactions with a form of damped oscillations to take into account the water-mediated interactions. The term (a) is composed of Lennard-Jones (LJ) and Coulombic interaction potential terms. The LJ parameters were adjusted to reproduce pairwise Radial Distribution Functions (RDF) computed from atomistic simulations (Figure 3.2).

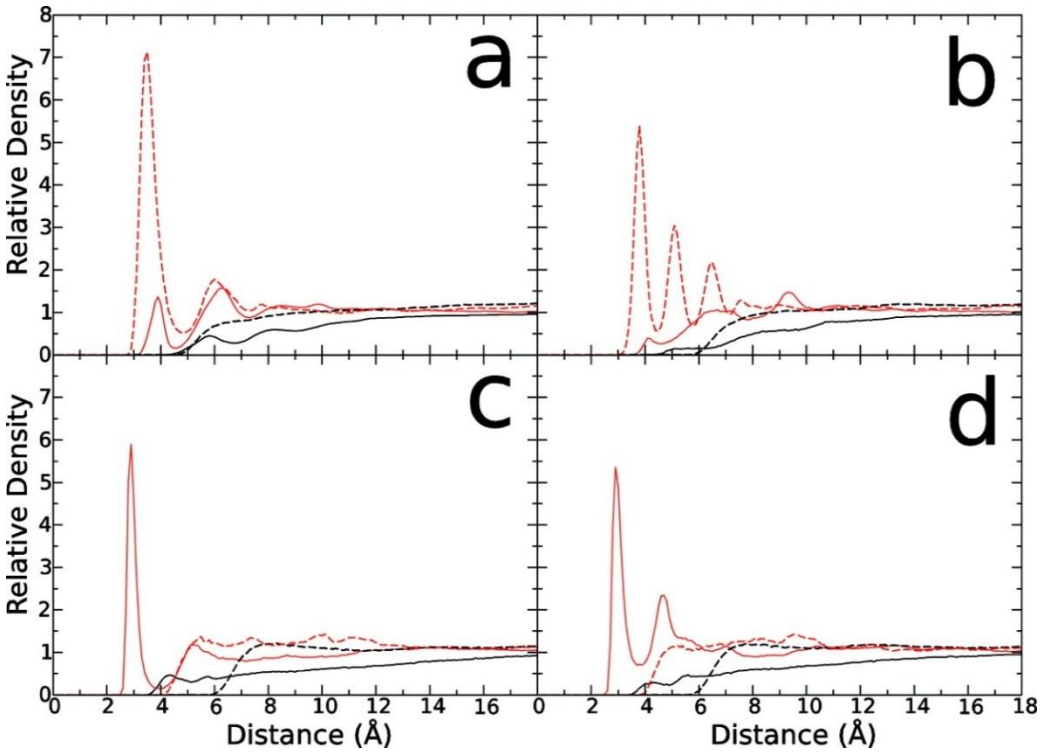

Figure 3.2 Comparison of radial distribution functions (RDF) of DNA sites–ions from two methods: All-atom Molecular Dynamics simulations (solid line) vs BROMOC simulations (dotted line). Cl^- anion is in black; K^+ cation is in red, (a) Phosphate, (b) sugar, (c) adenine, (d) cytosine.

The short-range (SR) water-mediated potential (W_{sr}) has the following functional form introduced by Im and Roux for ion-ion short-range (SR) potential (Im and Roux 2002):

$$W_{sr} = c_0 e^{\frac{c_1 - r}{c_2}} \cos[c_3(c_1 - r)\pi] + c_4 \left(\frac{c_1}{r}\right)^6 \quad (13)$$

All of the coefficients were empirically adjusted until reasonable agreement was achieved between ion−nucleotide RDFs obtained from explicit all-atom MD simulations (Figure 3.2) of ss-DNA and from GCMC simulations. The developed parameters for LJ and SR potentials are collected in Table 3.1.

Table 3.1 Parameters for non-electrostatic part of the effective ion–ion/DNA site interaction potential

Site /Ion	Ion	σ (Å)	ε (kcal/mol)	c_0	c_1	c_2	c_3	c_4
K^+	K^+	3.14	0.087	-0.600	4.40	0.90	0.80	0.25
Cl^-	K^+	3.59	0.114	-3.700	2.90	0.90	0.80	0.00
Cl^-	Cl^-	4.04	0.150	-0.500	4.90	0.90	0.80	0.25
P	K^+	3.25	0.125	-1.150	3.50	1.50	0.75	0.00
S	K^+	3.65	0.075	-0.750	3.75	2.90	1.50	0.10
A	K^+	4.65	0.200	-0.050	4.95	1.50	0.70	0.05
C	K^+	4.42	0.200	-0.025	4.65	1.50	0.70	0.05
P	Cl^-	5.45	0.100	-0.025	5.75	0.75	0.75	0.05
S	Cl^-	6.85	0.100	-0.025	6.35	3.00	0.50	0.05
A	Cl^-	6.69	0.200	-	-	-	-	-
C	Cl^-	6.49	0.200	-	-	-	-	-

P denotes phosphate bead,

S denotes sugar bead,

A denotes **A**denine bead,

C denotes **C**ytosine bead

The static-field electrostatic potential (W_{sf}) was evaluated by solving the Poisson−Boltzmann equation with a focusing method on a coarse grid (a grid spacing of 1.5 Å) followed by a second calculation on a finer grid (201 Å × 201 Å × 281 Å points with a grid spacing of 0.5 Å). The trans-membrane potential contribution was calculated with a modified version of the PB equation (Roux 2008). W_{rf} was calculated on grid with a grid spacing of 0.5 Å (Egwolf et al 2010; Im and Roux 2001). The GCMC/BD simulation trajectories were generated with a time step of 20 fs. Each production run was preceded by an equilibration run of 1 000 000 MC steps combined with 100 GCMC iterations to obtain well-equilibrated placement of the counter ions. In the translocation studies, each DNA polymer was placed such that its center of mass coincided with the geometric center of the nanopore. The main goal was to study the effect of the DNA on the ion dynamics in the pore. However, the DNA capturing rate (although important) is not the focus nor even achievable in the current study. All of the GCMC/BD simulations ranged from 1 to 5 μs.

3.4.4 All-atom MD simulations

To obtain equilibrium ion-density distributions in the pore, self-diffusion coefficients for nucleotides, position-dependent dielectric constants, as well as initial guesses on LJ parameters between ions and DNA sites, a series of MD simulations were performed. Equilibrium all-atom MD simulations for αHL/membrane systems were run for 25 ns with the NPT ensemble using the NAMD 2.7b1 program (Phillips et al 2005) package using a previously developed protocol from Comer et al (2011). The total number of atoms for MD simulations is ~270 000. Briefly, the all-atom system contains αHL toxin embedded into a POPC (1-palmitoyl-2-oleoyl-sn-glycero-3- phosphocholine) bilayer patch, ss-poly$(dA)_{40}$ or ss-poly$(dC)_{40}$ solvated by 1000 mM of KCl aqueous solution with 3′ entry to the pore. Average self-diffusion coefficients for

nucleotides were computed for free ss-poly(d(A/C))$_{40}$ in 1000 mM KCl from the mean-square displacement of the nucleotides' center of mass. The average self-diffusion coefficient was found to be ~0.001 Å^2/ps and is in accord with previous studies (Luan et al 2011). This value of the transport coefficient was used for BD simulations. The MD setup corresponds to one previously used by the Aksimentiev group and is known to faithfully reproduce experimental data on current blockades (Comer et al 2011).

The position-dependent dielectric constants were evaluated using average fluctuations in a dipole moment of the volume slice (5 Å) along the z-axis of the system using the following equation:

$$\varepsilon = \varepsilon_{\infty} + \frac{4\pi}{3\langle V\rangle k_B T}(\langle \mathrm{M}^2\rangle - \langle \mathrm{M}\rangle^2) \quad (14)$$

Where ⟨V⟩ is the average volume occupied by solvent molecules in the slice estimated by a grid-search algorithm. A similar approach was used in several MD studies of membrane proteins (Bockmann et al 2008). A high-frequency correction ε_{∞} has been set to a constant value of 2.0. The position-dependent profiles of the dielectric constants from equilibrium MD simulations (no applied voltage) suggest that the effective dielectric constant for water captured in the stem region (almost entire trans-membrane region of αHL channel; Figure 3.1, region B) in the presence of DNA is ~40.

3.4.5 Determination of the DNA−ion and ion−ion parameters.

As stated above, LJ-parameters describing interactions between nucleotide sites (base, sugar, phosphate) and ions (K^+, Cl^-) as well as ion−ion interactions were obtained from a series of separate simulations of ss-poly(dX)$_{14}$ in 1.0 M KCl (X = A, C, G, and T). Using charmm-gui.org, single-stranded B-DNA was built and solvated in a truncated octahedral box with 21177 TIP3 waters, 141 Cl^- anions, and 154 K^+ cations. All simulations were performed using NAMD 2.8

with the standard CHARMM27 force field, an integration time step of 2 fs, a cutoff of 12 Å, periodic boundary conditions, and particle-mesh Ewald (PME). The initial system was minimized performing 5000 steps followed by 300,000 steps of equilibration in the NpT ensemble at 1 atm and 300 K using a Langevin Piston and Lowe-Andersen thermostat. The DNA backbone was restrained using the minimized structure during the rest of the simulations to prevent self-interactions and to maximize DNA−ion interactions. After a short equilibration of 0.5 ns, a production run of 25.6 ns simulations in the NVT ensemble was performed for ss-poly$(dA)_{14}$, ss-poly$(dC)_{14}$, ss-poly$(dG)_{14}$, and ss-poly$(dT)_{14}$ using the last configuration from equilibration.

For RDF computation, atomistic DNA coordinates were converted to coarse grained DNA site coordinates according to de Pablo et al's coarse-grain model definition (Knotts et al 2007). The resulting ion-site RDF functions were used for fitting of the ion−DNA short-range parameters using the protocol described by Im and Roux (2002).

3.4.6 Translocation rates

DNA displacements (d) along the channel axis (z-axis) were computed as the dot product of the Geometric Center of Phosphates (GCP) coordinates and a vector along the z-axis (eq. 15).

$$d = [r(t) - r(0)] \cdot (0,0,1) \quad (15)$$

Translocation rates were computed at time t_r, that is, when the root-mean-square displacement of GCP (σ, eq. 16) for n independent simulations becomes equal to L. The L is an arbitrary length value and it is set to be L = 12 angstroms.

$$\bar{\sigma}_{GCP}(t) = \sqrt{\frac{\sum_i^n d_i^2(t)}{n-1}} \quad (16)$$

The root-mean-square displacement of GCP can be expressed as a function of the average GCP displacement (eq. 17) plus a diffusive displacement component f (eq. 18).

$$\bar{d}_{GCP}(t) = \frac{\sum_i^n d_i(t)}{n} \quad (17)$$

$$\bar{\sigma}^2_{GCP}(t) = \bar{d}^2_{GCP}(t) + \bar{f}^2(t) \quad (18)$$

The average GCP displacement is the voltage-driven displacement. For no external potential bias, the voltage-driven displacement tends to zero and the root-mean-square displacement leads to the diffusive displacement. Voltage-driven translocation rates (k_t) were computed using eq. 19, and translocation rates that include diffusive displacement (k_d) were computed using eq. 20.

$$k_t = \frac{\bar{d}_{GCP}(t_r)}{t_r} \quad (19)$$

$$k_d = \frac{\bar{\sigma}_{GCP}(t_r)}{t_r} \quad (20)$$

3.4.7 Root-Mean Square Displacements

To assess conformational dynamics of the confined polymer, 3 different Root-Mean Square Displacements (RMSD) were computed for beads representing every nucleotide (phosphate sites) from ss-DNA translocation through the nanopore simulations:

The absolute bead RMSD to characterize monomer dynamics:

$$RMSDa = \frac{1}{MN}\sqrt{\langle |r_i(t) - r_i(0)|^2 \rangle} \quad (21)$$

The bead RMSD relative to geometric center (GC) to assess chain extension:

$$RMSDr = \frac{1}{MN}\sqrt{\langle |r_i(t) - r_i(0) - r_{GC}(t) + r_{GC}(0)|^2 \rangle} \quad (22)$$

The RMSD of the chain geometric center (GC) to evaluate total displacement of an entire chain:

$$RMSDc = \frac{1}{M}\sqrt{\langle |r_{GC}(t) - r_{GC}(0)|^2 \rangle} \quad (23)$$

Where r is the position vector of the bead i or geometric center (GC), M is the number of chains (for ss-DNA M is equal to 1), and N is the number of beads per chain. RMSDs were computed without previous alignment. zRMSD denotes RMSDs computed using only the z coordinate.

3.5 Results

Here, we present some computational illustrations of the developed framework for simulating DNA dynamics in nanopores. All GCMC/BD simulations were run on a single core Xeon 2.4 GHz processor. The average run time for 1 μs of a GCMC/BD simulation for ss-poly(d(A/C))$_{25}$ blocking αHL ranges from 1 day in 300 mM KCl to 12 days in 1.0 M KCl. MD simulations, on the other hand, took up to 3 months to run using 128/256 cores on a supercomputer cluster to reach up to 100 ns of sampling.

3.5.1 Melting simulations of the ds-DNA: Debye- Hückel approximation vs explicit ions

A gold standard for evaluations of DNA force-field simulations with implicit and explicit ions is its ability to reproduce melting thermodynamics for ds-DNA (separation of strands). For melting simulations, we consider an aqueous 0.069 M monovalent salt (KCl) solution at a temperature of 317 K (experimental melting temperature (T_m) for the studied strand is 317.4 K (Sambriski et al 2009)). The ds-DNA sequence used for the simulations was 5′-AGTAGTAATCACACC-3′. Each base pair in the DNA coarse grain force field, characterized by the separation r_{ij} between intra- or inter-strand sites i and j, is described by characteristic energies $\varepsilon_{ij} \in [\varepsilon_{AT}, \varepsilon_{CG}]$ and characteristic lengths $\sigma_{ij} \in [\sigma_{AT}, \sigma_{CG}]$, where $\varepsilon_{ij} = \varepsilon_{ji}$; $\sigma_{ij} = \sigma_{ji}$; and A, T, C, and G correspond to adenine, guanine, cytosine, and thymine bases, respectively. A complementary base pair is considered to be hydrogen-bonded when the separation between bases is $r_{ij} < \sigma_{ij} + 2.0$ Å. The ratio between the unpaired bases and the total base pairs (f) is used to evaluate the melting process. The time step for melting simulations was set to 10 fs. This value is lower than the maximum time step allowing stable integration of the system's dynamics (previous studies used time steps up to 30 fs) (Knotts et al 2007; Sambriski et al 2009).

Using BROMOC, (f) values are computed each N simulation steps. From these consecutive measurements of the fluctuating quantity f, one can obtain the time average fraction of denatured bases (⟨f⟩) in a simulation. In our simulations, we've used the blocking method (Flyvbjerg and Petersen 1989) enabling evaluation of the statistical convergence for trajectories. Following de Pablo's protocol, we have included the solvent-induced contribution inside the DNA coarse-grain force field as well as an effective dielectric constant, which takes into account dependence on the temperature and KCl concentration. The Debye−Hückel implicit ion concentration was at to 0.069 M. Accounting for these terms only slightly reduces (⟨f⟩) value compared to similar simulations using the original force field described by Knotts et al (2007). Selecting an optimal value for the diffusivity of coarse-grained DNA sites is not a trivial issue. The self-diffusion coefficient for adenine was estimated from equilibrium MD simulations to be 6.8×10^{-4} Å^2/ps for periodic systems. Experimental data estimates transport coefficients between 1.3 and 1.8×10^{-3} Å^2/ps in the absence of an electric potential bias. To evaluate the effect of the diffusion constant on the melting temperature, we run several BD simulations with different transport coefficients. It was found that obtaining a statistically converged estimate for a melting temperature from multiple runs using elevated diffusion constants becomes extremely difficult. An increase in DNA diffusivity generates a modest but notable increase in (⟨f⟩) as expected (data is not shown). Several simulated systems did not show a significant fraction of ss-DNA at all. This indicates that one would need a large number of simulations to achieve a complete statistical convergence for melting simulations, and that the standard deviation of the average value can be significant. Similar conclusions have been reached recently by de Pablo and colleagues (Sambriski et al 2009).

To evaluate the explicit effect of ion−nucleotide interactions, we repeated GCMC/BD melting simulations for the same salt concentration. K^+ and Cl^- excess chemical potentials for a 0.069 M KCl salt solution were obtained from previous results for the excess chemical potential of monovalent salts (Im et al 2000) using polynomial interpolation. For melting simulations with explicit ions, we used a spherical system with a radius of 50 Å and a buffer region ranging from 40 to 50 Å. A total of 40 independent simulations were run to estimate (⟨f⟩), and the diffusion constant for DNA sites was set to 1.0×10^{-3} $Å^2$/ps. According to these results, the maximum fraction (⟨f⟩) of denatured GC (guanine−cytosine) base pairs is 0.62, and the distribution function is approximately normal, in good agreement with the experimentally reported value of 0.6 (Knotts et al 2007; Sambriski et al 2009). As expected, (⟨f⟩) increases when the attractive component of the Lennard-Jones potential for DNA-ion interactions is increased.

3.5.2 DNA translocation through cylindrical channels

A cylindrical nanopore provides arguably the simplest model for a biological or synthetic nanopore. The advantage of such a toy model is obvious; a transmembrane potential has an analytical solution in the limit of the Debye−Hückel approximation. An additional term accounting for repulsive interactions can easily be included in the potential function. In our simulations, a repulsive potential is smoothed using a polynomial radial function, and therefore discontinuities are avoided when calculating repulsive forces. Despite its simplicity, this model may provide a great platform for studies of the time-dependence of DNA translocation on ionic strength, temperature, or dielectric constant of the solution. To estimate the DNA translocation time, we calculated the fraction of DNA sites inside of the channel each N time steps. Thus, one can extrapolate the total DNA translocation time from the fraction of DNA sites inside the channel. For simulations, we consider an aqueous 1.0M of an implicit monovalent salt solution at

a temperature of 275.15 K with a membrane thickness of 50 Å, and the cylindrical nanopore radius is 9 Å, which approximates a constriction zone radius of αHL. A repulsive potential that prevents core−core overlap between DNA sites, the channel, and membrane was set to be 200 kcal/mol, and a switch region of 1.0 Å was set. Initially, a ss-poly$(dA)_{12}$ was positioned at the entrance of a cylindrical channel on the side where the electrostatic potential favors entrance into the nanopore confinement.

Generic cylindrical confinement without a heterogeneous wall charge distribution led to a Gaussian-like distribution of the translocation times. Table 3.2 collects results for ss-poly(dA) (Maglia et al 2010). Translocation across the cylindrical channel with a 3′ entrance with two biasing potentials of V_{mp} = 300 and 900 mV. Although all ss-DNAs were positioned near an entrance to the cylindrical channel, a capture of the monomer that will lead to a complete translocation (t_D) occurs only in a few cases for a constant simulation time, while partial DNA translocations through a cylindrical channel occur in all of them. This is in agreement with the rather broad distribution of translocation times observed experimentally (Maglia et al 2010). A large barrier to entrance is linked to the presence of an entropic barrier so that total translocation can only happen for a handful of relatively "low" probability captured states of flexible ss-DNA (Muthukumar 2007).

Table 3.2 Dependence of the capture $t_{capture}$ and translocation t_D times for 3'-poly$(dA)_{12}$ translocation across cylindrical channel on the diffusion constant and force-field parameter ε.

D ***(Å^2/ps)***	**ε** ***(kcal/mol)***	***V_{mp} (mV)***	***$t_{capture}$ (ns)***	**t_D** ***(ns)***
1.0×10^{-2}	0.01839	0.9	1.5	83.2
0.5×10^{-2}	0.01839	0.9	19.3	171.1
1.0×10^{-2}	0.1839	0.9	1.0	80.2
0.5×10^{-2}	0.1839	0.9	1.1	193.1
1.0×10^{-3}	0.1839	0.9	1.4	1264.3
1.0×10^{-2}	1.839	0.9	33.7	114.7
0.5×10^{-2}	1.839	0.9	41.3	221.8
1.0×10^{-2}	0.1839	0.3	35.5	303.2
0.5×10^{-2}	0.1839	0.3	222.1	610.2

Several DNA configurations blocking a model channel have a hairpin-like structure of the freely hanging tail that prevents DNA crossing. To explore the contribution of different factors affecting this process, several values for DNA diffusivity, the force field parameter controlling intra-molecular rigidity, and trans-membrane potential were used. The summary of key findings is shown in Table 3.2 As expected, complete translocation time increases when DNA diffusivity is decreased. The force-field parameter (ε) that controls the DNA flexibility has little impact on the translocation dynamics. Finally, a major factor for the cylindrical channel determining speed of translocation is an applied potential bias, while a self-diffusion of individual nucleotides has only a secondary role to play (Table 3.2). These findings are in agreement with the previous atomistic simulations (Luan and Aksimentiev 2008; Aksimentiev et al 2004) as well as with experimental data that suggest that DNA diffusion in the nanopore is hindered and the major driving force for translocation is the electrophoretic drift (Meller et al 2001).

3.5.3 Equilibrium ion distributions

Figure 3.3 shows the equilibrium distribution of K^+ and Cl^- along the nanopore axis. The ss-DNA molecule spans (on average) from −75 Å (extracellular cap) to 65 Å (intracellular milieu), which gives an average base-to-base distance of approximately 4.8 Å for ss-poly$(dA)_{40}$ (average from 10 separate simulations) and 4.9 Å ss-poly($dC)_{40}$. Similar measurements for the base-to-base distance (C1′ to C1′ distance) from equilibrium MD are 4.6 and 5.2 Å for ss-poly$(dA)_{40}$ and ss-poly$(dC)_{40}$, respectively. These distances differ slightly from reports on the observed fully stretched DNA conformations observed during steered MD simulations (Aksimentiev and Schulten 2005). However, the equilibrium MD and GCMC/BD simulations were run in the absence of strong biasing forces (up to 1.2 V) used in previous MD studies. The

distributions for both ions inside the channel drastically differ from that reported for a non-blocked nanopore (Noskov et al 2004; Aksimentiev et al 2004).

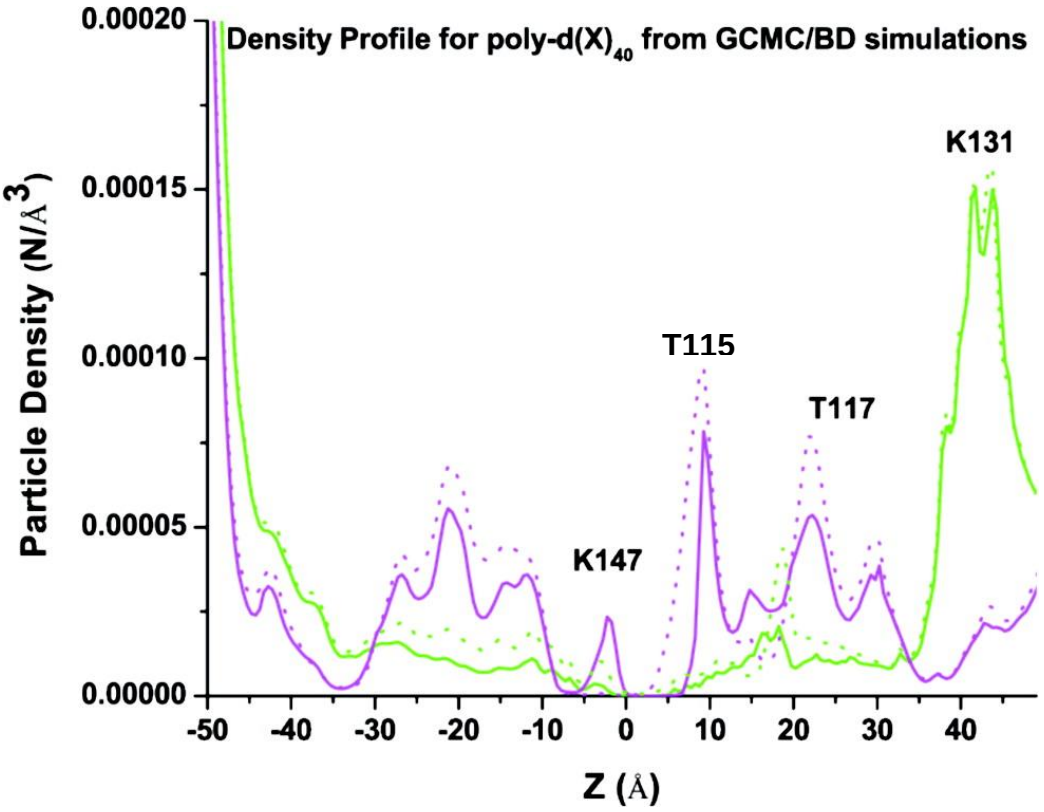

Figure 3.3 Ion density profile along the nanopore's stem region.

The results were obtained from GCMC-BD simulations with coarse-grained models of 5′-poly $d(A)_{40}$-3′ (shown in solid lines) and 5′-poly $d(C)_{40}$-3′ (shown in dotted lines) for K+ and Cl− show in magenta and green, respectively.

The presence of a DNA molecule in the wide extra-cellular cap (from 40 to 0 Å) leads to an increase in the number of K^+ ions and an apparent depletion of anions. The Cl^- concentration in the stem region (from −2 to −51 Å) approaches 0.0, with one notable exception around Z = 17 Å. The position of this peak correlates with the positions of several threonine residues (centered approximately at T115). Interestingly, there is no well-defined peak in the anion concentration profile around a crucial residue for DNA capture and translocation (K147) (Stoddart et al 2010), located in the constriction zone around Z = 0.0 Å. However, a peak at the same position for cation profile can be explained by the presence of negatively charged E111 residues. This may indicate that salt-bridging between phosphates and lysine side-chains are predominant, preventing interactions with small mobile ions. The density profile for K^+ shows an increase in the number of ions for both cap and stem regions of the pore. This may indicate that ion selectivity of the channel is reprogrammed by DNA making it a highly selective cation channel. MD simulations show the same trend with the anion-depleted area spanning for over 20−30 Å in the stem region, in agreement with previously published reports (Mathe et al 2005).

Both approaches show an apparent periodicity in the positions of peaks in the density profile for K^+ that is expected because of spacing phosphate charges in DNA. It is worth mentioning that the initial MD setup was produced with a Monte Carlo placement of counter ions, and a number of Cl^- ions were introduced in the stem region and the channel. It was found that it is difficult to obtain a converged density profile in nanosecond simulations, and anion density in the stem region was continuously decreasing as a function of simulation time. A similar trend was observed in simulations with coarse-grained models with a time-scale required to reach converged profiles in hundreds of nanoseconds. The density profiles for both studied polynucleotides display notable differences. For example, the cation density profile for ss-

poly$(dC)_{25}$ displays slightly greater ion densities than that for ss-poly$(dA)_{25}$ in the nanopore region with a well-defined peak around Z = −21 to −24 Å that correlates with the positions of N121 and N139 both of which are proposed to be playing an important role in the nucleotide contrast measurements (Stoddart et al 2010).

3.5.4 Translocation of ss-DNA oligomers through model biological nanopore αHL

An ultimate goal of nanopore-based sequencing is to enable high-sensitivity discrimination between signals produced by purine and pyrimidine bases. This discrimination in blockade levels may be enhanced by the mutations in the biological nanopore or chemical modifications of the translocated strand (Branton et al 2008; Stoddart et al 2010). The molecular design of pores would require an in-depth understanding of DNA−pore interactions as well as of DNA dynamics in the confinement. To test whether the coarse-grained description of DNA could capture differences in translocation dynamics, we considered two different homo-polymers. Experimental data on DNA dynamics in nanopores show that the distribution of translocation events is complex and cannot be described by a standard exponential distribution (Wiggin et al 2008; Stoddart et al 2010). From the histogram of translocation duration, one can obtain the most probable translocation time. However, these long-living states of DNA in a channel are outside the scope of this paper and beyond timescales accessible by atomistic simulations.

To simplify our comparisons, we have used the same initial conditions, homo-polynucleotides with the same number of nucleotides. In all of our studies with model cylindrical pores, ss-poly$(dC)_n$ strands translocate across model cylindrical pores considerably faster than ss-poly$(dA)_n$. In the absence of the stabilizing interactions between nanopore and ss-DNA, the size difference may explain this result. A bulkier adenine base in a cylindrical nanopore is expected to have greater hydrodynamic friction and therefore would slow down more than cytosine base

(Muthukumar 2007; Nikolaev and Gracheva 2011). The experimental data, however, shows a much more complex dependence of the translocation times on the chemistry of the base. An extension of the GCMC/BD algorithm with its realistic description of the heterogeneous charge distribution in the channel, dual buffers, and explicit account for ion dynamics to studies of real protein systems hold great promise. To test its performance and compare it to all-atom simulations, we have focused on studies of two homo-polymers with different bases, namely, poly$(dA)_n$ and poly$(dC)_n$.

3.5.5 (A/C) contrast in simulations with tethered polymer

Coarse-grained simulations are able to predict blocked currents that clearly show discrimination between A and C. To enable an efficient comparison to experimental data often reported for biotin/streptavidin tethered DNA, we constrain one of the ends of the DNA (5′), thus modeling the ion current blockade for the 3′ entry of ss-DNA. On the basis of the results of all-atom simulations, we set the dielectric constant in the stem region of the protein to $\varepsilon = 40$ in the presence of ss-DNA. For these proof-of-principle simulations, we used uniform bulk constants for ions and nucleotides in this work without scaling diffusion coefficients of ions and nucleotides inside the nanopore confinement. Under these conditions, the open-pore current for 1 M KCl and V_{mp} = 120 mV is ~186 ± 2 pA (55 pA for the K^+ component and 131 pA for Cl^-), while blocked currents are 7 ± 3 pA (5 pA for the K^+ component and 2 pA for Cl^-) and ~13 ± 2 pA (11 pA for the K^+ component and 2 pA for Cl^-) for the poly $d(A)_{40}$ and poly $d(C)_{40}$ blockades, respectively. An open-pore is weakly anion selective, but the presence of ss-DNA renders it highly cation selective instead. This finding is in accord with results of atomistic simulations reported earlier (Mathe et al 2005). In both cases, the average blocked current is between 3 and 8% of that for an open-pore depending on the nucleotide, showing a somewhat

deeper blockade than experimentally measured currents (12−15% in the experimental recordings).

The apparent difference may be related to the simplified treatment of nucleotide−ion interactions in the stem region. As a result, a more rigorous approach is required to fit interaction potentials between ions and nucleotides to include many-body effects. The use of implicit solvent may also lead to an increase in permeation barriers affecting blocked currents. Atomistic simulations also provide only indirect comparisons to experimental data as well, due to imperfect force fields, insufficient sampling, and the much higher voltages usually used (Aksimentiev 2010). It is important to point out the fact that blocked currents display an apparent dependence on the starting conformation of the captured polymer. Figure 3.4 shows the distribution of probabilities for residual currents for polyd$(A)_{40}$ and polyd$(C)_{40}$ blockades obtained from 20 independent simulations of 1 μs each.

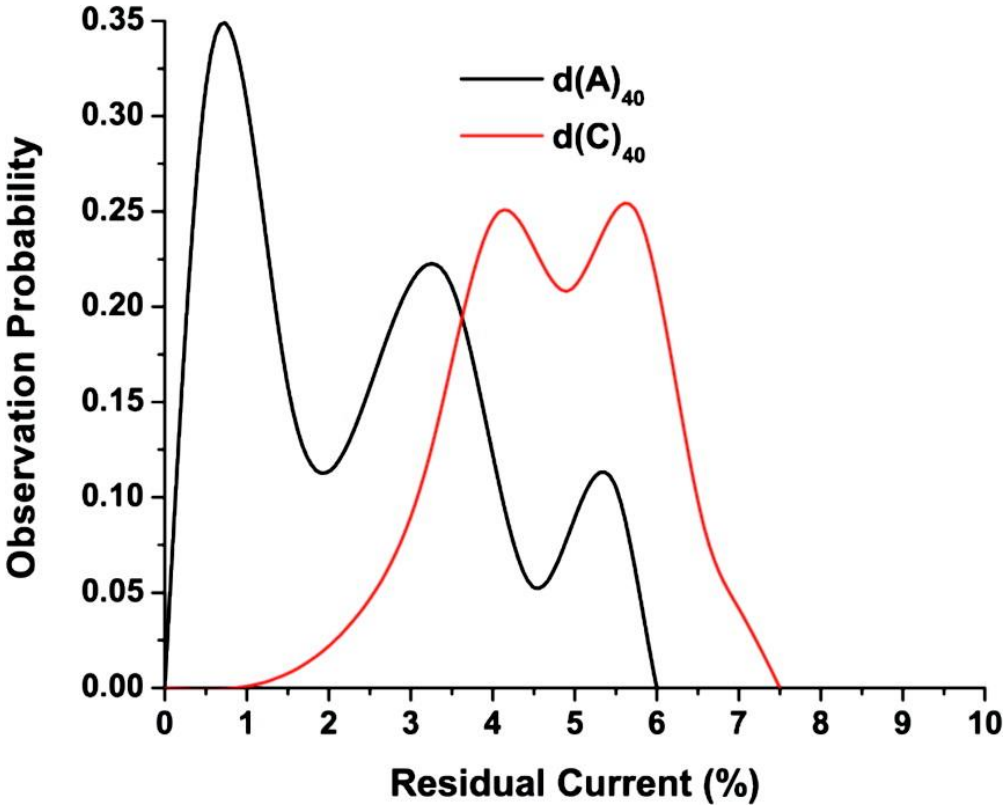

Figure 3.4 Distribution of residual currents determined from 20 separate simulations with ss-$d(A)_{40}$ and ss-$d(C)_{40}$ blocking the pore. C = 1 M of KCl and V_{mp} = 120 mV.

It is evident that ion currents are modulated by the conformational dynamics of the captured DNA. The noisy currents are well documented in a number of ss-DNA translocation studies across the nanopore (Branton et al 2008; Ashkenasy et al 2005). In all-atom MD simulations, it may be challenging to run multiple replicas of the system required to obtain a convergent estimate for the blocked currents, whereas the method presented in this paper allows for multiple runs of several microseconds. A comparison of the relative properties or a contrast in this case could be more meaningful. A common measure for the contrast is the difference between residual currents ΔI_{RES} poly(dA)−poly(dC), e.g. blocked current divided by an open-pore current. Ashkenasy et al. reported that ΔI_{RES} poly(dA)−poly(dC) for 3′ entry and immobilized DNA is ~−10%, while Purnell et al (2008) have reported ΔI_{RES} poly(dA)−poly(dC) to be around −2.9%. Theoretical estimates show ΔI_{RES} poly(dA)−poly(dC) to be around −3%, in good accord with published data from Purnell et al (2008) and previous simulations with all-atom force fields. It has been shown before that the degree of the blockade in αHL displays strong voltage dependence, which seems to be supported by the current simulations. Therefore, the model presented here allows for reasonable resolution between A and C. The model also allows for discrimination between purine and pyrimidine bases in terms of their translocation rates (Table 3.3) as seen in experiments (Branton et al 2008). In spite of all approximations used, the results show that the coarse-grained DNA model combined with explicit ions may offer a powerful instrument to study DNA dynamics in the nanopore.

3.5.6 Microsecond-range dynamics of ss-DNA in αHL

Finally, with a microsecond simulation range, it is possible to access slow dynamics of the confined ss-DNA. Table 3.3 shows a collection of different zRMSDs (computed using the z-axis only) allowing a simple description of different modes of the confined DNA molecule. Of

particular interest is zRMSDr, which characterizes displacement along the z-axis of the DNA phosphates with respect to the DNA geometric center (equivalent to zRMSDa removing DNA translation). Traditionally, in polymer theory, this function is used to characterize the extension/compaction movements of a polymer in solution. Calculations show that captured DNA undergoes "worm movement"-like dynamics, where the end to end distance for the capture portion of the DNA molecule fluctuates between 57 and 80 Å in just 1 microsecond of simulation. The amplitude of this movement is comparable to the vertical translocation itself. These slow modes may explain the excess noise in the electrophysiological recordings of the DNA blockade of ion currents (Tabard-Cossa et al 2007), and hence a strategy targeting suppression of these modes may help to improve the base contrast. They are shown to be DNA-orientation-dependent and likely are related to intrinsic conformational dynamics of DNA.

Table 3.3 Translocation rate changes on the type of ss-DNA inside the channel. Unit for velocity is Å/μs. C=0.5M and the applied voltage (V_{mp}) is 120mV.

	entrance	**Velocity (Å/μs)**	***z*RMSDa (Å)**	***z*RMSDc (Å)**	***z*RMSDr (Å)**
Poly(dA)$_{40}$	3’	1.6	5.1±1.5	2.8±1.5	4.1±0.9
	5’	2.7	7.0±1.9	2.7±1.6	6.3±1.8
Poly(dC)$_{40}$	3’	1.1	3.7±0.8	1.6±1.4	3.4±0.8
	5’	1.7	5.3±1.1	1.8±1.3	5.0±1.2

zRMSDa = absolute root mean square displacement of all phosphates.

zRMSDc = root mean square displacement of geometric center of phosphates.

zRMSDr = root mean square displacement of all phosphates relative to the geometric center. The standard errors were estimated from 20 separate simulations.

3.5.7 Voltage and concentration dependence of the ss-DNA translocation across αHL

BROMOC simulations were performed to examine the effect of salt concentration as well as voltage bias on the translocation rate. It is important to mention that these simulations are reported for already-captured DNA. Therefore, they do not account for the capture probability and its dependence on the applied voltage which is known to show a considerable dependence on the capture voltage (Maglia et al 2008; Meller 2003). To assess the effect of salt concentration on the translocation rate of single stranded DNA, three different salt (KCl) concentrations were used: 0.15, 0.3, and 1.0 M KCl. The translocation is faster when the ion concentration is decreased, which might be ascribed to an ion-shielding effect. When the number of ions that interact with ss-DNA is lower in the case of 0.15M as compared to the cases of 0.3M and 1.0M, the ion shield around ss-DNA is absent or less likely to be complete. Therefore, the effective volume of the ss-DNA molecule is smaller, and the net charge is more negative, thus speeding up the translocation process. To assess the effect of external applied voltages on the ss-DNA translocation rate, we applied four different voltages (50, 120, 200, and 300 mV) generally accessible to experiments. Translocation rates display only a modest increase as a function of applied voltage. This finding is consistent with available experimental data (Meller et al 2001) (Table 3.4).

Table 3.4 Translocation rate of poly-$(dA)_{25}$ as a function of salt (KCl) concentration and external electric potential. Unit for velocity is Å/μs. The standard errors were estimated from 10 separate simulations.

	50mV	**120 mV**	**200mV**	**300 mV**
0.15 M		2.8 ± 0.04		
0.3 M	1.2±0.04	1.8 ± 0.03	1.9±0.03	2.1 ± 0.03
1.0 M		1.6 ± 0.03		

3.5.8 Effect of DNA orientation on translocation rate

Table 3.3 summarizes findings on the orientational discrimination of the DNA transport across wt-αHL. The translocation rates were estimated as described in section 3.4.6. PolyA entering the nanopore at the 5′ end displays faster translocation rates when compared to the 3′ entrance. The standard deviations for velocity numbers are not shown in the table, however they are negligible and do not overlap, meaning that the values are statistically important. This is in good agreement with experimental findings, where it was reported that ss-DNA translocates up to 1.7 times faster depending on its orientation (Mathe et al 2005). It has been suggested that orientation discrimination is defined by the fine differences in interactions between captured DNA and the αHL pore. While protein−DNA contacts play an important role in the translocation of DNA, the results in Table 3.3 suggest that intrinsic dynamics of ss-DNA itself may be an important factor to consider. The captured strand undergoes "worm movement"-like dynamics that can be facilitated or inhibited by the confinement. Table 3.3 summarizes key characteristic functions of the polymer dynamics in the nanopore. It is evident that 5′ entry results in a considerable increase in most of the computed RMSDs characterizing the displacement of the strand along the pore.

3.6 Discussion

The combination of a well-established coarse-grained model with the GCMC-BD algorithm led to results that are in agreement with experimental data on the polymer translocation across a nanopore with non-uniform charge distribution. An advantage of the developed scheme is that it allows 3D sampling of the polymer dynamics inside the nanopore on a microsecond time scale. Furthermore, the developed scheme allows for investigation of the microscopic factors controlling DNA dynamics in the pore. To explore voltage-dependent dynamics, we focus on a truncated αHL system similar to that reported earlier, as well as a model state with a cylindrical pore.

3.6.1 Voltage effects on DNA translocation rates in model cylindrical pore

As a matter for comparison with a biological pore, voltage-driven translocation rates (k_t) and translocation rates with diffusive displacement (k_d) were computed as described in the Methods and Computational Models section for the single stranded adenine dodecamer (poly$(dA)_{12}$) in a cylindrical pore. The oligomer geometric center was positioned in the middle of the cylindrical pore. The nanopore was 50-Å-long with 9 Å radii, and an internal repulsive wall of 1 Å with a repulsion constant of 200 kcal/mole. The temperature used was 300 K; a dielectric constant of 80 and diffusivity for DNA of 0.001 $Å^2$/ps were also used. We used an implicit ionic solution with an ionic strength of 0.3 M. Only repulsive forces characterized the interactions between the phantom membrane and the DNA. During all translocation simulations, different external voltages were applied: 0, 150, 250, 500, and 1000 mV. Translocation simulations for each voltage were repeated 30 times using different random seed numbers. The rates (k_t and k_d) were computed at L = 12 Å (see section 3.4.6) and are plotted in Figure 3.5. As can be seen, the voltage-driven translocation rates component is important in the studied potential bias range.

Both rates display a linear dependence on the applied potential with similar slopes. At 0 mV, k_t intercepts at ~0 Å/μs, while k_d is positively displaced due to the small but statistically significant diffusive displacement component (f). The decomposition of the translocation rates clearly shows that applied force (voltage) is the main driver of translocation, while the diffusional component is only a secondary factor. Comparing these translocation rates with those in the more realistic pore, αHL, we observe that rates are considerably higher in the former. This can be explained due to the electrostatic interaction between DNA and αHL that is a crucial fact and acts as "friction" retarding DNA translocation. This "friction" can be the reason for the nonlinear translocation velocity/applied voltage dependence.

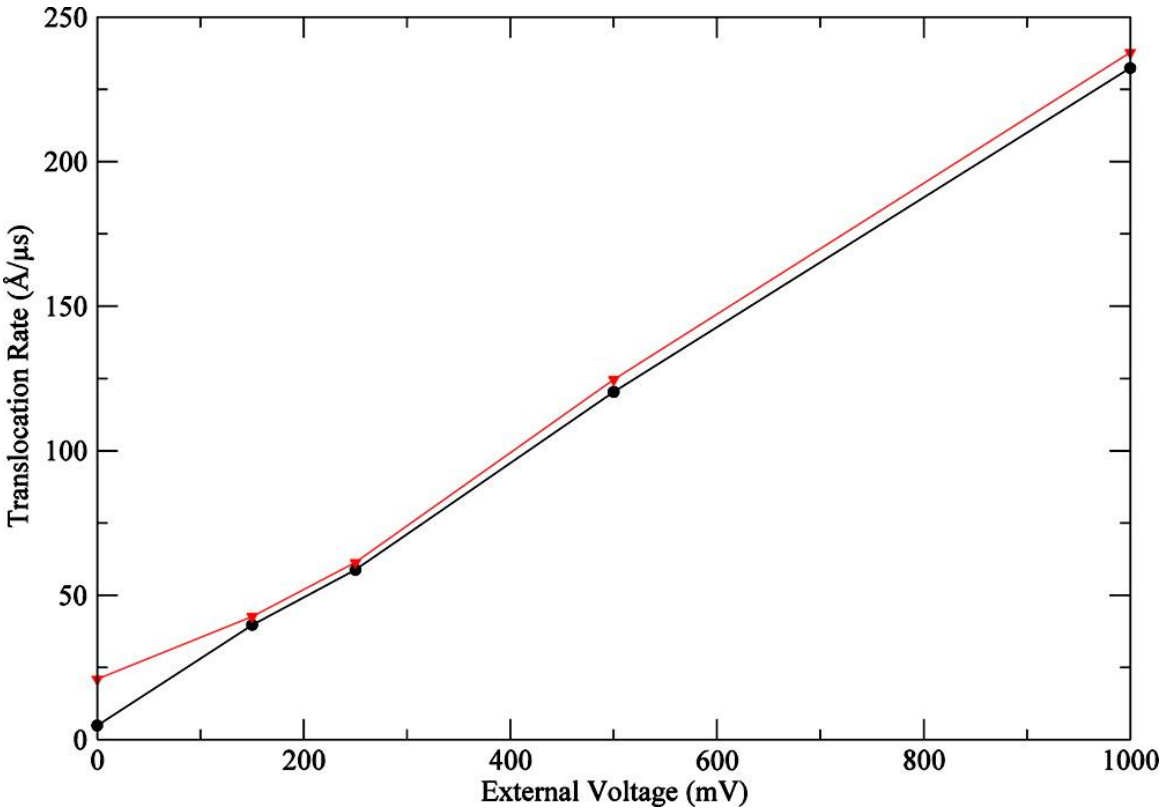

Figure 3.5 Dependence of translocation rates on the external voltage: for A-dodecamer in a 9 Å (width) × 50 Å (length) cylindrical pore. In black, voltage-driven translocation rates (k_t). In red, translocation rates with diffusive displacement (k_d).

3.6.2 DNA Translocation in a nanopore with a non-uniform charge distribution

To study the voltage dependence of polymer translocation in a nanopore with non-uniform charge distribution, we chose a truncated form of the αHL protein shown in Figure 3.6. The stem region was proposed to be a computationally amenable alternative to the full channel. It contains residues forming a proposed constriction zone and thus can provide a reasonable description of the actual pore, considerably reducing the computational burden. Reduction in the DNA translocation time in artificial and biological nanopores is one of the key factors in the development of potentially useful sequencing devices (Fologea et al 2005). First, we simulated ss-DNA transport across the truncated nanopore with all charges on. Figure 3.7 shows the time-dependence of the displacement of the 5′-ss-poly$(dA)_{25}$-3′ as a function of the applied voltage. The results collected in Figure 3.7 show no clear dependence of the displacement on the applied voltage in part due to limited simulation times. Non-exponential escape dynamics has also been reported experimentally, where an anomalously long residence time of the polymer in nanopores was measured (Wiggin et al 2008).

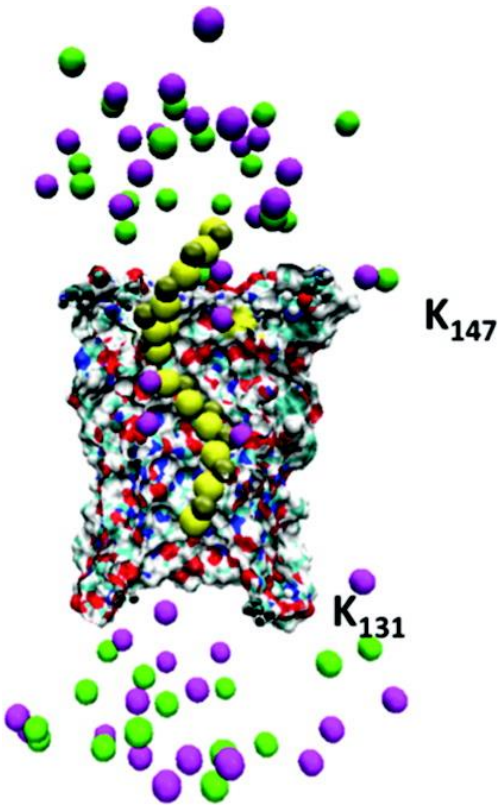

Figure 3.6 Trans-membrane segment of the model nanopore in surface representation. The implicit membrane zone is indicated by a solid black line. The nanopore orientation in the membrane is marked by the two lysine residues (K147 *cis* side and K131 *trans* side). K^+ and Cl^- ions are shown as magenta and green spheres, respectively. The initial positioning of the ss-$d(A)_{40}$ portion confined in the nanopore region is shown as ball and sticks.

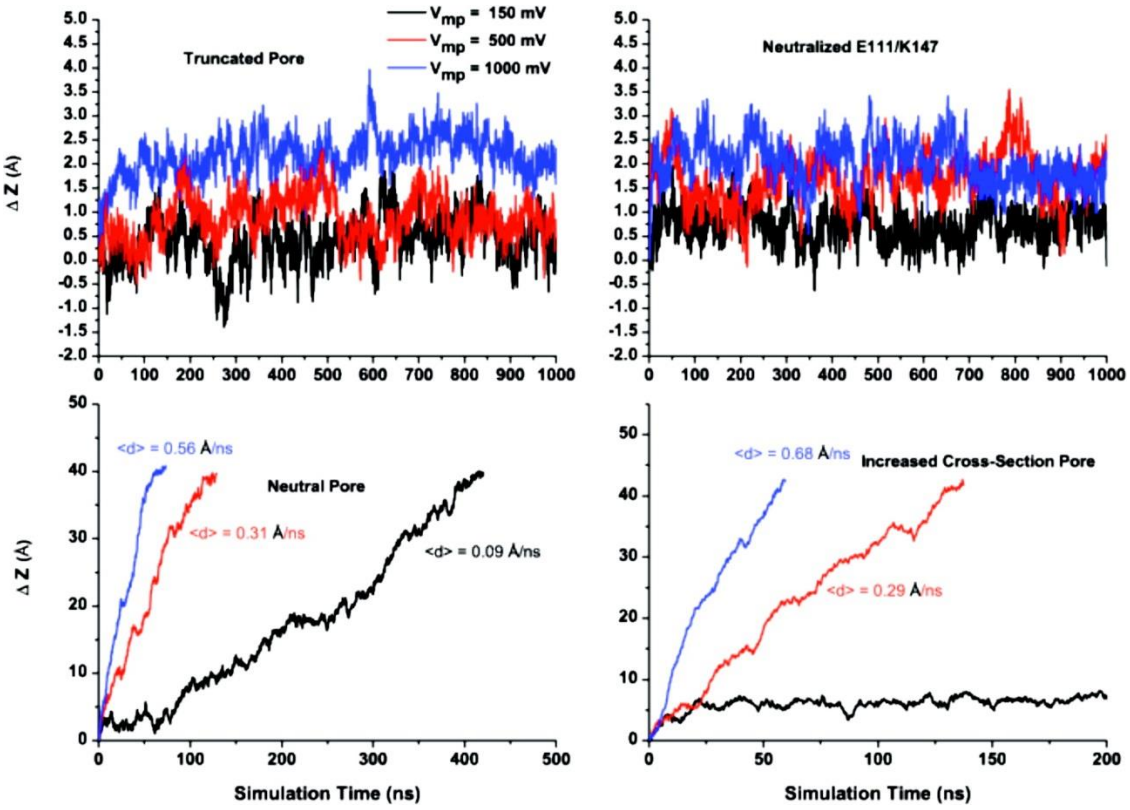

Figure 3.7 Effect of the nanopore confinement on the voltage-dependence of translocation. Top: Time series for the polymer displacement as a function of applied voltage along the *z-axis* of the truncated nanopore fully charged and with the neutralized first constriction zone, e.g., E111/K147 are shown on the left and right panels, respectively. Bottom left: Voltage-dependence of the DNA displacement in the neutralized pore. Velocity was determined from a linear fit of the time series for displacement. Bottom right panel: Same with an increased nanopore cross-section. The radius assigned to every atom has been scaled down by 50%, while all of the partial charges were kept on the amino acids forming the pore.

To elucidate the role of geometry in the translocation dynamics of DNA inside the pore, we neutralized pore-forming residues, e.g. retained the same accessible volume but removing the protein static field or increasing accessible volume across the pore. A salt concentration of 1 M of KCl was maintained in all of the simulations. Thus, it is expected that most of the nanopore charges will be effectively screened by the mobile counter ions. The complete neutralization of the beta barrel led to almost linear dependence of the translocation velocity on the applied voltage. This suggests that nanopore specific interactions with DNA play a role in the determination of translocation rates, while the confinement presented by the nanopore is insufficient to explain anomalous escape dynamics of the biopolymer. At the same time, a 2-fold increase in the solvent-accessible area allows for the almost complete elimination of the hindrance due to electrostatic effects and recovers the linear dependence of DNA translocation rates on the applied voltage seen in the model cylindrical pore. Interestingly, this nanopore clearly shows that there is a minimal voltage requirement for fast translocation of ss-DNA. The use of a membrane potential of 150 mV or lower is insufficient to enable complete translocation in 1 μs of simulation. At the same time, higher voltages produced essentially linear dependence of the displacement on simulation time.

Next, we examined the effect of the charges in the first constriction zone proposed to play a significant role in ss-DNA transport across αHL (Stoddart et al 2010; Maglia et al 2008). The removal of the charges at the first constriction zone alone is insufficient to provide a linear dependence on the applied voltage. This finding is in good agreement with the range of mutations aimed at decreasing the threshold barrier by replacing charged residues at or near the first constriction zone (Maglia et al 2008). Nevertheless, the nanopore with a neutral pair of residues (K147−E111) shows great displacements at high voltages. Experimentally, removal of

E111 (E111N) led to a 2-fold increase in the most probable translocation time (Maglia et al 2008).

3.7 Conclusion

The comprehensive theoretical scheme developed in this work extends the existing GCMC/BD algorithm to the simulation of ion and DNA dynamics in model and biological pores. It was found that the molecular introduction of the DNA molecule modifies the ion distribution along the nanopore axis, converting it into a cation selective channel. Atomistic simulations supported these results. It was also shown that ss-DNA affects the ion distribution in the stem region in a sequence-dependent mode both in atomistic and coarse-grained simulations. The results obtained using CG-GCMC/BD simulations appear to be consistent with the available experimental data. This indicates that both atomistic and coarse-grained approaches are able to capture the essential electrostatic interactions among ions, solvent, and protein. The proposed approach is capable of reproducing some of the key features for DNA translocation in nanopores, e.g., an asymmetric 5′ vs 3′ entrance and purine vs pyrimidine discriminative translocation. In a series of computational tests, it was shown that the developed protocol allowing for simulations reaching up to tens of microseconds is readily available at a relatively low computational cost, thus providing a platform for the rational design of a nanopore with programmed properties. This simulation time can even be increased by the parallelization of the BROMOC code. Several theoretical papers reporting an extension of coarse-grained DNA models to explicit ion simulations have been published providing the scientific community with at least three different force fields to be tested and thus offering an inexpensive computational tool that may enhance our understanding of polymer dynamics in nanopores. BROMOC will provide more accurate results by improving pairwise interaction potentials and diffusivity models. The short-term goal

is to adopt a robust methodological approach to develop nucleotide−ion parameters for the coarse-grained implementation of DNA. This can be done by utilizing a recently developed scheme based on reversed Monte Carlo from Lubartsev and Laaksonen (1999), allowing better effective potentials, which include a more realistic description of solvent-mediated effects based on matching distribution functions.

3.8 BROMOC has been applied in the studies of αHL and ss-DNA interactions.

To summarize chapter 3, we have achieved an important milestone in this research project: we successfully addressed the third goal. Now we have a computer program, BROMOC that allows us to perform inexpensive and long-time simulations on large-scale biological systems. Moreover, it is able to reproduce all the key features of the system observed experimentally. Subsequently, we have used this tool in the next steps of our research project. In particular, I used BROMOC to screen and confirm the effectiveness (as a successive candidate for sequencing purposes) of several promising mutant versions of αHL nanopore. These mutants were established and characterized by our experimental collaborators in Electronic Bioscience Inc. The following chapter of my thesis introduces the research work done on these mutant proteins, using several approaches including BROMOC studies, all-atom MD simulations, and experimental measurements.

CHAPTER 4 - What controls nucleotide contrast in the first sensing zone of alpha-hemolysin nanopore? Combined experimental and theoretical study

4.2 Abstract

The electrophoretic transport of single-stranded DNA through biological nanopores such as alpha-hemolysin (αHL) represents one of the most promising and cost-effective applications and may potentially revolutionize genomics. The design of a rational approach to nanopore modifications for enhancing transport rates, residual conductance and contrast between different nucleotides represents a holy grail of nanopore sequencing. Here, we present a combination of theoretical and experimental studies targeting selective modification of the nanopore region (the first constriction zone), which was proposed to be crucial for effective discrimination between purines and pyrimidines. We have attempted to modify the cross-section and chemical functionality of this region for wild type (WT) αHL and six mutants (E111**N**/M113**X**/K147**N; X = I, F, K, R, T, Y**). Electrophysiological recordings were supplemented with all-atom Molecular Dynamics simulations (MD) and the recently developed BROMOC protocol to investigate residual currents and pore-DNA interactions for two homo-polymers, e.g. poly$(dA)_{40}$ or poly$(dC)_{40}$. The calculations of the residual currents, conductance, and the contrast on poly$(dA)_{40}$/poly$(dC)_{40}$ blocked currents were shown to be in qualitative agreement with experimental recordings. The per-residue decomposition of interaction energies and contact analyses were used to define interacting regions within the pore. It was found that a single nucleotide interacts with several residues and ss-DNA displays considerable conformational flexibility while in the pore.

4.3 Introduction

One of the most promising technological applications for membrane proteins and nanopores is its use for rapid DNA sequencing, which is expected to revolutionize both large-scale genomics and individualized medicine (Branton et al 2008; Deamer and Akeson 2000; Deamer and Branton 2002; Derrington et al 2010; Hornblower et al 2007; Meller et al 2000; Purnell et al 2008). Originally suggested in 1996 (Kasianowicz et al 1996), nanopore sequencing offers great promise to realize the goal of the $1000 genome, changing the future of genomics and medicine. The idea of the method is very simple: a strand of DNA is driven through a protein nanopore (e.g αHL) by an applied electrical bias. Translocation of the DNA through the nanopore restricts the ionic current flowing through the nanopore in a manner that is dependent upon the structure and composition of the nucleotides present (Stoddart et al 2009; Stoddart et al 2010). Ideally, the current is used to directly infer the composition of the DNA strand. One of the most studied pores for DNA sequencing is alpha-hemolysin (WT-αHL) and its modifications.

The contrast between nucleotides translocating wild type-αHL (WT-αHL) in a 1 M KCl solution with applied bias of 100 to 150 mV is approximately 2-5 pA (Purnell et al 2008; Stoddart et al 2009; Mathe et al 2005) depending on the strand orientation. The translocation rate of ssDNA through the αHL nanopore at the same voltage is ~1 to 5 μsec/base (Deamer and Branton 2002) rendering accurate discrimination very challenging. The pores based on MspA toxin have higher reported contrast (Derrington et al 2010) ~5 to 20 pA, but the rate of free DNA translocation through the MspA is more than 10 fold greater than that for αHL (Butler et al 2008). Several nanopore modifications were proposed to slow down DNA translocation, possibly leading to an increase in nucleotide contrast required for better resolution (Bhattacharya et al 2012). To circumvent such limitations several biochemical techniques were developed in the last

decade. Use of motor proteins such as DNA polymerases have now been shown to slowly process the ssDNA through the nanopore (Lieberman et al 2010; Manrao et al 2012) at about 10 ms to 100 ms per nucleotide. Recently, two groups have demonstrated motor-protein assisted nanopore sequencing using the αHL (Cherf et al 2012) and MspA (Manrao et al 2012) protein pores. While examining very slow translocation across the MspA nanopore Manrao et al (Manrao et al 2012) showed that the DNA dynamics in the nanopore lumen is probably stochastic even though the motion is slowed by a motor protein such as phi29 polymerase. Event durations vary significantly in length leading to deletion errors when the event is too short and allowing backward translocation also to occur. When using a motor protein, however, it is only possible to read the same strand 1 or 2 times, so it will be necessary to read multiple copies of the same sequence in order to resolve these types of errors. Since many parallel pores will be required to read copies of the same DNA, large quantities of starting DNA will be required or the DNA will need to be amplified thus negating the very idea of an inexpensive sequencing method.

To realize the potential of nanopore sequencing to be inexpensive enough to be situated in small laboratories and clinics, one has to improve the pore's ability to resolve A, C, G and T blockades without having to resort to processing enzymes, complex amplification steps, expensive consumables, and large banks of sequencing apparatus. There is a general agreement that the main challenge is not manufacturing of the nanopore or intrinsic limits in resolution of the equipment, but the presence of the complex energy surface that governs coupled transport of DNA and ions. The conformational dynamics of the captured polymer results in large fluctuations in measured ion currents, thus compromising both the speed and the accuracy of the method. The a priori prediction of the ideal strategy for nanopore modification via site-directed mutagenesis is challenging. One has to map contact regions, identify the role of different

chemical functionalities giving rise to well-defined contrast and to relate these molecular details to actual electrophysiological recordings.

As it is extremely difficult to study ion transport and the associated conformational changes in the nanopore in atomic detail using experimental approaches, computational studies provide valuable information that will form the basis of better directed experimental investigations (Mathe et al 2005; Heng et al 2004; Lu et al 2006; Wells et al 2011; Aksimentiev et al 2008; Jha et al 2009; Guy et al 2012). In this study, we focus on the targeted modification of the main constriction zone of αHL nanopore both experimentally and computationally. The topology of the main constriction zone in αHL is established (Stoddart et al 2009; Stoddart et al 2010; Guy et al 2012), while details on the protein-DNA interactions and effect of nanopore modification on ss-DNA dynamics are less clear. The main constriction zone of αHL consists of a charged ring of E111 and K147 residues supplemented by hydrophobic M113. The second constriction zone is thought to be formed by N121, N123 and L135. One possible strategy to increase contrast is neutralization and/or removal of the first constriction zone (E111/M113/K147) thus providing only one sensing region of the nanopore that presumably is capable of nucleotide discrimination. The second approach may focus, as proposed earlier, on introduction of a positive charge (E111N/M113K or M113R/K147N) that may slow down translocation thus aiding resolution between translocating strands (Bhattacharya et al 2012; Guy et al 2012; Bond et al 2011).

In this article, we report on a number of mutant pores for the E111**N**/M113**X**/K147**N** identified by Stoddard et al (2009; 2010) as high-sensitivity systems. All-atom MD simulations were combined with Grand-Canonical Monte-Carlo / Brownian Dynamics (BROMOC)

simulations to investigate the interactions of ss-DNA with the biological (WT) αHL and mutant pores (table 4.1) developed by the Electronic BioSciences Inc. (EBS).

Table 4.1 The full description of systems under investigation

αHL pore	pore description
WT	Wild Type
NIN	E111N/M113**I**/K147N
NFN	E111N/M113**F**/K147N
NKN	E111N/M113**K**/K147N
NRN	E111N/M113**R**/K147N
NTN	E111N/M113**T**/K147N
NYN	E111N/M113**Y**/K147N

We hypothesize that neutral/hydrophobic residues in the confinement may hold a better potential for improvement of the purine/pyrimidine contrast. Furthermore, we show that nanopore modifications have direct impact on the conformational dynamics of the confined nucleotides and thus are intrinsically related to excess noise observed in the experimental measurements.

4.4 Methods

4.4.1 All-atom Molecular Dynamics (MD) simulations

Several previous theoretical studies showed that ss-DNA/protein interactions and the resulting nucleotide-dependent currents can be faithfully described with a reduced system comprised of a membrane-inserted stem region of the nanopore, where the sensing regions are located (Bhattacharya et al 2012; Guy et al 2012; Bond et al 2011). One of the key challenges for studies of nucleotide-dependent ion transport is robust sampling of a vast conformational space. The phantom nanopore method was used to obtain initial coordinates for ss-DNA conformation inside WT αHL (Wells et al 2007). The temperature replica-exchange method (REMD) implemented in CHARMM (Jiang and Roux 2010) was used to relax structures of the confined ss-DNA. To ensure a broader sampling of conformational dynamics for ss-DNA ten separate simulations were run with different starting structures for each of the studied systems extracted from clustering of REMD trajectories. The mutations were introduced with SCWRL4.0 protocol (Canutescu et al 2003), re-equilibrated and used for the production runs. The list of studied systems can be found in Table 4.1. All of the simulations were run with NAMD2.7b3 using the CHARMM-27 force-field with CMAP (corrective map) corrections for all of the simulations (Kale et al 1999).

The protein was embedded in the DPPC lipid bilayer with a hydrophilic cap placed on the cis-side of the nanopore above the membrane and the β-barrel region inside the lipid bilayer (Jo

et al 2007; Jo and Im 2011). The electro-neutrality of the system was achieved by solvation in 1.0M KCl in a box of ~70 Å x 70 Å x 130 Å (figure 4.1 A) with a total number of ~60,000 atoms in the system. This simple model allows for longer simulation times, providing richer information on the dynamics of DNA translocation as well as apparently more accurate evaluation of ion conductance. In total, seven different systems with all-atom representations of the nanopore were selected. For each system, four different (a3p; a5p; c3p and c5p) ss-DNA strands (poly$(dA)_{20}$ and poly$(dC)_{20}$) were chosen. The long-range corrections were introduced with the Particle-Mesh-Ewald method (PME) with periodic boundary conditions (PBC). The time step was set to 1 fs for all production runs. The temperature was set to 303 K in all of the simulations. Non-bonded interactions were truncated at 12 Å. We performed 2500 steps to minimize the system, and then the system was equilibrated for 10 ns in the NPT ensemble with Langevin piston pressure control in the absence of an external electric field. We kept a weak harmonic restraint of 1.0 kcal/mol/$Å^2$ on all Cα atoms of the protein in keeping with a protocol by Comer et al (2011) and Aksimentiev et al (2009). The harmonic restraints of 5.0 kcal/mol/ $Å^2$ was used on all heavy atoms of the first nucleotide of DNA (*cis*-side of the pore) to mimic biotin tethering. The equilibrium MD simulations were performed for 10 ns for each of the constructed systems. A uniform electric field equivalent to a potential drop across the lipid membrane of V=0.6 V was applied next for the production run in the NVT ensemble. The production simulations were 25 ns for each of the truncated systems resulting in 250 ns for each of the studied pores. The resulting conductance was obtained by a linear regression fit of the cumulative charge transport across the pore. The R^2 of the linear regression fits were between 0.98 and 0.99 suggesting sufficient sampling per conformation.

4.4.2 BROMOC simulations

The entire set of simulations was carried out with the Grand-Canonical Monte-Carlo/Brownian Dynamics BROMOC program suite (de Biase et al 2012). The main advantage of the method is that it allows multiple simulations to be run for dozens of microseconds, approaching experimental timeframes. The ss-DNA is represented by a coarse-grained model developed earlier by de Pablo's group (de Biase et al 2012; Knotts et al 2007). The ss-DNA strands ($Poly(dA)_{40}$ and $Poly(dC)_{40}$) with two different directions (3' – a3p and c3p; 5' – a5p and c5p) were generated and pre-equilibrated using a "ghost-pore" protocol. This protocol is an in-house approach to prepare the DNA molecules for the actual simulations. The nanopore and dielectric boundaries were represented as a combination of a static field containing the membrane potential terms (obtained by solution of Poisson-Boltzmann equation), the repulsive potential and the reaction field terms. The rigid model of a protein with a dielectric constant of $\varepsilon_p = 2$ was solvated with an implicit water model with a dielectric constant of $\varepsilon_w = 80$ and was embedded into implicit lipid bilayer ($\varepsilon_b = 2$) with a thickness of 38 Å at the position z = 30.1. The overall size of a rectangular simulation box was 57 x 57 x 209 $Å^3$. The salt (KCl) concentration was kept at 1.0M using two symmetric 3.0 Å buffers from 101.50 to 104.50 (z) and from -104.50 to -101.50 (-z).The applied external electric potential was 0.18V (Figure 4.1 B). All other details were similar to those used before (de Biase et al 2012). To mimic the streptavidin tethering, ss-DNA strands were fixed in the 'cap' region of the protein. For each mutant model (a3p; c3p; a5p; c5p entrances and an open-pore) 25 separate runs were performed with a length of 1μs each to obtain open-pore and blocked-pore currents.

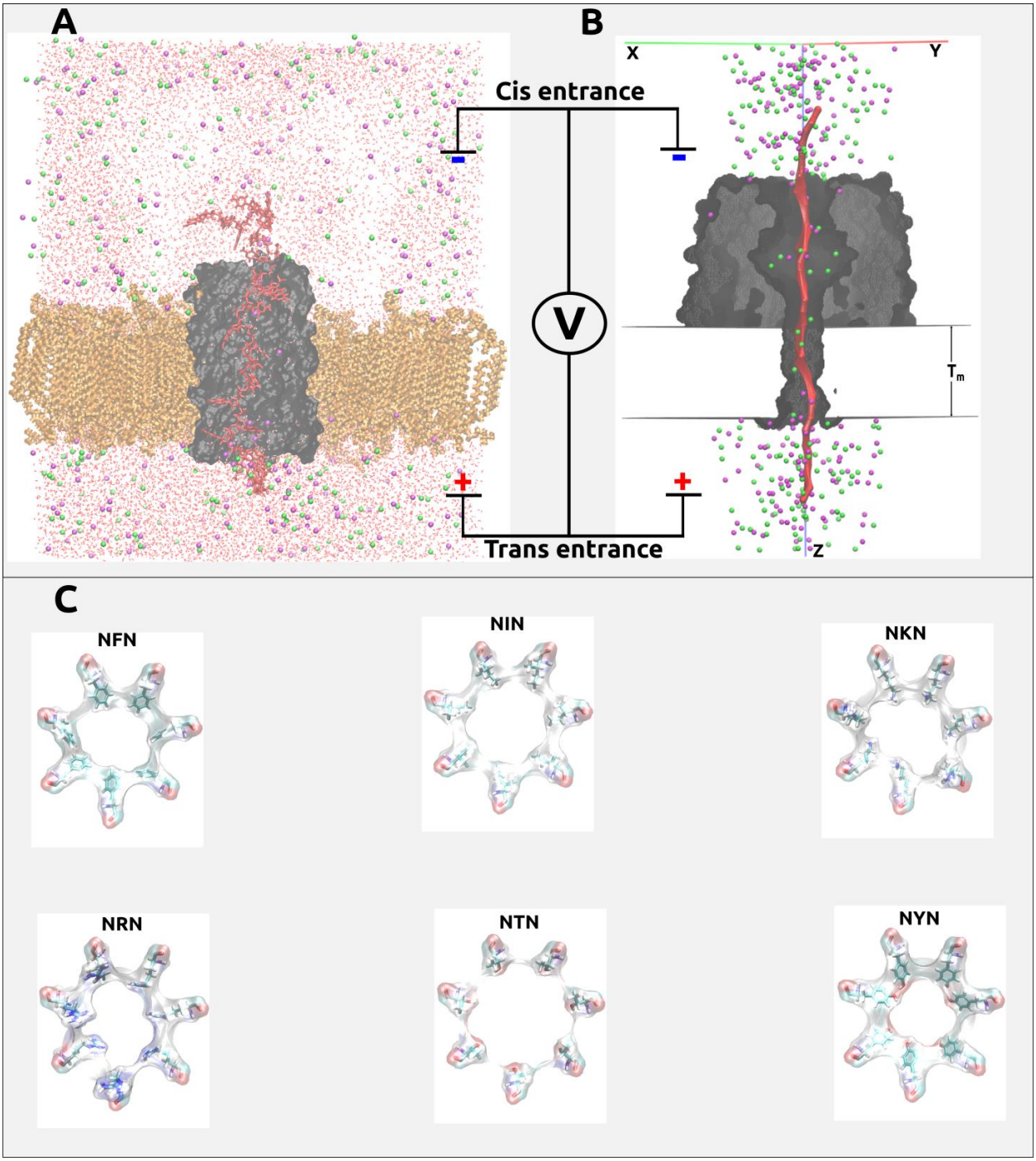

Figure 4.1 General schematic of computational setup of simulations.

For both **(A)** All-atom Molecular Dynamics (MD) simulation set up and **(B)** Brownian Dynamics (Bromoc) simulation set up the system includes truncated (in MD) or intact (in Bromoc) αHL protein (black surf) embedded into DPPC (orange sticks in MD) or implicit (T_m in Bromoc)

bilayer, single stranded (ss) DNA molecule (red line for both cases) is threaded through the αHL pore. All these are placed in an explicit (pink background in MD) or implicit (white background) water box, and explicit salt (purple (Cl- ions) and green (K+ ions) circles) solution is added.

(C) Top view of isolated amino acid residues at the 113 position. Targeted mutant introduction alters the physical radius of the nanpore among other changes. Six different mutants were under detailed focus.

4.5 Results and Discussion

4.5.1 Comparison of theoretical and experimental results on open-pore and blocked currents

We first attempted to test how the two different methods reproduce experimentally measured open-pore currents for the WT and mutant pores. The results are collected in table 4.2. The comparison plot is shown in Figure 4.2.

Table 4.2 Open-pore ion currents (I(pA)) obtained from different approaches. V(mV) = 180mV (BROMOC); 600mV (MD) and 120mV (experiment)

αHL pore	BROMOC (pA)	MD (pA)	Exp (pA)
WT	-293±6.4	-549±66.4	-214±
NIN	-358±12.7	-598±54.5	-245±
NFN	-342±10.6	-581±108.6	-229±
NKN	-439±7.7	-968±92.2	-252±
NRN	-417±8.5	-920±122	-239±
NTN	-370±9.1	-696±132.2	-247±
NYN	-348±7.9	-550±124.9	-215±

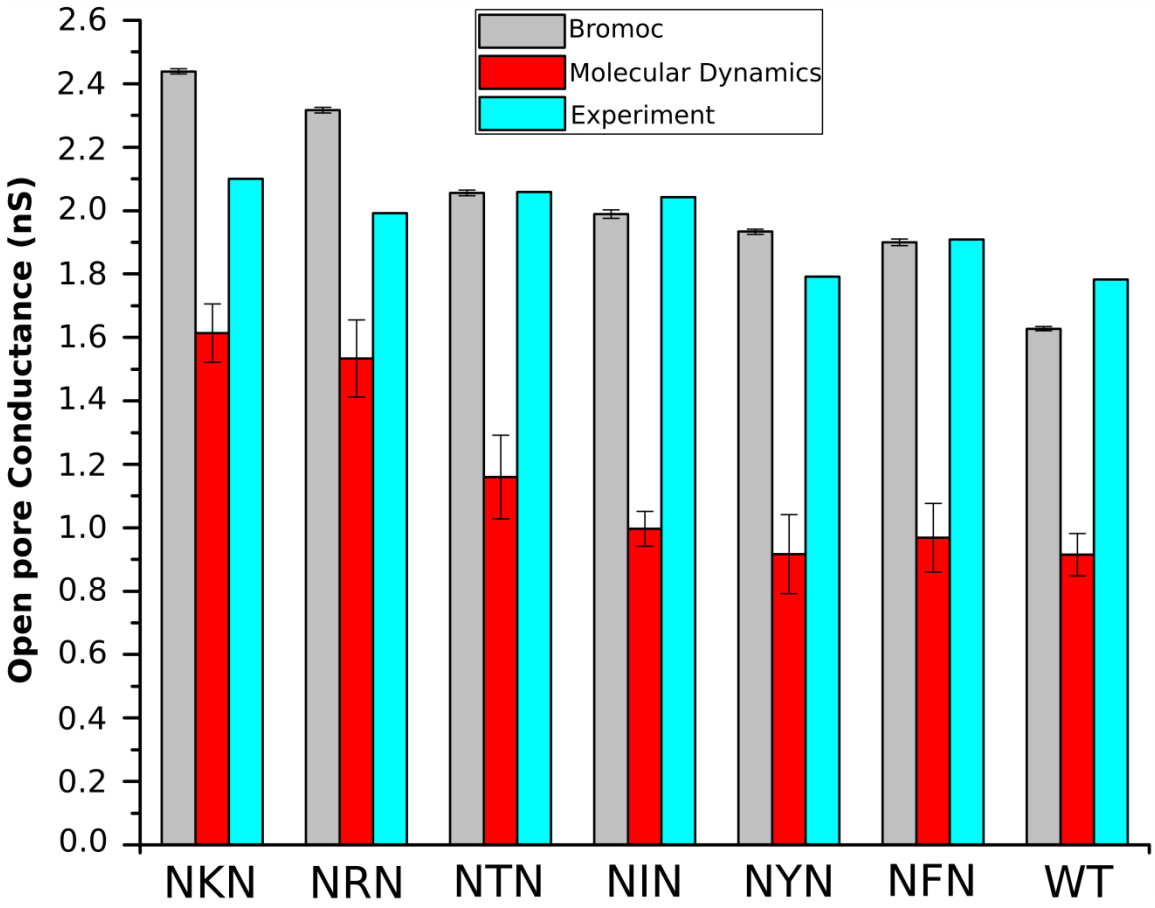

Figure 4.2 The comparison of open/unblocked conductance through wild type and mutant αHL pores obtained from theoretical simulations and experimental measurements.

Different pores (due to mutations) demonstrate different levels of conductance, with wild type (wt) being the least and NKN (E111**N**/M113**K**/K147**N**) being the most conductive among all studied pores. The same trend is successfully observed in all three approaches.

The conductance was calculated using the following equation: **G**(nS) = **I**(pA)/**V**(mV)

It is obvious that while both MD and BROMOC simulations show higher open-pore currents (due to slightly high electric field that has been used), they are still capable of reproducing general trends in conductance as a function of mutation in the lumen pore. All of the methods used in this study are capable of discriminating between high- and low- conducting pores. The result is not really surprising provided the fact that MD and BROMOC simulations sample and average at higher frequencies as compared to experimental measurements. On top of that, MD simulations were run at higher voltages than experimental measurements. The conformational dynamics of captured DNA contributes a lot to standard errors in computed currents. The standard deviation estimated from ten separate simulations was found to be around 10 to 30 % of the computed current. The results are in agreement with previous modeling studies of alpha-hemolysin (Bond et al 2011) and OmpF pores (Pezeshki et al 2009).

The linear correlations (R^2) between experimental and computational open-pore currents are 0.66 and 0.51 for BROMOC and MD simulations, respectively. It should be noted that both approaches significantly overestimate currents for E111N/M113K/K147N or E111N/M113R/**K**147N pores, suggesting that there might be conformational changes in the nanopore that are not captured by the simulations. If we remove these two pores from the correlation analysis, the resulting R^2 are 0.79 and 0.71, respectively. The results are comparable with data reported by Bond et al (2011), showing correlation coefficients of about 0.55. Nevertheless, both experimentally and computationally, introduction of charged side chains into the modified region (first constriction zone) led to an increase in open-pore current. Of note, the mutual correlation between BROMOC and MD results is very high ($R^2 > 0.9$). The initially suggested N**Y**N modification (Stoddart et al 2010) resulted in WT-like open-pore current, while T, I and F in the position 113 led to a higher open-pore current.

The figure 4.3 summarizes the results obtained for (A/C) contrast analysis. Based on this analysis, NIN and NTN mutants show the highest base contrast (17-18% in BROMOC, 4-6% in MD and experiment) among all proteins. And this is consistent for all three approaches. Also, both of the mutants (NKN and NRN) that introduced positively charged side-chains in the constriction led to a significant decrease in the (A/C) contrast and a broad spread of computed residual currents. Interestingly, BROMOC data displays consistently better results in relating blocked currents to experimental measurements. It also suggests that DNA dynamics inside the nanopore can be safely approximated by mean-field approaches where degrees of freedom may be effectively integrated out due to rapid protein dynamics. The use of higher voltages in MD simulations is also a significant source of uncertainty. Nevertheless, the recent breakthrough of several μs-long simulations of DNA in the MspA nanopore shows that MD-generated ensembles provide a sufficient description of conformational dynamics in the nanopore even in the limit of short runs of dozens of nanoseconds (Bhattacharya et al 2012). Another limitation for direct comparison between MD data and experiment is the use of truncated pores. The cap of αHL is involved in the interactions with ss-DNA and may be relevant (as suggested by BD simulations) for a complete description of the system.

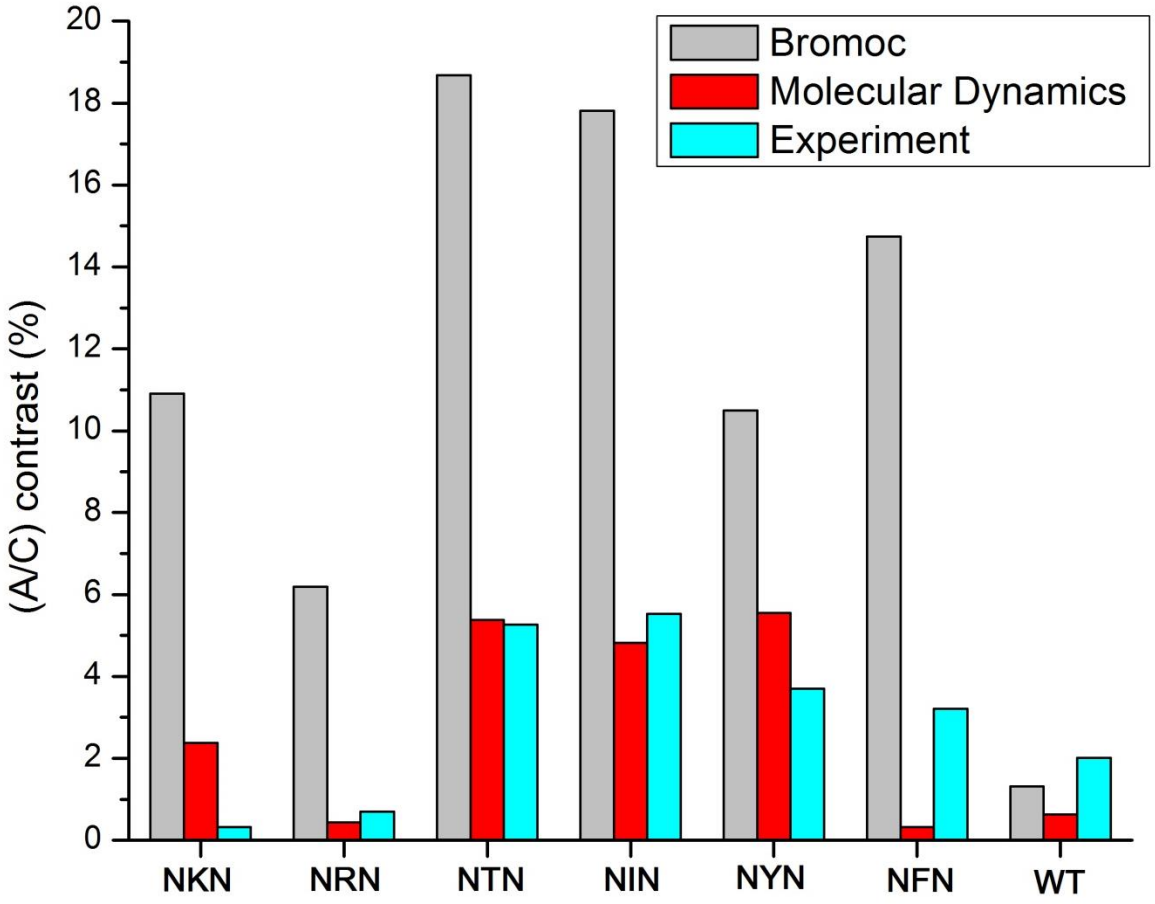

Figure 4.3 (A/C) contrast delivered by wild type and mutant αHL nanopores.

4.5.2 Mapping sensing zones in the WT and mutant alpha-hemolysin nanopores

To aid the design of the amino-acid substitutions we performed interaction analyses to map the apparent topology of the nanopore. The spatial analysis of the residue-DNA interactions are shown in Figure 4.4.

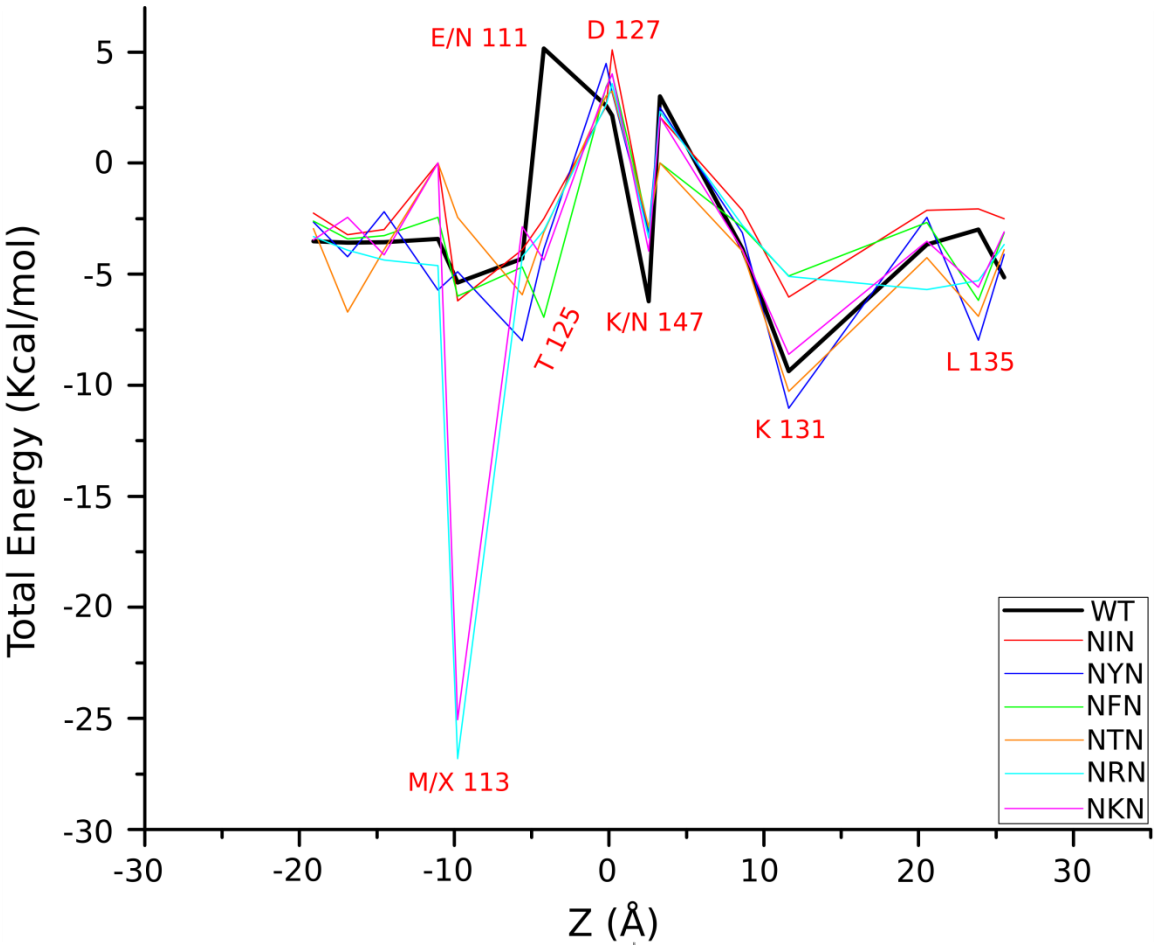

Figure 4.4 Total interaction energy between ss-DNA and αHL wild type and mutant proteins. The mutations in αHL change the interaction profile between the single-stranded DNA molecule and the protein itself. The amino acid (aa) residues that produce interaction changes are labeled on the figure. At the 113 position, X denotes all of the following aa residues: Ile, Tyr, Phe, Thr, Arg and Lys

We were interested primarily in the stem region, while decomposition of the protein-DNA interactions suggests an involvement of the cap region as well. Interaction analysis suggests persistent ionic and hydrogen bonded protein-DNA interactions between several regions of the pore, particularly in the stem. While the most confined region of the αHL (near K147 residues by the junction of the protein cap and stem) has strong ionic interactions with the phosphate charge of DNA, it does not display a large degree of discrimination between A and C. The ss-DNA also makes long-living contacts with M113 as well as with a series of polar residues located nearby. Noticeably, strong interactions at the position of E111 observed in wild type have almost disappeared in the mutant channels. For instance, some mutated amino acid residues (K113 and R113) at the primary constriction resulted in the interactions transitioning from repulsive to attractive, leading to a decrease in the number of degrees of freedom of the ss-DNA oligomer. Another interesting difference has been observed at the second constriction (L135 and T125), where the interactions observed between the DNA and the wild type protein has become stronger in the case of almost all mutants, except NIN. The second constriction zone shows some of the strongest combined interactions located near the *trans* side of the nanopore within the stem.

Significant interactions near the *cis* entrance of the nanopore observed through simulation may be useful for engineering optimal αHL mutants for DNA sequencing applications as well. Although the bases closest to the confinement region of the nanopore appear to affect the current blockade the most, this site may also significantly influence the translocation dynamics and create significant biological noise in ion current readouts. An analysis of contacts and interaction energy decomposition indicates that hydrogen bonding is an essential factor for preferential interactions between cytosine and two asparagines residues N121 and N139 and it is also

supplemented by stabilizing interactions with a threonine (T115). One of the most important residues providing hydrophobic interactions with the translocating polymer is the Leucine at 135 position. Average protein-DNA interactions are relatively small, contributing between 1 and 5 kcal/mol to the base stabilization. Thus, these residues form an initial list for the mutagenesis strategy.

4.5.3 Ion density as a function of nanopore mutation

Figure 4.5 summarizes the information obtained from ion density calculations. We took a closer look at what happens with ions inside the first constriction of αHL nanopore(s) when one performs site-specific mutations.

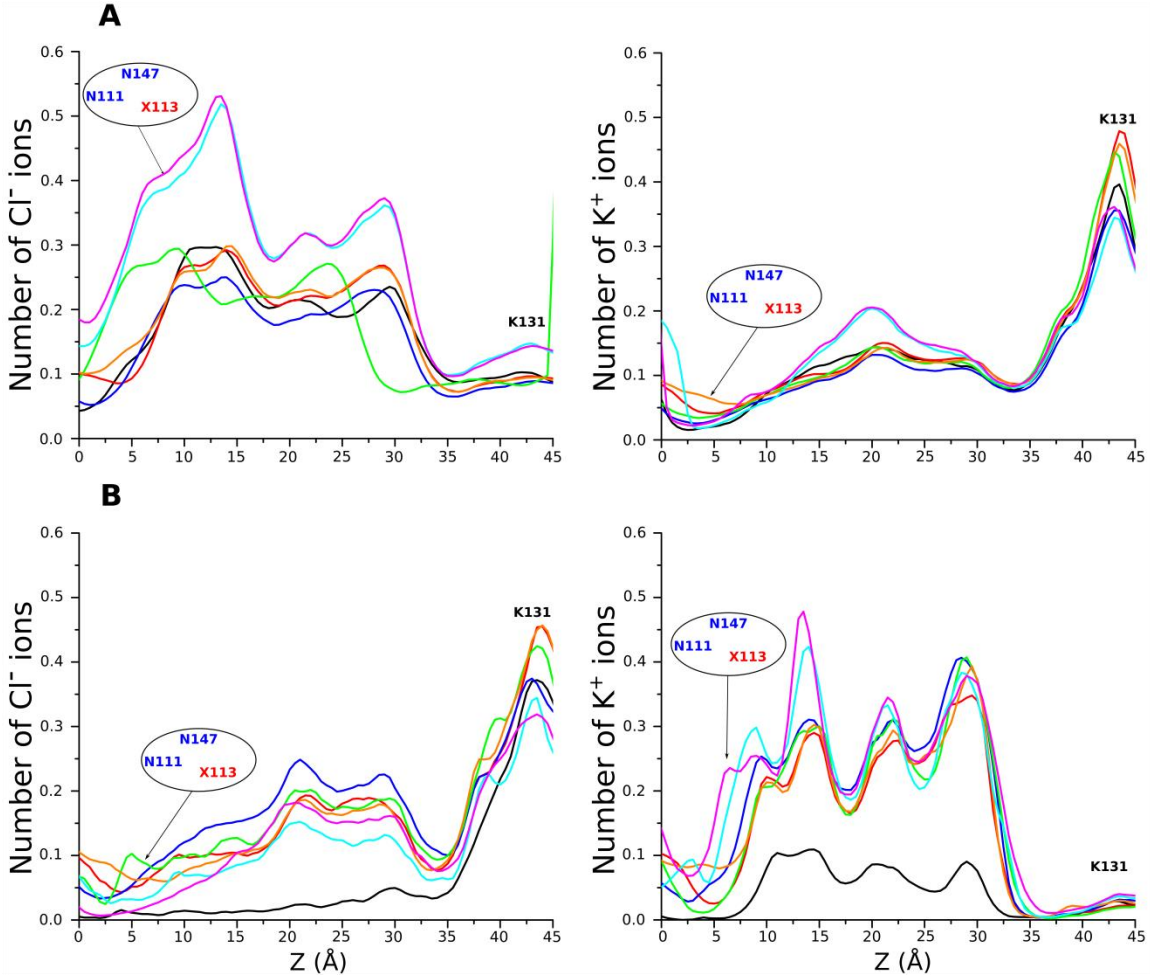

Figure 4.5 Ion density profile inside the stem (β-barrel) region of wild type and mutant αHL pores.

The number of potassium and chlorine ions inside the trans membrane stem region for wild type (wt) and mutant pores in the absence of ss-DNA inside **(A)**. The number of the same ions is changing (decreasing) in the presence of ss-DNA inside the nanopore **(B)**.

The location of mutated amino acid residues (in circle) is indicated alongside the z-axis. X refers to Ile, Tyr, Phe, Thr, Arg and Lys residues.

WT (black), NIN (red), NYN (blue), NFN (green), NTN (orange), NRN (cyan), NKN (magenta)

First, we shall consider the case for open-pore(s) (figure 4.5, panel A). One general observation is that in all pores (WT and mutant) the number of potassium (K^+) ions is smaller than the number of chlorine ions (Cl^-) around the first constriction zone. There, we can conclude that the main charge carrier is the anion. The other observation is that the number of ions is directly proportional to conductance levels, i.e. we see a higher number of ions for more conductive pores. In particular, NKN (2.44nS) and NRN (2.32nS) pores give the highest number of ions (~0.6), whereas the NYN (1.93nS), NFN (1.9nS) and WT (1.63nS) show lower number of ions (~0.2), among all pores.

Now, in the case when the pores are blocked with a ss-DNA molecule (figure 4.5, panel B) the number of potassium (K^+) ions is higher than the chlorine (Cl^-) ions in all pores. This is expected, since the backbone of ss-DNA molecule is negatively charged, therefore the positively charged ions (K^+) prefer to be inside the constriction. The wild type (WT) αHL nanopore is blocked the most, whereas NRN and NKN pores show low blockade levels (or high number of ions).

4.5.4 DNA dynamics inside the nanopore

As it is hypothesized in the current work, the conformational dynamics of a ss-DNA molecule is affected by the specific mutations introduced in the first constriction region. One way to assess that effect is to examine the changes in end-to-end distance of the DNA strand. Figure 4.6 provides a detailed illustration of DNA end-to-end distance fluctuations as a function of mutation.

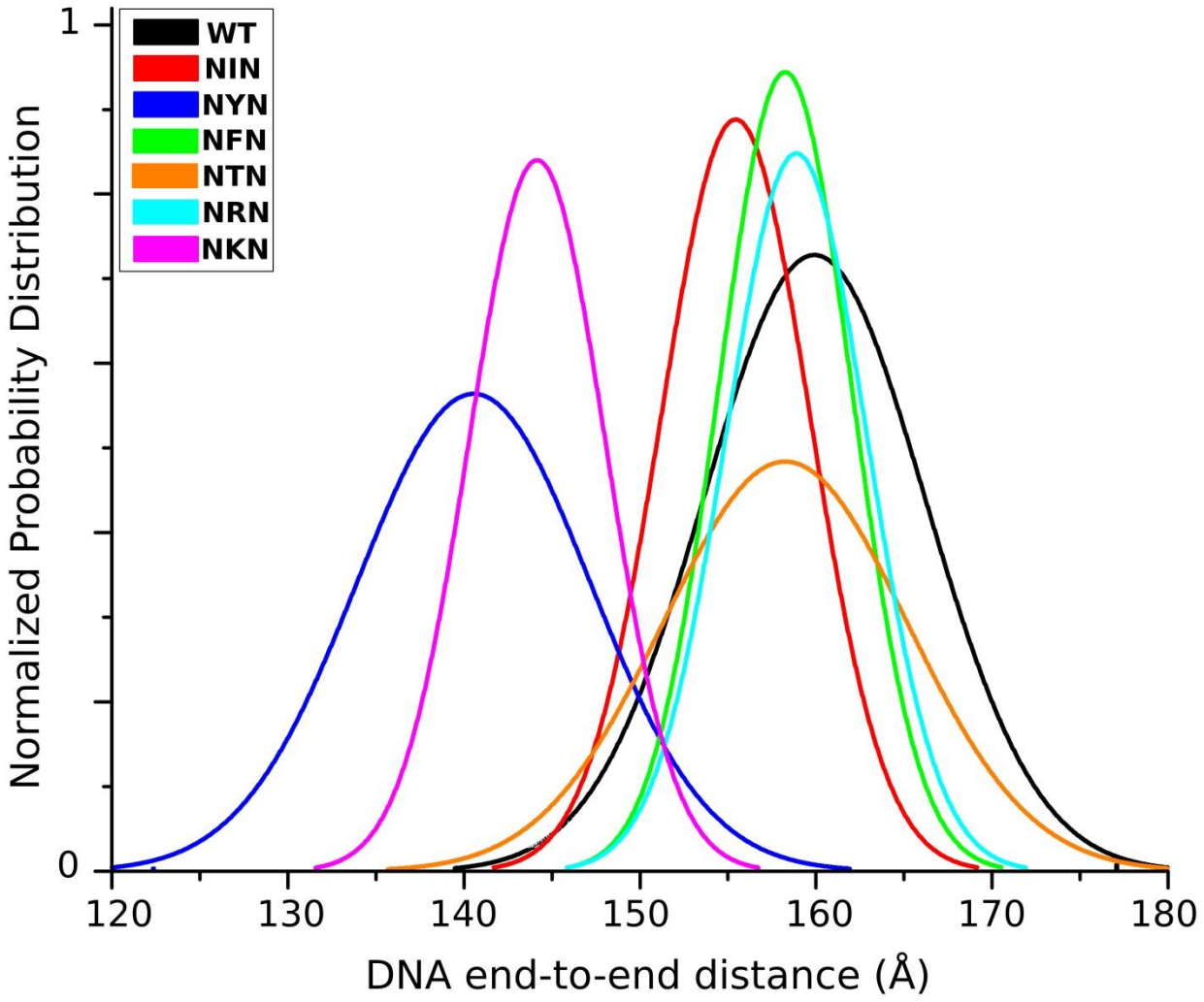

Figure 4.6 ss-DNA dynamics (changes in contour length) observed during BROMOC simulations.

The end-to-end distance of ss-DNA is different inside different αHL nanopores. It ranges from 120 to 160 angstroms depending on the nanopore nature. It also depends on the orientation and geometry of ss-DNA.

The end-to-end distance of double stranded helical B-DNA composed of 40 base pairs (bp) will be around (40 bp x 3.14 Å (helical rise)) 125.6 Å. In our simulations, the DNA strand is stretched due to the fact that it is represented with a coarse-grained approach described earlier by de Pablo et al (2012) and Knotts et al (2007). In particular it varies from 120 to 180 Å (see figure 4.6). The pores that showed high levels of open-pore and residual currents seem to produce longer end-to-end distances (more stretched ss-DNA strand). For example, in NRN and NTN mutant nanopores the distance distribution for ss-DNA peaks ~ 150 – 165 Å. This is expected considering the fact that certain mutations lead to more extended ss-DNA conformations, which in turn facilitates the movement of ions through the nanopore therefore producing higher levels of currents. This feature is also important since it provides quantitative information about how many nucleotides can occupy the sensing region of the nanopore. In terms of sequencing, the ideal case is to have a single nucleotide in the sensing region. Subsequently, a more stretched ss-DNA strand is better as compared to a strand with a more coiled conformation.

4.6 Conclusions

The wild type and six mutants of αHL protein were studied in detail. Open-pore and residual ion currents were calculated and compared with electrophysiological recordings provided by our colleagues from Electronic Biosciences Inc. Based on the results, both approaches (theory and experiment) qualitatively agree on “good” and “bad” nanopores. The computational approach allowed us to obtain details on the nature of nanopore-DNA interactions, energy and topology. The ion density analysis correlates with conductance results. The DNA conformation inside the channel may be directly related to the conductivity of the channel itself. The end-to-end distance and its fluctuations were computed and analyzed for wt and mutant αHL nanopores.

This study is one step further towards nanopore sequencing and bio-polymer translocation studies and provides valuable insights into the molecular level of interaction mechanism.

4.7 Summary of chapter 4

To summarize chapter 4, I can say that the two other goals outlined in this research have been addressed with a positive outcome. We managed to confirm the experimental results about the nanopores that show improved (A/C) contrast as compared to the wild type nanopore. We also successfully attempted to analyze the DNA-nanopore interactions, providing molecular details on the energy profiles of those interactions. The DNA dynamics inside the nanopore(s) were also examined.

CHAPTER 5 - CONCLUSION

This research project was initiated to extend the current understanding of molecular mechanisms of bio-polymer transport through biological ion channels and to relate this knowledge to the construction of better/more efficient nanopores for sequencing purposes. I had three major objectives:

Objective 1: (a) to establish a clear understanding of the behaviour of a DNA molecule within the nanopore.

Objective 2: (b) to confirm the targeted mutagenesis and to provide molecular details for the improvement of the (A/C) contrast.

Chapters 3 and 4 successfully cover all the aspects of objectives 1 & 2. We were able to validate specific versions of αHL nanopores that exhibit considerably improved (A/C) contrast (relative to the wild type αHL nanopore). The energy profile was obtained and the DNA dynamics inside the nanopore(s) were analyzed.

Objective 3: (c) to aid the development of a computer tool for long-time DNA-nanopore studies. Chapter 3 addresses objective 3 completely.

One of the main achievements of this project was the development and validation of a computer tool that can perform long-time (up to millisecond scale) DNA-αHL studies. It has been proven that this program can accurately reproduce all the characteristic features observed in the real experiments. It can fill the time gap created between real-time experiments and all-atom Molecular Dynamics simulations by utilizing the sets of effective potentials (from MD) to propagate the system of interests over longer time scales.

We managed to gain information on DNA dynamics inside the nanopore and to relate it to the actual measurements. For example, we have confirmed that the direction of the DNA inside the

nanopore affects a) the translocation speed b) the blocked ion current. Subsequently, we established a molecular mechanism responsible for these effects. The developed method (BROMOC) can be used to study the dependence of translocation rates on the salt concentration and the external electric potential (these are properties that can easily be measured experimentally). It is important to state that the developed technology is fast and scalable allowing us to screen large numbers of nanopores for their ability to separate different nucleotides in a DNA sequences, thus offering a computational platform for future studies. However, there still are challenges to develop nanopore sequencing further. One, which was not addressed in my thesis, is the so-called "excess noise". It seems to be dependent on the DNA sequence, its length, osmolarity of the bathing solution and it represents a significant challenge to improving the method's resolution. Accordingly, future studies will focus on the identification of the sources of excess noise in electrophysiological recordings and the formulation of a rational strategy to either filter it out or control it. In particular, we intend to use this information to design a strategy to slow down the DNA movement inside the nanopore or to modify the nanopore to increase the separation between nucleotides. Further study of the DNA conformational dynamics inside the nanopore and relating those differences to the conductivity of the nanopore is necessary. There is evidence from our preliminary results that the DNA conformation affects the ion dynamics producing different conductive states in the same nanopore via mechanisms that are similar to fast gating in ion channels. I plan to screen mutants of αHL that may affect these "gating" dynamics e.g. by reducing the preferential stability of one of the DNA conformations in the nanopore. We have already established (in collaboration with Electronic BioSciences Inc.) that there are several mutants of αHL which can be further tested for nanopore sequencing. In the future, we shall include the remaining nucleotide bases (thymine

and guanine) in our studies. We shall investigate the interactions between the DNA and other suggested sensing regions in the nanopore and apply targeted mutagenesis on those regions. Another part of the system that needs to be carefully studied is the bathing solution and the dependence of the signal on the nature of the salt carrier. The DNA molecule remains partially hydrated inside the nanopore, and there is a high probability that its conformational dynamics may be controlled by a) solvents with different polarities e.g. binary mixtures (water-alcohols for example) or b) different charge carriers. In this work we used primarily KCl solutions, but plan to include (in accordance with experimental recordings) NaCl, RbCl and CsCl as well as a varying anion series.

I think that nanopore sequencing has the potential to become one of the main genome sequencing techniques available to a broad sector of society. But until then, the challenges need to be addressed properly. Currently, αHL or its variations can only differentiate between Adenine and Cytosine homo-polymers separately. No research has been reported to show discrimination by αHL among all four types of nucleotides either in the same strand or separately. This indicates that nanopore sequencing has a long way to go to become a fully functional and commercially available technique. One of the bright sides of the nanopore sequencing development is that αHL is now being used as a stochastic sensor for a detection of different kinds of analyte compounds. These include small molecules, and also proteins such as thrombin (Rotem et al 2012).

BIBLIOGRAPHY

- Akeson, M., Branton, D., Kasianowicz, J. J., Brandin, E., & Deamer, D. W. (1999). Microsecond time-scale discrimination among polycytidylic acid, polyadenylic acid, and polyuridylic acid as homopolymers or as segments within single RNA molecules. Biophysical Journal, 77(6), 3227-3233.
- Aksimentiev, A., & Holyst, R. (1999). Phase behavior of gradient copolymers. Journal of Chemical Physics, 111(5), 2329-2339.
- Aksimentiev, A., Moorthi, K., & Holyst, R. (2000). Scaling properties of the morphological measures at the early and intermediate stages of the spinodal decomposition in homopolymer blends. Journal of Chemical Physics, 112(13), 6049-6062.
- Aksimentiev, A., Balabin, I. A., Fillingame, R. H., & Schulten, K. (2004). Insights into the molecular mechanism of rotation in the Fo sector of ATP synthase. Biophysical Journal, 86(3), 1332-1344.
- Aksimentiev, A., Heng, J. B., Timp, G., & Schulten, K. (2004). Microscopic Kinetics of DNA Translocation through synthetic nanopores. Biophysical Journal, 87(3), 2086-2097.
- Aksimentiev, A., & Schulten, K. (2004). Extending molecular modeling methodology to study insertion of membrane nanopores. Proceedings of the National Academy of Sciences U S A, 101(13), 4337-4338.
- Aksimentiev, A., Schulten, K., Heng, J., Ho, C., & Timp, G. (2004). Molecular dynamics simulations of a nanopore device for DNA sequencing. Biophysical Journal, 86(1), 480a-480a.

- Aksimentiev, A., & Schulten, K. (2005). Imaging alpha-hemolysin with molecular dynamics: Ionic conductance, osmotic permeability, and the electrostatic potential map. Biophysical Journal, 88(6), 3745-3761.
- Aksimentiev, A., Brunner, R., Cohen, J., Comer, J., Cruz-Chu, E., Hardy, D., Schulten, K. (2008). Computer modeling in biotechnology: a partner in development. Methods in Molecular Biology, 474, 181-234.
- Aksimentiev, A. (2010). Deciphering ionic current signatures of DNA transport through a nanopore. Nanoscale, 2(4), 468-483.
- Apetrei, A., Asandei, A., Park, Y., Hahm, K. S., Winterhalter, M., & Luchian, T. (2010). Unimolecular study of the interaction between the outer membrane protein OmpF from E. coli and an analogue of the HP(2-20) antimicrobial peptide. Journal of Bioenergetics and Biomembranes, 42(2), 173-180.
- Ashkenasy, N., Sanchez-Quesada, J., Bayley, H., & Ghadiri, M. R. (2005). Recognizing a single base in an individual DNA strand: A step toward DNA sequencing in nanopores. Angewandte Chemie-International Edition, 44(9), 1401-1404.
- Bajaj, H., Tran, Q. T., Mahendran, K. R., Nasrallah, C., Colletier, J. P., Davin-Regli, A., Winterhalter, M. (2012). Antibiotic Uptake through Membrane Channels: Role of Providencia stuartii OmpPst1 Porin in Carbapenem Resistance. Biochemistry, 51(51), 10244-10249.
- Basilio, D., Juris, S. J., Collier, R. J., & Finkelstein, A. (2009). Evidence for a Proton-Protein Symport Mechanism in the Anthrax Toxin Channel. Journal of General Physiology, 133(3), 307-314.

- Bayley, H., Braha, O., & Gu, L. Q. (2000). Stochastic sensing with protein pores. Advanced Materials, 12(2), 139-142.
- Bekker, H., Berendsen, H. J. C., & Vangunsteren, W. F. (1995). Force and Virial of Torsional-Angle-Dependent Potentials. Journal of Computational Chemistry, 16(5), 527-533.
- Benner, S., Chen, R. J. A., Wilson, N. A., Abu-Shumays, R., Hurt, N., Lieberman, K. R., Akeson, M. (2007). Sequence-specific detection of individual DNA polymerase complexes in real time using a nanopore. Nat Nano, 2(11), 718-724.
- Bezrukov, S. M., & Kasianowicz, J. J. (1993). Current noise reveals protonation kinetics and number of ionizable sites in an open protein ion channel. Physical Review Letters, 70(15), 2352-2355.
- Bezrukov, S. M., Vodyanoy, I., Brutyan, R. A., & Kasianowicz, J. J. (1996). Dynamics and free energy of polymers partitioning into a nanoscale pore. Macromolecules, 29(26), 8517-8522.
- Bezrukov, S. M., & Winterhalter, M. (2000). Examining Noise Sources at the Single-Molecule Level: 1/f Noise of an Open Maltoporin Channel. Physical Review Letters, 85(1), 202.
- Bhakdi, S., & Tranumjensen, J. (1991). Alpha-Toxin of Staphylococcus-Aureus. Microbiological Reviews, 55(4), 733-751.
- Bhattacharya, S., Derrington, I. M., Pavlenok, M., Niederweis, M., Gundlach, J. H., & Aksimentiev, A. (2012). Molecular Dynamics Study of MspA Arginine Mutants Predicts Slow DNA Translocations and Ion Current Blockades Indicative of DNA Sequence. ACS Nano, 6(8), 6960-6968.

- Biro, I., Pezeshki, S., Weingart, H., Winterhalter, M., & Kleinekathofer, U. (2010). Comparing the Temperature-Dependent Conductance of the Two Structurally Similar E. coil Porins OmpC and OmpF. Biophysical Journal, 98(9), 1830-1839.
- Bockmann, R. A., de Groot, B. L., Kakorin, S., Neumann, E., & Grubmuller, H. (2008). Kinetics, statistics, and energetics of lipid membrane electroporation studied by molecular dynamics simulations. Biophysical Journal, 95(4), 1837-1850.
- Bond, P. J., Guy, A. T., Heron, A. J., Bayley, H., & Khalid, S. (2011). Molecular Dynamics Simulations of DNA within a Nanopore: Arginine-Phosphate Tethering and a Binding/Sliding Mechanism for Translocation. Biochemistry, 50(18), 3777-3783.
- Bowman, G. R., Huang,X, Pande, VS. (2008). Using generalized ensemble simulations and Markov state models to identify conformational states. Methods, 49, 197-201.
- Bowman, G. R., Beauchamp, K. A., Boxer, G., & Pande, V. S. (2009). Progress and challenges in the automated construction of Markov state models for full protein systems. Journal of Chemical Physics, 131(12).
- Bowman, G. R., Huang, X. H., & Pande, V. S. (2009). Using generalized ensemble simulations and Markov state models to identify conformational states. Methods, 49(2), 197-201.
- Braha, O., Gu, L. Q., Zhou, L., Lu, X. F., Cheley, S., & Bayley, H. (2000). Simultaneous stochastic sensing of divalent metal ions. Nature Biotechnology, 18(9), 1005-1007.
- Branton, D., Deamer, D. W., Marziali, A., Bayley, H., Benner, S. A., Butler, T., . . . Schloss, J. A. (2008). The potential and challenges of nanopore sequencing. Nature Biotechnology, 26(10), 1146-1153.

- Brauser, A., Schroeder, I., Gutsmann, T., Cosentino, C., Moroni, A., Moroni, A., Winterhalter, M. (2012). Modulation of enrofloxacin binding in OmpF by Mg2+ as revealed by the analysis of fast flickering single-porin current. Journal of General Physiology, 140(1), 69-82.
- Butler, T. Z., Gundlach, J. H., & Troll, M. (2007). Ionic Current Blockades from DNA and RNA Molecules in the {alpha}-Hemolysin Nanopore. Biophysical Journal, 93(9), 3229-3240.
- Butler, T. Z., Pavlenok, M., Derrington, I. M., Niederweis, M., & Gundlach, J. H. (2008). Single-molecule DNA detection with an engineered MspA protein nanopore. Proceedings of the National Academy of Sciences, 105(52), 20647-20652.
- Buyukdagli, S., Sanrey, M., & Joyeux, M. (2006). Towards more realistic dynamical models for DNA secondary structure. Chemical Physics Letters, 419(4-6), 434-438.
- Canutescu, A. A., Shelenkov, A. A., & Dunbrack, R. L. (2003). A graph-theory algorithm for rapid protein side-chain prediction. Protein Science, 12(9), 2001-2014.
- Carr, R., Comer, J., Ginsberg, M. D., & Aksimentiev, A. (2011). Atoms-to-microns model for small solute transport through sticky nanochannels. Lab on a Chip, 11(22), 3766-3773.
- Carr, R., Comer, J., Ginsberg, M. D., & Aksimentiev, A. (2011). Modeling Pressure-Driven Transport of Proteins Through a Nanochannel. IEEE Transactions on Nanotechnology, 10(1), 75-82.
- Cherf, G. M., Lieberman, K. R., Rashid, H., Lam, C. E., Karplus, K., & Akeson, M. (2012). Automated forward and reverse ratcheting of DNA in a nanopore at 5-angstrom precision. Nature Biotechnology, 30(4), 344-348.

- Chimerel, C., Movileanu, L., Pezeshki, S., Winterhalter, M., & Kleinekathofer, U. (2008). Transport at the nanoscale: temperature dependence of ion conductance. European Biophysics Journal with Biophysics Letters, 38(1), 121-125.
- Comer, J., Dimitrov, V., Zhao, Q., Timp, G., & Aksimentiev, A. (2009). Microscopic Mechanics of Hairpin DNA Translocation through Synthetic Nanopores. Biophysical Journal, 96(2), 593-608.
- Comer, J. R., Wells, D. B., & Aksimentiev, A. (2011). Modeling nanopores for sequencing DNA. Methods in Molecular Biology, 749, 317-358.
- Comer, J., & Aksimentiev, A. (2012). Predicting the DNA Sequence Dependence of Nanopore Ion Current Using Atomic-Resolution Brownian Dynamics. Journal of Physical Chemistry C, 116(5), 3376-3393.
- Comer, J., Ho, A., & Aksimentiev, A. (2012). Toward detection of DNA-bound proteins using solid-state nanopores: Insights from computer simulations. Electrophoresis, 33(23), 3466-3479.
- Cruz-Chu, E. R., Aksimentiev, A., & Schulten, K. (2006). Water-silica force field for simulating nanodevices. Journal of Physical Chemistry B, 110(43), 21497-21508.
- Danelon, C., Nestorovich, E. M., Winterhalter, M., & Bezrukov, S. M. (2003). Interaction of antibiotics with the OmpF channel: effect on translocation. Biophysical Journal, 84(2), 534A-534A.
- Danelon, C., Suenaga, A., Winterhalter, M., & Yamato, I. (2003). Molecular origin of the cation selectivity in OmpF porin: single channel conductances vs. free energy calculation. Biophysical Chemistry, 104(3), 591-603.

- Danelon, C., Lindemann, M., Borin, C., Fournier, D., & Winterhalter, M. (2004). Channel-forming membrane proteins as molecular sensors. IEEE Transactions on Nanobioscience, 3(1), 46-48.
- Daura, X., Affentrauger, R. and Mark, A.E. (2010). On the relative merits of equilibrium and non-equilibrium simulations for the estimation of free-energy differences. ChemPhysChem, 11, 3734-3743.
- De Biase, P. M., Solano, C. J. F., Markosyan, S., Czapla, L., & Noskov, S. Y. (2012). BROMOC: Brownian Dynamics/Monte-Carlo Program Suite to Study Ion and DNA Permeation in Nanopores. Journal of Chemical Theory and Computation, 8(7), 2540-2551.
- Deamer, D. W., & Akeson, M. (2000). Nanopores and nucleic acids: prospects for ultrarapid sequencing. Trends Biotechnology, 18(4), 147-151.
- Deamer, D. W., & Branton, D. (2002). Characterization of nucleic acids by nanopore analysis. Accounts of Chemical Research, 35(10), 817-825.
- Derrington, I. M., Butler, T. Z., Collins, M. D., Manrao, E., Pavlenok, M., Niederweis, M., & Gundlach, J. H. (2010). Nanopore DNA sequencing with MspA. Proceedings of the National Academy of Sciences, 107(37), 16060-16065.
- Dorvel, B., Sigalov, G., Zhao, Q., Comer, J., Dimitrov, V., Mirsaidov, U., Timp, G. (2009). Analyzing the forces binding a restriction endonuclease to DNA using a synthetic nanopore. Nucleic Acids Research, 37(12), 4170-4179.
- Drukker, K., & Schatz, G. C. (2000). A model for simulating dynamics of DNA denaturation. Journal of Physical Chemistry B, 104(26), 6108-6111.

- Drukker, K., Wu, G. S., & Schatz, G. C. (2001). Modes simulations of DNA denaturation dynamics. Journal of Chemical Physics, 114(1), 579-590.
- Durdagi, S., Subbotina, J., Lees-Miller, J., Guo, J., Duff, H. J., & Noskov, S. Y. (2010). Insights into the Molecular Mechanism of hERG1 Channel Activation and Blockade by Drugs. Current Medicinal Chemistry, 17(30), 3514-3532.
- Durdagi, S., & Noskov, S. Y. (2011). Consistency of constructed hERG1nanoporedomain and pharmacophore models: A 3D-QSAR, molecular docking, and pharmacophore modeling study. Biochemistry and Cell Biology-Biochimie Et Biologie Cellulaire, 89(2), 266-267.
- Durdagi, S., & Noskov, S. Y. (2011). Mechanism of K+/Na+ selectivity in potassium channels from the perspective of the non-selective bacterial channel NaK. Channels, 5(3), 198-200.
- Durdagi, S., Duff, H. J., & Noskov, S. Y. (2011). Combined Receptor and Ligand-Based Approach to the Universal Pharmacophore Model Development for Studies of Drug Blockade to the hERG1nanoporeDomain. Journal of Chemical Information and Modeling, 51(2), 463-474.
- Durdagi, S., Zhao, C., Cuervo, J. E., & Noskov, S. Y. (2011). Atomistic models for free energy evaluation of drug binding to membrane proteins. Current Medicinal Chemistry, 18(17), 2601-2611.
- Durdagi, S., Guo, J. Q., Lees-Miller, J. P., Noskov, S. Y., & Duff, H. J. (2012). Structure-Guided Topographic Mapping and Mutagenesis to Elucidate Binding Sites for the Human Ether-a-Go-Go-Related Gene 1 Potassium Channel (KCNH2) Activator NS1643. Journal of Pharmacology and Experimental Therapeutics, 342(2), 441-452.

- Egorov, A. V., Komolkin, A. V., Chizhik, V. I., Yushmanov, P. V., Lyubartsev, A. P., & Laaksonen, A. (2003). Temperature and concentration effects on Li+-ion hydration. A molecular dynamics simulation study. Journal of Physical Chemistry B, 107(14), 3234-3242.
- Egwolf, B., Luo, Y., Walters, D. E., & Roux, B. (2010). Ion Selectivity of alpha-Hemolysin with beta-Cyclodextrin Adapter. II. Multi-Ion Effects Studied with Grand Canonical Monte Carlo/Brownian Dynamics Simulations. Journal of Physical Chemistry B, 114(8), 2901-2909.
- Elber, R., & West, A. (2010). Atomically detailed simulation of the recovery stroke in myosin by Milestoning. Proceedings of the National Academy of Sciences of the United States of America, 107(11), 5001-5005.
- Ermak, D. L., & Mccammon, J. A. (1978). Brownian Dynamics with Hydrodynamic Interactions. Journal of Chemical Physics, 69(4), 1352-1360.
- Faraldo-Gomez, J. D., & Roux, B. (2006). Characterization of conformational equilibria through Hamiltonian replica-exchange simulations: Prevailing over large energy barriers, close confinement and strong entropic and solvation effects. Abstracts of Papers of the American Chemical Society, 232, 292-292.
- Faraldo-Gomez, J. D., & Roux, B. (2007). Characterization of conformational equilibria through Hamiltonian and temperature replica-exchange simulations: Assessing entropic and environmental effects. Journal of Computational Chemistry, 28(10), 1634-1647.
- Faraldo-Gomez, J. D., Kutluay, E., Jogini, V., Zhao, Y. X., Heginbotham, L., & Roux, B. (2007). Mechanism of intracellular block of the KcsA K+ channel by tetrabutylammonium: Insights from X-ray crystallography, electrophysiology and replica-

exchange molecular dynamics simulations. Journal of Molecular Biology, 365(3), 649-662.

- Finkelstein, A. (2009). Proton-coupled protein transport through the anthrax toxin channel. Philosophical Transactions of the Royal Society B-Biological Sciences, 364(1514), 209-215.
- Flyvbjerg, H., & Petersen, H. G. (1989). Error-Estimates on Averages of Correlated Data. Journal of Chemical Physics, 91(1), 461-466.
- Fologea, D., Uplinger, J., Thomas, B., McNabb, D. S., & Li, J. L. (2005). Slowing DNA translocation in a solid-state nanopore. Nano Letters, 5(9), 1734-1737.
- Frenkel D., & Smit B. (2002). Understanding molecular dynamics: From algorithms to applications (2nd ed.). San Diego, CA: Academic Press
- Gameiro, P., Neves, P., & Winterhalter, M. (2007). Fluorescence quenching as a tool to investigate interaction of quinolone antibiotics with bacterial protein OmpF. Biophysical Journal, 554A-555A.
- Gan, W. X., Yang, S. C., & Roux, B. (2009). Atomistic View of the Conformational Activation of Src Kinase Using the String Method with Swarms-of-Trajectories. Biophysical Journal, 97(4), L8-L10.
- Gibbs, S. J., Barren, B., Beck, K. E., Proft, J., Zhao, X., Noskova, T., . . . Braun, J. E. (2009). Hsp40 couples with the CSPalpha chaperone complex upon induction of the heat shock response. PLoS One, 4(2), e4595.
- Gornall, J. L., Mahendran, K. R., Pambos, O. J., Steinbock, L. J., Otto, O., Chimerel, C., Keyser, U. F. (2011). Simple Reconstitution of Protein Pores in Nano Lipid Bilayers. Nano letters, 11(8), 3334-3340.

- Graff, A., Winterhalter, M., & Meier, W. (2001). Nanoreactors from polymer-stabilized liposomes. Langmuir, 17(3), 919-923.
- Gu, L. Q., Braha, O., Cheley, S., & Bayley, H. (2000). Control of charge selectivity in transmembrane protein pores by using non-covalent molecular adapters. Biophysical Journal, 78(1), 397a-397a.
- Gumbart, J., Wang, Y., Aksimentiev, A., Tajkhorshid, E., & Schulten, K. (2005). Molecular dynamics simulations of proteins in lipid bilayers. Current Opinion in Structural Biology, 15(4), 423-431.
- Guy, A. T., Piggot, T. J., & Khalid, S. (2012). Single-Stranded DNA within Nanopores: Conformational Dynamics and Implications for Sequencing; a Molecular Dynamics Simulation Study. Biophysical Journal, 103(5), 1028-1036.
- Gyarfas, B., Olasagasti, F., Benner, S., Garalde, D., Lieberman, K. R., & Akeson, M. (2009). Mapping the Position of DNA Polymerase-Bound DNA Templates in a Nanopore at 5 Ã Resolution. ACS Nano, 3(6), 1457-1466.
- Hajjar, E., Bessonov, A., Molitor, A., Kumar, A., Mahendran, K. R., Winterhalter, M., Ceccarelli, M. (2010). Toward Screening for Antibiotics with Enhanced Permeation Properties through Bacterial Porins. Biochemistry, 49(32), 6928-6935.
- Hajjar, E., Mahendran, K. R., Kumar, A., Bessonov, A., Petrescu, M., Weingart, H., Ceccarelli, M. (2010). Bridging Timescales and Length Scales: From Macroscopic Flux to the Molecular Mechanism of Antibiotic Diffusion through Porins. Biophysical Journal, 98(4), 569-575.

- Heng, J. B., Ho, C., Kim, T., Timp, R., Aksimentiev, A., Grinkova, Y. V., Timp, G. (2004). Sizing DNA using a nanometer-diameter pore. Biophysical Journal, 87(4), 2905-2911.
- Heng, J. B., Aksimentiev, A., Ho, C., Dimitrov, V., Sorsch, T., Miner, J., Timp, G. (2005). Beyond the Gene Chip. Bell Labs Technical Journal, 10(3), 5-22.
- Heng, J. B., Aksimentiev, A., Ho, C., Marks, P., Grinkova, Y. V., Sligar, S., Timp, G. (2005). Stretching DNA using the electric field in a synthetic nanopore. Nano Letters, 5(10), 1883-1888.
- Heng, J. B., Aksimentiev, A., Ho, C., Marks, P., Grinkova, Y. V., Sligar, S., Timp, G. (2006). The electromechanics of DNA in a synthetic nanopore. Biophysical Journal, 90(3), 1098-1106.
- Hornblower, B., Coombs, A., Whitaker, R. D., Kolomeisky, A., Picone, S. J., Meller, A., & Akeson, M. (2007). Single-molecule analysis of DNA-protein complexes using nanopores. Nature Methods, 4, 315-317.
- Im, W., Seefeld, S., & Roux, B. (2000). A Grand Canonical Monte Carlo-Brownian dynamics algorithm for simulating ion channels. Biophysical Journal, 79(2), 788-801.
- Im, W., & Roux, B. (2001). Brownian dynamics simulations of ions channels: A general treatment of electrostatic reaction fields for molecular pores of arbitrary geometry. Journal of Chemical Physics, 115(10), 4850-4861.
- Im, W., & Roux, B. (2002). Ion permeation and selectivity of OmpF porin: A theoretical study based on molecular dynamics, brownian dynamics, and continuum electrodiffusion theory. Journal of Molecular Biology, 322(4), 851-869.

- James, C. E., Mahendran, K. R., Molitor, A., Bolla, J. M., Bessonov, A. N., Winterhalter, M., & Page, J. M. (2009). How beta-Lactam Antibiotics Enter Bacteria: A Dialogue with the Porins. PLoS One, 4(5).
- Jha, S., Martin, H. S. C., Howorka, S., & Coveney, P. V. (2009). Determination of Free Energy Profiles for the Translocation of Polynucleotides through alpha-Hemolysin Nanopores using Non-Equilibrium Molecular Dynamics Simulations. Journal of Chemical Theory and Computation, 5(8), 2135-2148.
- Jiang, W., Hodoscek, M., & Roux, B. (2009). Computation of Absolute Hydration and Binding Free Energy with Free Energy Perturbation Distributed Replica-Exchange Molecular Dynamics. Journal of Chemical Theory and Computation, 5(10), 2583-2588.
- Jiang, W., & Roux, B. (2010). Free Energy Perturbation Hamiltonian Replica-Exchange Molecular Dynamics (FEP/H-REMD) for Absolute Ligand Binding Free Energy Calculations. Journal of Chemical Theory and Computation, 6(9), 2559-2565.
- Jo, S., Kim, T., & Im, W. (2007). Automated Builder and Database of Protein/Membrane Complexes for Molecular Dynamics Simulations. PLoS One, 2(9).
- Jo, S., Kim, T., Iyer, V. G., & Im, W. (2008). Software news and updates - CHARNIM-GUI: A web-based grraphical user interface for CHARMM. Journal of Computational Chemistry, 29(11), 1859-1865.
- Jo, S., Vargyas, M., Vasko-Szedlar, J., Roux, B., & Im, W. (2008). PBEQ-Solver for online visualization of electrostatic potential of biomolecules. Nucleic Acids Research, 36, W270-W275.

- Jo, S., Lim, J. B., Klauda, J. B., & Im, W. (2009). CHARMM-GUI Membrane Builder for Mixed Bilayers and Its Application to Yeast Membranes. Biophysical Journal, 97(1), 50-58.
- Jo, S., & Im, W. (2011). CHARMM-GUI: Brining Advanced Computational Techniques to Web Interface. Biophysical Journal, 100(3), 156-156.
- Jo, S., Song, K. C., Desaire, H., MacKerell, A. D., & Im, W. (2011). Glycan Reader: Automated Sugar Identification and Simulation Preparation for Carbohydrates and Glycoproteins. Journal of Computational Chemistry, 32(14), 3135-3141.
- Jo, S., Song, K., MacKerell, A. D., & Im, W. (2011). First Step Towards Glycan Modeling: Charmm-Gui Glycan Reader and Glycan Database. Biophysical Journal, 100(3), 156-156.
- Kale, L., Skeel, R., Bhandarkar, M., Brunner, R., Gursoy, A., Krawetz, N., . . . Schulten, K. (1999). NAMD2: Greater scalability for parallel molecular dynamics. Journal of Computational Physics, 151(1), 283-312.
- Kasianowicz, J. J., & Bezrukov, S. M. (1995). Protonation dynamics of the alpha-toxin ion channel from spectral analysis of pH-dependent current fluctuations. Biophysical Journal, 69(1), 94-105.
- Kasianowicz, J. J., Brandin, E., Branton, D., & Deamer, D. W. (1996). Characterization of individual polynucleotide molecules using a membrane channel. Proceedings of the National Academy of Sciences of the United States of America, 93(24), 13770-13773.
- Kjellander, R., Lyubartsev, A. P., & Marcelja, S. (2001). McMillan-Mayer theory for solvent effects in inhomogeneous systems: Calculation of interaction pressure in aqueous electrical double layers. Journal of Chemical Physics, 114(21), 9565-9577.

- Knotts, T. A., Rathore, N., & de Pablo, J. J. (2006). A coarse-grain model of DNA. Abstracts of Papers of the American Chemical Society, 232, 417-417.
- Knotts, T. A., Deublein, S., & de Pablo, J. J. (2007). Unraveling the behavior of DNA through multiscale modeling. Abstracts of Papers of the American Chemical Society, 234.
- Knotts, T. A., Rathore, N., Schwartz, D. C., & de Pablo, J. J. (2007). A coarse grain model for DNA. Journal of Chemical Physics, 126(8).
- Kumar, R., Iyer, V. G., & Im, W. (2007). CHARMM-GUI: A graphical user interface for the CHARMM users. Abstracts of Papers of the American Chemical Society, 233, 273-273.
- Larsson, H. P., Wang, X., Lev, B., Baconguis, I., Caplan, D. A., Vyleta, N. P., . . . Noskov, S. Y. (2010). Evidence for a third sodium-binding site in glutamate transporters suggests an ion/substrate coupling model. Proceedings of the National Academy of Sciences UNITED STATES OF AMERICA, 107(31), 13912-13917.
- Lathrop, D. K., Ervin, E. N., Barrall, G. A., Keehan, M. G., Kawano, R., Krupka, M. A., Hibbs, A. H. (2010). Monitoring the Escape of DNA from a Nanopore Using an Alternating Current Signal. Journal of the American Chemical Society, 132(6), 1878-1885.
- Lee, K. I., Jo, S., Rui, H., Egwolf, B., Roux, B., Pastor, R. W., & Im, W. (2012). Web interface for brownian dynamics simulation of ion transport and its applications to beta-barrel pores. Journal of Computational Chemistry, 33(3), 331-339.

- Lev, B. B., Salahub, D. R., & Noskov, S. Y. (2010). Na(+), K (+) and Tl(+) hydration from QM/MM computations and MD simulations with a polarizable force field. Interdisciplinary Sciences, 2(1), 12-20.
- Lev, B., Zhang, R., de la Lande, A., Salahub, D., & Noskov, S. Y. (2010). The QM-MM interface for CHARMM-deMon. Journal of Computational Chemistry, 31(5), 1015-1023.
- Levenberg, I. G., & Noskov, A. I. (1966). [The sanitary inspection of feeding corn infected with corn smut]. Veterinariia, 43(10), 82-83.
- Li, J. L., & Talaga, D. S. (2010). The distribution of DNA translocation times in solid-state nanopores. Journal of Physics-Condensed Matter, 22(45).
- Lieberman, K. R., Cherf, G. M., Doody, M. J., Olasagasti, F., Kolodji, Y., & Akeson, M. (2010). Processive Replication of Single DNA Molecules in a Nanopore Catalyzed by phi29 DNA Polymerase. Journal of the American Chemical Society, 132(50), 17961-17972
- Lobaskin, V., Lyubartsev, A., & Linse, P. (2001). Effective macroion-macroion potentials in asymmetric electrolytes. Physical Review E, 63(2).
- Lolicato, M., Reina, S., Messina, A., Guarino, F., Winterhalter, M., Benz, R., & De Pinto, V. (2011). Generation of artificial channels by multimerization of beta-strands from natural porin. Biological Chemistry, 392(7), 617-624.
- Lovelle, M., Mach, T., Mahendran, K. R., Weingart, H., Winterhalter, M., & Gameiro, P. (2011). Interaction of cephalosporins with outer membrane channels of Escherichia coli. Revealing binding by fluorescence quenching and ion conductance fluctuations. Physical Chemistry Chemical Physics, 13(4), 1521-1530.

- Rotem, D., Jayasinghe, L., Salichou, M., & Bayley, H. (2012). Protein detection by nanopore equipped with aptamers. Journal of The American Chemical Society, 134, 2781-2787.
- Lu, D., Aksimentiev, A., Shih, A. Y., Cruz-Chu, E., Freddolino, P. L., Arkhipov, A., & Schulten, K. (2006). The role of molecular modeling in bionanotechnology. Physical Biology, 3(1), S40-53.
- Lu, X. J.; Olson, W. K. (2003). 3DNA: a software package for the analysis, rebuilding and visualization of three-dimensional nucleic acid structures. Nucleic Acids Research, 31, 5108-5021
- Luan, B. Q., & Aksimentiev, A. (2008). Electro-osmotic screening of the DNA charge in a nanopore. Physical Review E, 78(2).
- Luan, B. Q., Martyna, G., & Stolovitzky, G. (2011). Characterizing and Controlling the Motion of ssDNA in a Solid-State Nanopore. Biophysical Journal, 101(9), 2214-2222.
- Lubensky, D. K., & Nelson, D. R. (1999). Driven Polymer Translocation Through a Narrow Pore. Biophysical Journal, 77(4), 1824-1838.
- Luo, K. F., Ala-Nissila, T., Ying, S. C., & Bhattacharya, A. (2008). Sequence dependence of DNA translocation through a Nanopore. Physical Review Letters, 100(5). Luo, Y., Egwolf, B., Walters, D. E., & Roux, B. (2010). Ion Selectivity of alpha-Hemolysin with a beta-Cyclodextrin Adapter. I. Single Ion Potential of Mean Force and Diffusion Coefficient. Journal of Physical Chemistry B, 114(2), 952-958.
- Luzzati, V., Mathis, A., Masson, F., & Witz, J. (1964). Structure Transitions Observed in DNA + Poly a in Solution as Function of Temperature + Ph. Journal of Molecular Biology, 10(1), 28-&.

- Lyubartsev, A. P., & Laaksonen, A. (1995). Calculation of Effective Interaction Potentials from Radial-Distribution Functions - a Reverse Monte-Carlo Approach. Physical Review E, 52(4), 3730-3737.
- Lyubartsev, A. P., & Nordenskiold, L. (1995). Monte-Carlo Simulation Study of Ion Distribution and Osmotic-Pressure in Hexagonally Oriented DNA. Journal of Physical Chemistry, 99(25), 10373-10382.
- Lyubartsev, A. P., & Laaksonen, A. (1997). Osmotic and activity coefficients from effective potentials for hydrated ions. Physical Review E, 55(5), 5689-5696.
- Lyubartsev, A. P., & Laaksonen, A. (1999). Effective potentials for ion-DNA interactions. Journal of Chemical Physics, 111(24), 11207-11215.
- Lyubartsev, A. P., & Laaksonen, A. (2000). Determination of effective pair potentials from ab initio simulations: application to liquid water. Chemical Physics Letters, 325(1-3), 15-21.
- Lyubartsev, A. P., & Marcelja, S. (2002). Evaluation of effective ion-ion potentials in aqueous electrolytes. Physical Review E, 65(4).
- Lyubartsev, A. P., Karttunen, M., Vattulainen, I., & Laaksonen, A. (2003). On coarse-graining by the inverse Monte Carlo method: Dissipative particle dynamics simulations made to a precise tool in soft matter modeling. Soft Materials, 1(1), 121-137.
- Lyubartsev, A. P. (2005). Multiscale modeling of lipids and lipid bilayers. European Biophysics Journal with Biophysics Letters, 35(1), 53-61.
- Lyubartsev, A. P. (2007). Interacting electrons in one dimension: a path integral Monte Carlo study. Journal of Physics a-Mathematical and Theoretical, 40(26), 7151-7157.

- Lyubartsev, A., Tu, Y. Q., & Laaksonen, A. (2009). Hierarchical Multiscale Modelling Scheme from First Principles to Mesoscale. Journal of Computational and Theoretical Nanoscience, 6(5), 951-959.
- Lyubartsev, A., Mirzoev, A., Chen, L. J., & Laaksonen, A. (2010). Systematic coarse-graining of molecular models by the Newton inversion method. Faraday Discussions, 144, 43-56.
- Mach, T., Neves, P., Spiga, E., Weingart, H., Winterhalter, M., Ruggerone, P., . . . Gameiro, P. (2008). Facilitated permeation of antibiotics across membrane channels - Interaction of the quinolone moxifloxacin with the OmpF channel. Journal of the American Chemical Society, 130(40), 13301-13309.
- Machlup, S. (1954). Noise in Semiconductors: Spectrum of a Two-Parameter Random Signal. Journal of Applied Physics, 25(3), 341-343.
- MacKerell, A. D. (1998). Developments in the CHARMM all-atom empirical energy function for biological molecules. Abstracts of Papers of the American Chemical Society, 216, U696-U696.
- Maglia, G., Restrepo, M. R., Mikhailova, E., & Bayley, H. (2008). Enhanced translocation of single DNA molecules through alpha-hemolysin nanopores by manipulation of internal charge. Proceedings of the National Academy of Sciences of the United States of America, 105(50), 19720-19725.
- Maglia, G., Heron, A. J., Stoddart, D., Japrung, D., & Bayley, H. (2010). Analysis of Single Nucleic Acid Molecules with Protein Nanopores. Methods in Enzymology, Vol 475: Single Molecule Tools, Pt B, 475, 591-623.

- Mahendran, K. R., Chimerel, C., Mach, T., & Winterhalter, M. (2009). Antibiotic translocation through membrane channels: temperature-dependent ion current fluctuation for catching the fast events. European Biophysics Journal with Biophysics Letters, 38(8), 1141-1145.
- Mahendran, K. R., Hajjar, E., Mach, T., Lovelle, M., Kumar, A., SoUnited States of America, I., . . . Ceccarelli, M. (2010). Molecular Basis of Enrofloxacin Translocation through OmpF, an Outer Membrane Channel of Escherichia coli - When Binding Does Not Imply Translocation. Journal of Physical Chemistry B, 114(15), 5170-5179.
- Mahendran, K. R., Kreir, M., Weingart, H., Fertig, N., & Winterhalter, M. (2010). Permeation of Antibiotics through Escherichia coli OmpF and OmpC Porins: Screening for Influx on a Single-Molecule Level. Journal of Biomolecular Screening, 15(3), 302-307.
- Mahendran, K. R., Singh, P. R., Arning, J., Stolte, S., Kleinekathofer, U., & Winterhalter, M. (2010). Permeation through nanochannels: revealing fast kinetics. Journal of Physics-Condensed Matter, 22(45).
- Majek, P., & Elber, R. (2010). Milestoning without a Reaction Coordinate. Journal of Chemical Theory and Computation, 6(6), 1805-1817.
- Manrao, E. A., Derrington, I. M., Laszlo, A. H., Langford, K. W., Hopper, M. K., Gillgren, N., Gundlach, J. H. (2012). Reading DNA at single-nucleotide resolution with a mutant MspA nanopore and phi29 DNA polymerase. Nature Biotechnology, 30(4), 349-U174.

- Maragliano, L., Cottone, G., Ciccotti, G., & Vanden-Eijnden, E. (2010). Mapping the Network of Pathways of CO Diffusion in Myoglobin. Journal of the American Chemical Society, 132(3), 1010-1017.
- Mardis, E. R. (2011). A decade's perspective on DNA sequencing technology. Nature, 470, 198-203
- Mathe, J., Aksimentiev, A., Nelson, D. R., Schulten, K., & Meller, A. (2005). Orientation discrimination of single-stranded DNA inside the alpha-hemolysin membrane channel. Proceedings of the National Academy of Sciences of the United States of America, 102(35), 12377-12382.
- Meller, A., Nivon, L., Brandin, E., Golovchenko, J., & Branton, D. (2000). Rapid nanopore discrimination between single polynucleotide molecules. Proceedings of the National Academy of Sciences of the United States of America, 97(3), 1079-1084.
- Meller, A., Nivon, L., & Branton, D. (2001). Single molecule characterization of polynucleotides using a trans-membrane channel. Biophysical Journal, 80(1), 147a-148a.
- Meller, A., Nivon, L., & Branton, D. (2001). Voltage-driven DNA translocations through a nanopore. Physical Review Letters, 86(15), 3435-3438.
- Meller, A. (2003). Dynamics of polynucleotide transport through nanometre-scale pores. Journal of Physics-Condensed Matter, 15(17), R581-R607.
- Menestrina, G., Dalla Serra, M., & Prevost, G. (2001). Mode of action of beta-barrel pore-forming toxins of the staphylococcal alpha-hemolysin family. Toxicon, 39(11), 1661-1672.
- Mergell, B., Ejtehadi, M. R., & Everaers, R. (2003). Modeling DNA structure, elasticity, and deformations at the base-pair level. Physical Review E, 68(2).

- Metzker, M. L. (2010). Sequencing technologies – the next generation. Nature Reviews/Genetics, 11, 31-46.
- Mirsaidov, U., Comer, J., Dimitrov, V., Aksimentiev, A., & Timp, G. (2010). Slowing the translocation of double-stranded DNA using a nanopore smaller than the double helix. Nanotechnology, 21(39).
- Mirzoev, A., & Lyubartsev, A. P. (2011). Effective solvent mediated potentials of Na+ and Cl- ions in aqueous solution: temperature dependence. Physical Chemistry Chemical Physics, 13(13), 5722-5727.
- Modi, N., Singh, P. R., Mahendran, K. R., Schulz, R., Winterhalter, M., & Kleinekathofer, U. (2011). Probing the Transport of Ionic Liquids in Aqueous Solution through Nanopores. Journal of Physical Chemistry Letters, 2(18), 2331-2336.
- Modi, N., Winterhalter, M., & Kleinekathofer, U. (2012). Computational modeling of ion transport through nanopores. Nanoscale, 4(20), 6166-6180.
- Muthukumar, M. (2007). Mechanism of DNA transport through pores. Annual Review of Biophysics and Biomolecular Structure, 36, 435-450.
- Nakane, J. J., Akeson, M., & Marziali, A. (2003). Nanopore sensors for nucleic acid analysis. Journal of Physics: Condensed Matter, 15(32), R1365-1393.
- Nardin, C., Widmer, J., Winterhalter, M., & Meier, W. (2001). Amphiphilic block copolymer nanocontainers as bioreactors. European Physical Journal E, 4(4), 403-410.
- Nestorovich, E. M., Winterhalter, M., & Bezrukov, S. M. (2001). Ampicillin translocation through OmpF studied on a single channel level. Biophysical Journal, 80(1), 128A-128A.

- Nestorovich, E. M., Danelon, C., Winterhalter, M., & Bezrukov, S. M. (2002). Designed to penetrate: Time-resolved interaction of single antibiotic molecules with bacterial pores. Proceedings of the National Academy of Sciences of the United States of America, 99(15), 9789-9794.
- Nestorovich, E. M., Rostovtseva, T. K., & Bezrukov, S. M. (2003). Residue Ionization and Ion Transport through OmpF Channels. Biophysical Journal, 85(6), 3718-3729.
- Neves, P., Berkane, E., Gameiro, P., Winterhalter, M., & de Castro, B. (2005). Interaction between quinolones antibiotics and bacterial outer membrane porin OmpF. Biophysical Chemistry, 113(2), 123-128.
- Neves, P., SoUnited States of America, I., Winterhalter, M., & Gameiro, P. (2009). Fluorescence Quenching as a Tool to Investigate Quinolone Antibiotic Interactions with Bacterial Protein OmpF. Journal of Membrane Biology, 227(3), 133-140.
- Nikolaev, A., & Gracheva, M. E. (2011). Simulation of ionic current through the nanopore in a double-layered semiconductor membrane. Nanotechnology, 22(16).
- Noskov, S. Y., Im, W., & Roux, B. (2004). Ion permeation through the alpha-hemolysin channel: Theoretical studies based on Brownian dynamics and Poisson-Nernst-Plank electrodiffusion theory. Biophysical Journal, 87(4), 2299-2309.
- Ovchinnikov, V., Karplus, M., & Vanden-Eijnden, E. (2011). Free energy of conformational transition paths in biomolecules: The string method and its application to myosin VI. Journal of Chemical Physics, 134(8).
- Pan, A. C., Sezer, D., & Roux, B. (2008). Finding transition pathways using the string method with swarms of trajectories. Journal of Physical Chemistry B, 112(11), 3432-3440.

- Papoian, G. A., & Savelyev, A. (2010). Chemically accurate coarse graining of double-stranded DNA. Proceedings of the National Academy of Sciences of the United States of America, 107(47), 20340-20345.
- Parrinello, M., & Laio, A. (2002). Escaping free-energy minima. Proceedings of the National Academy of Sciences of the United States of America, 99(20), 12562-12566.
- Pezeshki, S., Chimerel, C., Bessonov, A. N., Winterhalter, M., & Kleinekathofer, U. (2009). Understanding Ion Conductance on a Molecular Level: An All-Atom Modeling of the Bacterial Porin OmpF. Biophysical Journal, 97(7), 1898-1906.
- Phillips, J. C.; Braun, R.; Wang, W.; Gumbart, J.; Tajkhorshid, E.; Villa, E.; Chipot, C.; Skeel, R. D.; Kale, L.; Schulten, K.(2005). Scalable molecular dynamics with NAMD. Journal of Computational Chemistry, 26, 1781-1802
- Purnell, R. F., Mehta, K. K., & Schmidt, J. J. (2008). Nucleotide identification and orientation discrimination of DNA Homopolymers immobilized in a protein nanopore. Nano Letters, 8(9), 3029-3034.
- Qin, F. (2004). Restoration of Single-Channel Currents Using the Segmental k-Means Method Based on Hidden Markov Modeling. Biophysical Journal, 86(3), 1488-1501.
- Rabin, Y., & Tanaka, M. (2005). DNA in nanopores: Counterion condensation and coion depletion. Physical Review Letters, 94(14).
- Rostovtseva, T. K., Komarov, A., Bezrukov, S. M., & Colombini, M. (2002). Dymamics of nucleotides in VDAC channels: Structure-specific noise generation. Biophysical Journal, 82(1), 188a-188a.

- Rotan, O., Sokolova, V., Gilles, P., Hu, w., Dutt, S., Schrader, T., & Epple, M. (2013). Transport of supramolecular drugs across the cell membrane by calcium phosphate nanoparticles. Materialwissenschaft Und Werkstofftechnik, 44(2-3), 176-182
- Roux, B. (2008). The Membrane Potential and its Representation by a Constant Electric Field in Computer Simulations. Biophysical Journal, 95(9), 4205-4216.
- Roux, B., Pan, A. C., & Sezer, D. (2008). Finding transition pathways using the string method with swarms of trajectories. Journal of Physical Chemistry B, 112(11), 3432-3440.
- Roux, B., Gan, W. X., & Yang, S. C. (2009). Atomistic View of the Conformational Activation of Src Kinase Using the String Method with Swarms-of-Trajectories. Biophysical Journal, 97(4), L8-L10.
- Roux, B., Berneche, S., Egwolf, B., Lev, B., Noskov, S. Y., Rowley, C. N., & Yu, H. (2011). Ion selectivity in channels and transporters. The Journal of General Physiology, 137(5), 415-426.
- Sales-Pardo, M., Guimera, R., Moreira, A. A., Widom, J., & Amaral, L. A. N. (2005). Mesoscopic modeling for nucleic acid chain dynamics. Physical Review E, 71(5). Sambriski, E. J., Oldham, A. B., Knotts, T. A., & de Pablo, J. J. (2008). COMP 254-Thermodynamic and transport properties of DNA from Monte Carlo simulations of a coarse-grained model. Abstracts of Papers of the American Chemical Society, 235.
- Sambriski, E. J., Schwartz, D. C., & de Pablo, J. J. (2009). A Mesoscale Model of DNA and Its Renaturation. Biophysical Journal, 96(5), 1675-1690.

- Sanger, F., Nicklen, S., & Coulson, A. R. (1977). DNA sequencing with chain-terminating inhibitors. Proceedings of the National Academy of Sciences of the United States of America, 74 (12), 5463–5467
- Schloss, J. A. (2008). How to get genomes at one ten-thoUnited States of Americandth the cost. Nature Biotechnology, 26(10), 1113-1115.
- Schmitt, T. J., & Knotts, T. A. (2011). Thermodynamics of DNA hybridization on surfaces. Journal of Chemical Physics, 134(20).
- Schmitt, T. J., Rogers, J. B., & Knotts, T. A. (2013). Exploring the mechanisms of DNA hybridization on a surface. Journal of Chemical Physics, 138(3).
- Sigalov, G., Comer, J., Timp, G., & Aksimentiev, A. (2008). Detection of DNA sequences using an alternating electric field in a nanopore capacitor. Nano Letters, 8(1), 56-63.
- Simakov, N. A., & Kurnikova, M. G. (2010). Soft Wall Ion Channel in Continuum Representation with Application to Modeling Ion Currents in alpha-Hemolysin. Journal of Physical Chemistry B, 114(46), 15180-15190.
- Singh, P. R., Ceccarelli, M., Lovelle, M., Winterhalter, M., & Mahendran, K. R. (2012). Antibiotic Permeation across the OmpF Channel: Modulation of the Affinity Site in the Presence of Magnesium. Journal of Physical Chemistry B, 116(15), 4433-4438.
- Somasundaran, M., Zapp, M. L., Beattie, L. K., Pang, L. Z., Byron, K. S., Bassell, G. J., & Singer, R. H. (1994). Localization of Hiv Rna in Mitochondria of Infected-Cells - Potential Role in Cytopathogenicity. Journal of Cell Biology, 126(6), 1353-1360.

- Song, L., Hobaugh, M. R., Shustak, C., Cheley, S., Bayley, H., & Gouaux, J. E. (1996). Structure of staphylococcal alpha-hemolysin, a heptameric transmembrane pore. Science, 274 (5294), 1859-1866.
- Stoddart, D., Heron, A. J., Mikhailova, E., Maglia, G., & Bayley, H. (2009). Single-nucleotide discrimination in immobilized DNA oligonucleotides with a biological nanopore. Proceedings of the National Academy of Sciences of the United States of America, 106(19), 7702-7707.
- Stoddart, D., Heron, A. J., Klingelhoefer, J., Mikhailova, E., Maglia, G., & Bayley, H. (2010). Nucleobase Recognition in ssDNA at the Central Constriction of the alpha-Hemolysin Pore. Nano Letters, 10(9), 3633-3637.
- Stoddart, D., Maglia, G., Mikhailova, E., Heron, A. J., & Bayley, H. (2010). Multiple Base-Recognition Sites in a Biological Nanopore: Two Heads are Better than One. Angewandte Chemie-International Edition, 49(3), 556-559.
- Subbotina, J. O., Johannes, J., Lev, B., & Noskov, S. Y. (2010). Halothane solvation in water and organic solvents from molecular simulations with new polarizable potential function. Journal of Physical Chemistry B, 114(19), 6401-6408.
- Subbotina, J., Yarov-Yarovoy, V., Lees-Miller, J., Durdagi, S., Guo, J. Q., Duff, H. J., & Noskov, S. Y. (2010). Structural refinement of the hERG1 pore and voltage-sensing domains with ROSETTA-membrane and molecular dynamics simulations. Proteins-Structure Function and Bioinformatics, 78(14), 2922-2934.
- Suginta, W., Mahendran, K. R., Chumjan, W., Hajjar, E., Schulte, A., Winterhalter, M., & Weingart, H. (2011). Molecular analysis of antimicrobial agent translocation through

the membrane porin BpsOmp38 from an ultraresistant Burkholderia pseudomallei strain. Biochimica Et Biophysica Acta-Biomembranes, 1808(6), 1552-1559.

- Szabo, I., Bathori, G., Tombola, F., Coppola, A., Schmehl, I., Brini, M., Ghazi, A., De Pinto, V., & Zoratti, M. (1998). Double-stranded DNA can be translocated across a planar membrane containg purified mitochondrial porin. FASEB Journal, 12, 495-502
- Tabard-Cossa, V., Trivedi, D., Wiggin, M., Jetha, N. N., & Marziali, A. (2007). Noise analysis and reduction in solid-state nanopores. Nanotechnology, 18(30).
- Tajkhorshid, E., Aksimentiev, A., Balabin, I., Gao, M., Isralewitz, B., Phillips, J. C., Schulten, K. (2003). Large scale simulation of protein mechanics and function. Advanced in Protein Chemistry, 66, 195-247.
- Tarasov, V. A., Filatov, M. V., Kisliakova, T. V., Noskov, F. S., Koloskov, A. V., Stavrovietski, V. V., Kiselevski, M. V. (1999). Combined surgical and immunotherapeutic treatment of patients with fourth stage colon cancer. Hybridoma, 18(1), 99-102.
- Timp, W., Mirsaidov, U. M., Wang, D. Q., Comer, J., Aksimentiev, A., & Timp, G. (2010). Nanopore Sequencing: Electrical Measurements of the Code of Life. IEEE Transactions on Nanotechnology, 9(3), 281-294.
- Timp, W., Comer, J., & Aksimentiev, A. (2012). DNA Base-Calling from a Nanopore Using a Viterbi Algorithm. Biophysical Journal, 102(10), L37-L39.
- Tran, Q. T., Mahendran, K. R., Hajjar, E., Ceccarelli, M., Davin-Regli, A., Winterhalter, M., Pages, J. M. (2010). Implication of Porins in beta-Lactam Resistance of Providencia stuartii. Journal of Biological Chemistry, 285(42), 32273-32281.

- van Dijk, M., & Bonvin, A. M. J. J. (2009). 3D-DART: a DNA structure modelling server. Nucleic Acids Research, 37, W235-W239.
- Vanden-Eijnden, E., Venturoli, M., Ciccotti, G., & Elber, R. (2008). On the assumptions underlying milestoning. Journal of Chemical Physics, 129(17).
- Venkatesan, B. M., Polans, J., Comer, J., Sridhar, S., Wendell, D., Aksimentiev, A., & Bashir, R. (2011). Lipid bilayer coated Al2O3 nanopore sensors: towards a hybrid biological solid-state nanopore. Biomedical Microdevices, 13(4), 671-682.
- Wanunu, M., Morrison, W., Rabin, Y., Grosberg, A. Y., & Meller, A. (2010). Electrostatic focusing of unlabelled DNA into nanoscale pores using a salt gradient. Nature Nanotechnology, 5(2), 160-165.
- Weingart, H., Petrescu, M., & Winterhalter, M. (2008). Biophysical Characterization of In- and Efflux in Gram-Negative Bacteria. Current Drug Targets, 9(9), 789-796.
- Wells, D. B., Abramkina, V., & Aksimentiev, A. (2007). Exploring transmembrane transport through alpha-hemolysin with grid-steered molecular dynamics. Journal of Chemical Physics, 127(12).
- Wells, D. B., Bhattacharya, S, Carr, R, Maffeo, C, Ho, A., Comer, J and Aksimentiev, A. (2011). Optimization of the molecular dynamics method for simulations of DNA and ion transport through biological nanopores. Nanopore-based technology: single molecular characterization and DNA sequencing: Humana Press.
- Wells, D. B., Belkin, M., Comer, J., & Aksimentiev, A. (2012). Assessing Graphene Nanopores for Sequencing DNA. Nano Letters, 12(8), 4117-4123.

- White, R. J., Ervin, E. N., Yang, T., Chen, X., Daniel, S., Cremer, P. S., & White, H. S. (2007). Single Ion-Channel Recordings Using Glass Nanopore Membranes. Journal of the American Chemical Society, 129(38), 11766-11775.
- Wiggin, M., Tropini, C., Tabard-Cossa, V., & Marziali, A. (2007). Interactions of DNA with nanopores: Lessons for sensor development. Biophysical Journal, 520a-520a.
- Wiggin, M., Tropini, C., Tabard-Cossa, V., Jetha, N. N., & Marziali, A. (2008). Nonexponential Kinetics of DNA Escape from alpha-Hemolysin Nanopores. Biophysical Journal, 95(11), 5317-5323.
- Wilson, N. A., Abu-Shumays, R., Gyarfas, B., Wang, H., Lieberman, K. R., Akeson, M., & Dunbar, W. B. (2009). Electronic Control of DNA Polymerase Binding and Unbinding to Single DNA Molecules. ACS Nano, 3(4), 995-1003.
- Yang, S., & Roux, B. (2008). Src kinase conformational activation: thermodynamics, pathways, and mechanisms. PLoS Computational Biology, 4(3).
- Zhang, B., Zhang, Y., & White, H. S. (2004). The Nanopore Electrode. Analytical Chemistry, 76(21), 6229-6238.
- Zhao, C., & Noskov, S. Y. (2011). The role of local hydration and hydrogen-bonding dynamics in ion and solute release from ion-coupled secondary transporters. Biochemistry, 50(11), 1848-1856.
- Zhao, Q., Comer, J., Dimitrov, V., Yemenicioglu, S., Aksimentiev, A., & Timp, G. (2008). Stretching and unzipping nucleic acid hairpins using a synthetic nanopore. Nucleic Acids Research, 36(5), 1532-1541.

• Zhao, Q., Jayawardhana, D. A., Wang, D., & Guan, X. (2009). Study of Peptide Transport through Engineered Protein Channels. The Journal of Physical Chemistry B, 113(11), 3572-3578.

APPENDIX

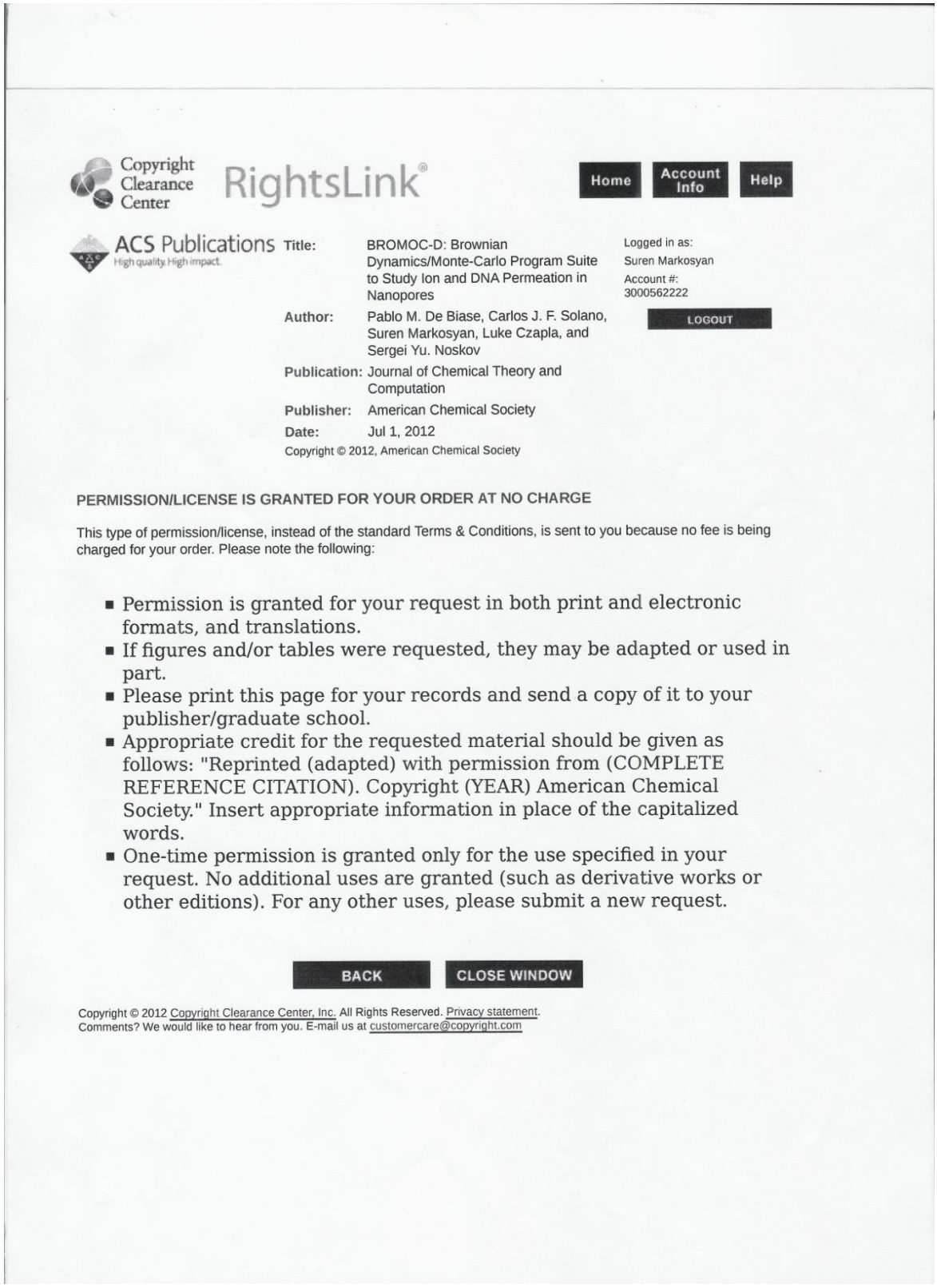

Copyright Clearance Center RightsLink®

Home | Account Info | Help

ACS Publications
High quality. High impact.

Title: BROMOC-D: Brownian Dynamics/Monte-Carlo Program Suite to Study Ion and DNA Permeation in Nanopores

Author: Pablo M. De Biase, Carlos J. F. Solano, Suren Markosyan, Luke Czapla, and Sergei Yu. Noskov

Publication: Journal of Chemical Theory and Computation

Publisher: American Chemical Society

Date: Jul 1, 2012

Copyright © 2012, American Chemical Society

Logged in as:
Suren Markosyan
Account #:
3000562222

LOGOUT

PERMISSION/LICENSE IS GRANTED FOR YOUR ORDER AT NO CHARGE

This type of permission/license, instead of the standard Terms & Conditions, is sent to you because no fee is being charged for your order. Please note the following:

- Permission is granted for your request in both print and electronic formats, and translations.
- If figures and/or tables were requested, they may be adapted or used in part.
- Please print this page for your records and send a copy of it to your publisher/graduate school.
- Appropriate credit for the requested material should be given as follows: "Reprinted (adapted) with permission from (COMPLETE REFERENCE CITATION). Copyright (YEAR) American Chemical Society." Insert appropriate information in place of the capitalized words.
- One-time permission is granted only for the use specified in your request. No additional uses are granted (such as derivative works or other editions). For any other uses, please submit a new request.

BACK | CLOSE WINDOW

Copyright © 2012 Copyright Clearance Center, Inc. All Rights Reserved. Privacy statement.
Comments? We would like to hear from you. E-mail us at customercare@copyright.com

Suren markosyan <smarkosyan3@gmail.com>

Permission Letter

2 messages

Suren markosyan <smarkosyan3@gmail.com> Thu, Aug 29, 2013 at 11:52 AM
To: Pablo De Biase <pablodebiase@gmail.com>

Hi Pablo

I plan to use our research paper

("BROMOC-D: Brownian Dynamics/Monte-Carlo Program Suite to
Study Ion and DNA Permeation in Nanopores" that was published in the Journal of Chemical Theory and Computation, 2012, 8 (7), pp 2540–2551, DOI: 10.1021/ct3004244)

in my Master's thesis. According to the regulations of the University of Calgary, I have to obtain permission letter from every single co-author on the paper.

Please reply to this email and confirm your permission to use the paper in my thesis.

Thank you in advanced

With best regards

Suren Markosyan, M.Sc.
University of Calgary
Department of Bio Sciences

Pablo M. De Biase <pablodebiase@gmail.com> Thu, Aug 29, 2013 at 12:09 PM
To: Suren markosyan <smarkosyan3@gmail.com>

Permission given

On Thu, Aug 29, 2013 at 11:52 AM, Suren markosyan <smarkosyan3@gmail.com> wrote:

> Hi Pablo
>
> I plan to use our research paper
>
> ("BROMOC-D: Brownian Dynamics/Monte-Carlo Program Suite to
> Study Ion and DNA Permeation in Nanopores" that was published in the Journal of Chemical Theory and Computation, 2012, 8 (7), pp 2540–2551, DOI: 10.1021/ct3004244)
>
> in my Master's thesis. According to the regulations of the University of Calgary, I have to obtain permission letter from every single co-author on the paper.
>
> Please reply to this email and confirm your permission to use the paper in my thesis.
>
> Thank you in advanced
>
> With best regards

Suren markosyan <smarkosyan3@gmail.com>

Permission letter

2 messages

Suren markosyan <smarkosyan3@gmail.com> Thu, Aug 29, 2013 at 11:50 AM
To: Carlos José Fernández Solano <cjfqct@hotmail.com>

Hi Carlos

I plan to use our research paper

("BROMOC-D: Brownian Dynamics/Monte-Carlo Program Suite to
Study Ion and DNA Permeation in Nanopores" that was published in the Journal of Chemical Theory and Computation, 2012, 8 (7), pp 2540–2551, DOI: 10.1021/ct3004244)

in my Master's thesis. According to the regulations of the University of Calgary, I have to obtain permission letter from every single co-author on the paper.

Please reply to this email and confirm your permission to use the paper in my thesis.

Thank you in advanced

With best regards

Suren Markosyan, M.Sc.
University of Calgary
Department of Bio Sciences

Carlos José Fernández Solano <cjfqct@gmail.com> Sat, Aug 31, 2013 at 2:32 AM
To: Suren markosyan <smarkosyan3@gmail.com>

Hi Suren,

First of all, congratulations for your Master's thesis. I wish you the best of lucky.

Of course, I confirm my permission to use the paper "BROMOC-D: Brownian Dynamics/Monte-Carlo Program Suite to Study Ion and DNA Permeation in Nanopores" in your thesis.

Please let me know anything you need.

Best Regards,

Carlos José Fernán dez Solano

El 29/08/2013, a las 19:50, Suren markosyan <smarkosyan3@gmail.com> escribió:
[Quoted text hidden]

Gmail by Google

Suren markosyan <smarkosyan3@gmail.com>

Permission letter

2 messages

Suren markosyan <smarkosyan3@gmail.com> Thu, Aug 29, 2013 at 11:51 AM
To: Luke Czapla <luke.czapla@yahoo.com>

Hi Luke

I plan to use our research paper

("BROMOC-D: Brownian Dynamics/Monte-Carlo Program Suite to
Study Ion and DNA Permeation in Nanopores" that was published in the Journal of Chemical Theory and Computation, 2012, 8 (7), pp 2540–2551, DOI: 10.1021/ct3004244)

in my Master's thesis. According to the regulations of the University of Calgary, I have to obtain permission letter from every single co-author on the paper.

Please reply to this email and confirm your permission to use the paper in my thesis.

Thank you in advanced

With best regards

Suren Markosyan, M.Sc.
University of Calgary
Department of Bio Sciences

Luke Czapla <luke.czapla@yahoo.com> Thu, Aug 29, 2013 at 12:09 PM
Reply-To: Luke Czapla <luke.czapla@yahoo.com>
To: Suren markosyan <smarkosyan3@gmail.com>

Hi Suren, of course you may use our paper for your master's thesis! Good luck to you!

-Luke

From: Suren markosyan <smarkosyan3@gmail.com>
To: Luke Czapla <luke.czapla@yahoo.com>
Sent: Thursday, August 29, 2013 1:51 PM
Subject: Permission letter
[Quoted text hidden]

Suren markosyan <smarkosyan3@gmail.com>

Permission Letter

2 messages

Suren markosyan <smarkosyan3@gmail.com> Thu, Aug 29, 2013 at 11:52 AM
To: Sergei Noskov <noskovsy@gmail.com>

Hi Sergei

I plan to use our research paper

("BROMOC-D: Brownian Dynamics/Monte-Carlo Program Suite to
Study Ion and DNA Permeation in Nanopores" that was published in the Journal of Chemical Theory and Computation, 2012, 8 (7), pp 2540–2551, DOI: 10.1021/ct3004244)

in my Master's thesis. According to the regulations of the University of Calgary, I have to obtain permission letter from every single co-author on the paper.

Please reply to this email and confirm your permission to use the paper in my thesis.

Thank you in advanced

With best regards

Suren Markosyan, M.Sc.
University of Calgary
Department of Bio Sciences

Sergei Noskov <noskovsy@gmail.com> Thu, Aug 29, 2013 at 12:01 PM
To: Suren markosyan <smarkosyan3@gmail.com>

You have my full permission to use it.

Sincerely

Sergei Noskov

Отправлено с iPhone

Aug 29, 2013, в 11:52 AM, Suren markosyan <smarkosyan3@gmail.com> написал(а):

[Quoted text hidden]